Constraints on the power spectrum of primordial perturbations from small-scale structure

Amandeep Singh Josan

The University of Nottingham

Thesis submitted to the University of Nottingham
for the degree of Doctor of Philosophy, September 2010

"We are all in the gutter, but some of us are looking at the stars"

– Oscar Wilde

Supervisor: Dr Anne M. Green

Examiners: Professor Edmund J. Copeland
                 Professor Bernard J. Carr

Abstract

In this thesis the Big Bang and inflation theory are reviewed. The success of inflation is largely due to the predicted generation of inhomogeneities. We review the dynamical equations of motion for an accelerating expansion of the Universe and the flow equations which describe the evolution of the Hubble slow-roll parameters. We use cosmological perturbation theory to find a new expression relating comoving curvature perturbations generated during inflation to density perturbations responsible for structure formation. Primordial black holes (PBHs) may form from primordial perturbations. We compile and update constraints on the abundance of PBHs. We then use our new relationship to translate these abundance limits into constraints on the power spectrum of primordial curvature perturbation. In addition we investigate the possible formation of ultracompact dark matter minihalos (UCMHs) which may also form from primordial pertubations. If dark matter is in the form of weakly interacting massive particles (WIMPs) then WIMP annihilation may produce a detectable gamma-ray signature. We calculate the potential constraints which would arise from a detection by the Fermi satellite. Finally, we investigate single field models of inflation using a stochastic technique to generate a large ensemble of models. Using a numerical approach along with a modified flow algorithm we find models of inflation compatible with all cosmological data which have large perturbations on small scales. Significant PBH formation occurs in models in which inflation can continue indefinitely and is ended via a secondary mechanism. We use our PBH constraints to eliminate such models which overproduce PBHs. In this work we demonstrate that PBH constraints, although weak, are effective at constraining models of inflation. We also demonstrate that a gamma-ray detection from UCMHs could potentially constrain the power spectrum of curvature perturbation on small scales very tightly in the near future.

Acknowledgements

I would firstly like to thank my supervisor Dr Anne Green for her guidance throughout my PhD. I would also like to thank Prof. Ed Copeland for encouraging me along the way and Will Hartley for patiently re-teaching me the basics of computer programming. I am also grateful to all the people in the Particle Theory and Astronomy groups who have helped with various computer crises or indulged me when I asked obscure questions.

I want to thank my parents and my sisters for their unwavering support over the years. My parents finally have a doctor in the family and although I can't help with their dodgy knees or hips, I can tell them all about black holes.

I also want to thank my friends who kept me from going insane. Their constant contact and frequent get-togethers kept me grounded and made me appreciate whats important. I particularly want to dedicate this thesis to one of my oldest friends, Imran Khan, who passed away during my PhD. I deeply miss our conversations and hearing about his latest adventures. He was the most loyal friend I could imagine. I wish I could pick up the phone and talk to you again.

Lastly, I would like reserve my deepest appreciation and affection to Carrie. You put up with me over the years and provided unconditional love, support and fantastic food, especially when times were low. I am so happy that you moved across the world for me. I hope I can be as supportive to you if ever you need.

Contents

List of Figures

List of Tables

Constraints on the power spectrum of primordial perturbations from small-scale structure

Chapter 1

Introduction

1.1 Cosmology

Observational cosmology has driven the study of the origins of the Universe from speculative theories to testable models. In particular, the discovery of the Cosmic Microwave Background (CMB) has put the Big Bang theory on sound theoretical footing. Subsequent observations have greatly enhanced our understanding of the Universe and taken us into an era of precision cosmology. An important extension to the the Big Bang model is the theory of cosmological inflation.

The paradigm of cosmological inflation during the early Universe was first proposed in 1980 by Alan Guth [1]. It postulates that subsequent to the Big Bang there was a period of accelerated expansion of the Universe. It is arguably the most successful model for explaining several puzzling features of the Big Bang theory which include the horizon, flatness and monopole problems. One of the most interesting features of inflation is that it naturally results in the generation of inhomogeneities in the Universe in the form of scalar curvature perturbations and gravitational waves in the form of tensor perturbations [2, 3, 4].

In the last two decades there has been much study in the area of inflation model building. Particular models of inflation make predictions about the primordial perturbations which are then compared to observational constraints. These constraints come from a variety of cosmological and astrophysical observations. However, these observations

generally only probe a very narrow range of large scales. Exceptions to this are constraints obtained from Primordial Black Holes (PBHs) [5, 6] and more recently, from Ultra Compact Mini Halos (UCMHs) [7]. Although less well constrained than large-scale observational data, these objects potentially probe perturbations over a very large range of small scales.

In this thesis we review the 'standard cosmology' in chapter 1 and perturbation theory in Chapter 2. We then investigate constraints from PBHs and UCMHs in Chapter 3 and Chapter 4. Finally we investigate PBH constraints on models of inflation generated via a stochastic method in Chapter. 5.

Throughout, we use greek subscript and superscript letters to denote spacetime coordinates and Latin letters to denote spatial coordinates. We adopt the summation convention to imply a sum over pairs of identical superscript and subscript spacetime indices. We also adopt the metric signature $(-, +, +, +)$ and the usual convention of labelling contravariant quantities using superscript indices and covariant quantities using subscript indices. We also set the speed of light and the Planck constant to one throughout, $c = \hbar = 1$. The Planck mass is $m_{\mathrm{Pl}} \equiv G^{-1/2} \approx 10^{19} \mathrm{GeV}$ and is a factor of $\sqrt{8\pi}$ larger than the reduced Planck mass, which we do not use in this thesis.

1.2 The Big-Bang

In the early part of the 20th century Edwin Hubble performed methodical observations of galaxy redshifts as a function of distance [8]. These observations revealed that almost all galaxies in the Universe are travelling away from us. Hubble discovered that the more distant a galaxy the more rapid the recession. The relationship between the separation of two galaxies d and their relative recession velocity v is given by Hubble's law:

$$v = Hd \,, \tag{1.1}$$

where $H \equiv H(t)$ is the Hubble parameter and is given by

$$H = \frac{\dot{a}}{a} \,, \tag{1.2}$$

where overdots represent derivatives with respect to time $\mathrm{d}/\mathrm{d}t$ and $a \equiv a(t)$ is the scale factor which characterizes the expansion of the Universe. The measured value of the Hubble parameter today H_0 is [9]

$$H_0 = 71 \pm 2.5 \,\mathrm{km\ s^{-1} Mpc^{-1}}, \tag{1.3}$$

where throughout we will use a subscript '0' to denote the current epoch.

The revelation of an expanding Universe naturally led to the conclusion that the Universe started from a much smaller early state. This then expanded to the present Universe with the expansion still continuing today. The initial state from which the entire visible Universe expanded is known as **the Big Bang**.

The standard mathematical description of an expanding Universe is constructed by the consideration of distance measures. The distance between two nearby points in a four dimensional space-time is given by the following line element:

$$\mathrm{d}s^2 = \sum_{\mu,\nu} g_{\mu\nu} \mathrm{d}x^\mu \mathrm{d}x^\nu, \tag{1.4}$$

where $g_{\mu\nu}$ is the metric and μ and ν are indices which can take values $0, 1, 2$ and 3. Here x^0 is assigned the time coordinate and x^1, x^2 and x^3 are the spatial coordinates. If the Universe has a constant curvature which can be flat, hyperbolic or spherical on the largest scales, then the most general line element in polar coordinates is given by the Friedmann-Robertson-Walker (FRW) metric line element:

$$\mathrm{d}s^2 = -\mathrm{d}t^2 + a(t)^2 \left[\frac{\mathrm{d}r^2}{1 - Kr^2} + r^2(\mathrm{d}\theta^2 + \sin^2\theta \mathrm{d}\phi^2) \right], \tag{1.5}$$

where K is the measure of spatial curvature with $K = 0$ corresponding to flat spatial curvature, $K = -1$ to hyperbolic spatial curvature and $K = 1$ to spherical spatial curvature. Here and throughout we have set the speed of light to $c = 1$.

The evolution of the scale factor is described by the Einstein equations [10]:

$$G_{\mu\nu} \equiv R_{\mu\nu} - \frac{1}{2}Rg_{\mu\nu} = 8\pi G T_{\mu\nu}, \tag{1.6}$$

where $R_{\mu\nu}$ is the Ricci tensor, R is the Ricci scalar and $T_{\mu\nu}$ is the energy-momentum tensor which can be written $T^\mu_\nu = \mathrm{diag}(-\rho, \mathrm{P}, \mathrm{P}, \mathrm{P})$ where ρ is the energy density of the Universe and P is its pressure. From the Einstein equations one can derive the

Friedmann equation:

$$H^2 \equiv \left(\frac{\dot{a}}{a}\right)^2 = \frac{8\pi G\rho}{3} - \frac{K}{a^2} \ . \tag{1.7}$$

From Eq. (1.6) one can also derive the acceleration equation:

$$\left(\frac{\ddot{a}}{a}\right) = -\frac{4\pi G}{3}(\rho + 3P) \ . \tag{1.8}$$

One further useful equation is obtained by considering the conservation of energy to give the fluid equation:

$$\dot{\rho} + 3H(\rho + P) = 0 \ . \tag{1.9}$$

These equations together describe the expansion and geometry of the Universe in terms of the density and pressure of material contained within it. One can solve Eq. (1.7) and Eq. (1.9) for the case of a flat Universe ($K = 0$) to find the behaviour of a matter or radiation dominated Universe:

For a matter dominated Universe:

$$\rho_{\mathrm{m}} \propto \frac{1}{a^3} \ , \qquad a \propto t^{2/3} \ . \tag{1.10}$$

For a radiation dominated Universe:

$$\rho_{\mathrm{r}} \propto \frac{1}{a^4} \ , \qquad a \propto t^{1/2} \ . \tag{1.11}$$

A useful quantity to consider is the critical density ρ_{crit} defined as the total energy density required to make the Universe flat ($K = 0$). Using Eq. (1.7) this is given by

$$\rho_{\mathrm{crit}}(t) = \frac{3H^2}{8\pi G} \ . \tag{1.12}$$

1.3 Energy content of the Universe

It is convenient to define the energy density ρ_X of a particular substance X in the Universe as a fraction of the critical density ρ_{crit}. The resulting density parameter Ω for each component of the energy density is given by

$$\Omega_{\mathrm{X}} = \frac{\rho_{\mathrm{X}}}{\rho_{\mathrm{crit}}} \ . \tag{1.13}$$

From Eq. (1.13) if the total density parameter $\Omega_{\mathrm{tot}} = 1$ then the Universe is spatially flat ($K = 0$) with a density given by Eq. (1.12).

The total energy within the Universe is made up from various components and so Ω_{tot} can be divided into each component such as matter Ω_{m} and radiation Ω_{r}. These can be further subdivided into the various different types of matter such as Ω_{stars}, Ω_{dust}, Ω_{PBH}, Ω_{UCMH} etc..

The current 'standard cosmological model' places values on the energy content of the Universe finding [9]

$$\Omega_{\mathrm{b}} \approx 0.04 , \tag{1.14}$$

$$\Omega_{\mathrm{DM}} \approx 0.22 , \tag{1.15}$$

$$\Omega_{\Lambda} \approx 0.73 , \tag{1.16}$$

where Ω_{b} is the density parameter for baryonic matter, Ω_{DM} for non-baryonic cold dark matter and Ω_{Λ} for the cosmological constant (or dark energy) which is thought to be responsible for the observed accelerated expansion of the Universe [11, 12]. (For a review of dark energy see Refs. [13, 14]).

1.4   Cosmic Microwave Background

The Cosmic Microwave Background (CMB) radiation, discovered in 1965 by Arno Penzias and Robert Wilson [15], quickly led to the Big Bang theory becoming an accepted model for the early Universe. The near perfect thermal black body spectrum has a temperature of 2.725 K with wavelength such that observations are in the microwave range. The significant point here is that the uniform black body spectrum implies the early Universe was in thermal equilibrium. Of particular interest to cosmologists, however, are the small variations (anisotropies) in this almost uniform temperature at the level of approximately one part in 10^5. These temperature anisotropies were first detected in 1992 by the Russian RELIKT-1 experiment and soon after by COsmic Background Explorer (COBE) satellite [16]. More recently the anisotropies have been measured to high precision by the Wilkinson Microwave Anisotropy Probe (WMAP) [9].

These observations imply that the Universe emerged from the Big Bang as a very hot and dense expanding fluid. The current understanding is that this fluid was comprised

of an ionized plasma of protons and electrons and photons. High energy photon inter-actions through Thomson scattering prevented neutral atoms from forming. Due to this photon scattering the Universe was, therefore, opaque. It is assumed that some initial perturbations were present in this dense fluid. Overdense regions collapsed through gravitational attraction until the photon pressure countered this collapse. This resulted in the generation of acoustic oscillations within the plasma with regions of high density plasma being hotter than low density regions.

As the Universe further expanded and cooled, the photon energy dropped until the ion-izing interaction of photons with ionized atoms could no longer occur. Neutral atoms could then form resulting in an epoch known as **recombination**. The sudden drop in photon scattering known as **decoupling** resulted in these photons travelling uninter-rupted ever since. Photons from this era therefore provide a snapshot of conditions just prior to decoupling.

At decoupling, photons which were in overdense regions had to begin their uninter-rupted journey after decoupling by first overcoming the gravitational potential energy within this region. These photons therefore emerged from the decoupling epoch with less energy (or lower temperature) than those photons in underdense regions. This is known as the Sachs-Wolfe effect [17]. This along with the acoustic oscillations de-scribed above and other effects are precisely the origin of the temperature anisotropy that we observe today. The observed surface the CMB photons occupy on the celes-tial sphere centred on our location is known as the **surface of last scattering**. This represent the earliest time accessible to us through observations. Information about conditions prior to this epoch may be accessible through gravitational wave detection in the future.

1.5 Problems with the Big-Bang

1.5.1 Horizon problem

The size of the observable Universe is given by the distance light could have travelled during the lifetime of the Universe taking into account the entire expansion history. At

any given instant, taking into account the dynamics of the expansion of the Universe at that time, one can define a Hubble length as $d_{\mathrm{H}} = H^{-1}$. This determines the size of a region within which causality can operate. This length scale is often called a **horizon** [18].

Observations of the CMB have shown that the Universe is highly isotropic with all parts of the sky being the same temperature to one part in 10^5. This suggests that the Universe must have been in thermal equilibrium at some point in its history. In order for this to occur the entire visible Universe must have been in causal contact at one time. Photons from the CMB were free to travel uninterrupted since the time of decoupling approximately 400,000 years after the Big Bang. This means that the size of the horizon at the time of decoupling was approximately 400,000 light years across. This corresponds to a region on the sky today which subtends an angle of around 2 degrees across. The CMB photons from one part of the sky have taken almost the age of the Universe to reach us and likewise with the CMB on the opposite part of the sky. These regions are certainly greater than 2 degrees apart and so it is not possible, within the standard Big Bang picture, for these two regions to have ever been in causal contact to thermally equalize. One of the biggest problems with the Big Bang theory is understanding why the temperature of the Universe is so uniform across such large distances.

1.5.2 Flatness problem

The present day value for the total density parameter Ω_{tot} has been shown to be very close to one ($\Omega_{\mathrm{tot}} = 1.0023^{+0.0056}_{-0.0054}$ [19]) i.e. that the energy density of the Universe is very close to the critical energy density (see Sec. 1.3). From Eq. (1.13) this implies that the Universe is spatially flat. The Friedmann equation given by Eq. (1.7) can be rewritten in terms of the density parameter as

$$\Omega_{\mathrm{tot}} - 1 = \frac{K}{a^2 H^2} . \tag{1.17}$$

Using the matter and radiation domination relations for $a(t)$ given in Sec. 1.2, $\Omega_{\mathrm{tot}} - 1 \propto t$ in a radiation dominated Universe and $\Omega_{\mathrm{tot}} - 1 \propto t^{2/3}$ in a matter dominated Universe i.e. $\Omega_{\mathrm{tot}} = 1$ is unstable. Even a small deviation from $\Omega_{\mathrm{tot}} = 1$ at early

times results in rapid departure away from one at late times. The question must then be asked, why is the Universe so close to being flat today when any small deviation from flatness at early times is greatly amplified in time.

1.5.3 Monopole problem

Within particle physics the concept of symmetry breaking leads to the production of relics such as magnetic monopoles (also cosmic strings and topological defects) in the early Universe. In an expanding Universe the energy density of these relics reduces as matter ($\rho \propto a^{-3}$). In the early radiation dominated Universe $\rho \propto a^{-4}$, therefore one would expect relics to rapidly dominate the Universe.

1.6 Inflation

Inflation seeks to resolve the problems discussed above by adding a period of rapidly accelerating expansion soon after the Big Bang. In this scenario the scale factor is accelerating:

$$\ddot{a} > 0 . \tag{1.18}$$

From Eq. (1.8), this requires

$$P < -\frac{1}{3}\rho . \tag{1.19}$$

This implies that for an accelerating expansion, the Universe must be dominated by some substance with negative pressure.

The quasi-exponential expansion associated with inflation results in regions which were causally connected before the onset of inflation being stretched to scales far beyond the horizon after inflation. Our current horizon continually grows as photons from more distant regions of the Universe have time to reach us. Despite this our observable Universe is still contained within a region that was initially much smaller before the onset of inflation and therefore causally connected. This resolves the horizon problem as two regions of the Universe which appear beyond each others horizon were, in fact, well within each others horizon in the early Universe and so were able to reach thermal equilibrium.

The flatness problem can also be confronted by inflation theory by considering the denominator in Eq. (1.17). During inflation H remains almost constant whilst a increases almost exponentially. From Eq. (1.17) any spatial curvature K which exists initially is quickly suppressed by the rapid expansion of a. Therefore, rather than flat space being unstable, Ω_{tot} is now driven to one during inflation. Heuristically, one can imagine that any spacetime curvature that existed before inflation is stretched to such a vast degree (far beyond observable scales) that after inflation the observable Universe is effectively flat.

The monopole problem is also solved by simply ensuring that any relics produced by symmetry breaking are quickly diluted away during inflation.

Any theory of the early Universe must solve the above problems and also must provide a means for generating the inhomogeneities observed in the Universe. The Big Bang does not provide any natural explanation for these inhomogeneities (with the exception of topological defect theories [20, 21, 22, 23]) and so must assume these were present as part of the initial conditions.

As briefly mentioned in Sec. 1.1, the success of inflation theory derives, in a large part, from the prediction of the generation of inhomogeneities. During inflation the quasi-exponential expansion of the Universe results in the amplification of vacuum quantum fluctuations. These perturbations are stretched to far beyond the horizon becoming classical spacetime curvature perturbations in the process [2, 4, 24, 25]. Once outside of the horizon, spatial curvature perturbations cannot evolve further as they are larger than regions of causal contact. They are then said to be 'frozen' [1]. Some time after inflation has ended, perturbations re-entered the horizon where they are able to evolve through gravitational collapse or expand through radiation pressure. The evolution of these perturbations after inflation has ended is thought to eventually lead to the rich structure we see in the Universe today. The exact nature of the inhomogeneities generated by inflation is still not well understood. Many models of inflation have been proposed, most with different predictions for the evolution of perturbations. With the exception of PBHs and possible DM substructures, our only opportunity of testing models of inflation come from a very narrow range of large-scale observations. These

---

[1]we ignore the possible generation of isocurvature perturbations throughout this thesis.

observations do, however, provide strong constraints on the range of scales where they are relevant.

1.7 Slow-roll inflation

A simple way to achieve an accelerated expansion of the Universe is with a scalar field φ known as the inflaton field. This field evolves along a potential $V(\varphi)$ given by a particular model of inflation. Assuming homogeneity, the energy-momentum tensor of the inflaton field is given by

$$T_{\mu\nu} = \partial_\mu\varphi\partial_\nu\varphi - g_{\mu\nu}\left(\frac{1}{2}g^{\alpha\beta}\partial_\alpha\varphi\partial_\beta\varphi - V(\varphi)\right), \tag{1.20}$$

where the energy density and pressure of an homogeneous inflaton field are

$$\rho_\varphi = \frac{1}{2}\dot\varphi^2 + V(\varphi), \tag{1.21}$$

$$P_\varphi = \frac{1}{2}\dot\varphi^2 - V(\varphi). \tag{1.22}$$

The dynamics of an expanding FRW Universe are given by the equations of motion of the background (Friedmann equations). Using Eq. (1.7) and Eq. (1.8) (setting $K = 0$) along with Eq. (1.21) and Eq. (1.22), these are given by

$$H^2 = \frac{8\pi}{3m_{\mathrm{Pl}}^2}\left[\frac{1}{2}\dot\varphi^2 + V(\varphi)\right], \tag{1.23}$$

$$\left(\frac{\ddot a}{a}\right) = \frac{8\pi}{3m_{\mathrm{Pl}}^2}\left[V(\varphi) - \dot\varphi^2\right], \tag{1.24}$$

where $m_{\mathrm{Pl}} \equiv G^{-1/2} \approx 10^{19}\mathrm{GeV}$ is the Planck mass. The equation of motion of the inflaton field φ is given by the conservation of the energy-momentum tensor:

$$\ddot\varphi + 3H\dot\varphi + V'(\varphi) = 0, \tag{1.25}$$

where primes represent derivatives with respect to the field φ.

From Eq. (1.24) an accelerated expansion of the scale factor ($\ddot a > 0$) is obtained if $\dot\varphi^2 < V(\varphi)$. If we take the limiting case

$$\dot\varphi^2 \ll V(\varphi), \tag{1.26}$$

then one obtains an almost exponential expansion with a limit approaching a constant Hubble parameter. This limit is known as a de Sitter Universe. With this limiting case the following approximation also becomes valid:

$$\ddot{\varphi} \ll 3H\dot{\varphi} \ . \tag{1.27}$$

Substituting these approximations into the Einstein equations, Eq. (1.23) and Eq. (1.25), the approximations are equivalent to

$$H^2 \approx \frac{8\pi V(\varphi)}{3m_{\mathrm{Pl}}^2} , \tag{1.28}$$

$$3H\dot{\varphi} \approx -V'(\varphi) . \tag{1.29}$$

We see from Eq. (1.25) that this second approximation can be interpreted as the friction term of Eq. (1.25) dominating resulting in the inflaton field rolling very slowly down the potential. As a result Eq. (1.26) and Eq. (1.27) are known as the **slow-roll approximations** and result in **slow-roll inflation**. For slow-roll inflation to occur these slow-roll approximations must hold. It can be shown that the slow-roll approximations are valid when

$$\epsilon_{\mathrm{V}} \ll 1 , \qquad \eta_{\mathrm{V}} \ll 1 , \tag{1.30}$$

where ϵ_{V} and η_{V} are known as the potential slow-roll parameters and are defined as

$$\epsilon_{\mathrm{V}} = \frac{m_{\mathrm{Pl}}^2}{16\pi} \left(\frac{V'(\varphi)}{V(\varphi)} \right)^2 , \tag{1.31}$$

$$\eta_{\mathrm{V}} = \frac{m_{\mathrm{Pl}}^2}{8\pi} \left(\frac{V''(\varphi)}{V(\varphi)} \right) , \tag{1.32}$$

with $\epsilon_{\mathrm{V}} = 1$ being defined as the end of inflation. The potential slow-roll parameters, therefore, describe the form of the potential which, in turn, determines the dynamics of the inflaton field along this potential through Eqs. (1.28) & (1.29).

1.8 Hamilton-Jacobi Formalism

As discussed in the previous section, the condition for slow-roll inflation is an approximation only valid in the limit approaching de Sitter expansion, or equivalently, where Eqs. (1.28) & (1.29) apply. In a situation where $\epsilon_{\mathrm{V}} \lesssim 1$ and $\eta_{\mathrm{V}} \lesssim 1$, the slow-roll

approximations given by Eqs. (1.30) are clearly violated. However, this does not imply inflation has ceased as the condition $\dot{\varphi}^2 < V(\varphi)$ and therefore $\ddot{a} > 0$ may still be valid. What this means is that slow-roll inflation is no longer occurring but inflation may continue, albeit not of the slow-roll variety. Indeed, since the end of inflation is defined by $\epsilon_V = 1$, one would expect that any single field model of slow-roll inflation must necessarily pass through this regime of slow-roll violation.

It is evident that to fully track the evolution of the inflaton field to the end of inflation with the formalism presented in Sec. 1.7 will be impossible. The description of the dynamics given by Eq. (1.28) and Eq. (1.29) becomes insufficient as $\epsilon_V \sim 1$ or $\eta_V \sim 1$ due to the breakdown of the slow-roll approximations given by Eq. (1.26) and Eq. (1.27). This poses a problem when it comes to fully evolving and describing particular models of inflation numerically as we do in Chapter 5.

To overcome this, Eq. (1.23) and Eq. (1.25) can be simply re-written with $H(\varphi)$ as the fundamental quantity instead of $V(\varphi)$. Assuming a monotonic field evolution Eq. (1.23) and Eq. (1.25) can be re-written as [26, 27]

$$[H'(\varphi)]^2 - \frac{12\pi}{m_{Pl}^2}H^2(\varphi) = -\frac{32\pi^2}{m_{Pl}^4}V(\varphi)\,, \tag{1.33}$$

$$\dot{\varphi} = -\frac{m_{Pl}^2}{4\pi}H'(\varphi)\,, \tag{1.34}$$

where Eq. (1.33) is called the Hamilton-Jacobi equation.

One can think of the Hamilton-Jacobi equation as providing a description of the dynamics of inflation in terms of geometrical properties, $H(\varphi)$, rather than the potential, $V(\varphi)$, motivated from particle physics. Using $H(\varphi)$ as the fundamental quantity the following slow-roll parameters can be derived:

$$\epsilon_H = \frac{m_{Pl}^2}{4\pi}\left(\frac{H'(\varphi)}{H(\varphi)}\right)^2\,, \tag{1.35}$$

$$\eta_H = \frac{m_{Pl}^2}{4\pi}\left(\frac{H''(\varphi)}{H(\varphi)}\right)\,. \tag{1.36}$$

These parameters are often called the Hubble slow-roll parameters to distinguish them from the potential slow-roll parameters given by Eqs. (1.31) & (1.32). We emphasize that despite the unfortunate name, the Hubble slow-roll parameters Eqs. (1.35) & (1.36) are derived without invoking the slow-roll approximations [28]. Rather, the derivation

of the Hubble slow-roll parameters is exact and does not rely on taking the limiting case of exponential expansion as seen for the potential slow-roll parameters.

The acceleration equation given by Eq. (1.24), can now be rewritten in terms of the Hubble slow-roll parameter:

$$\left(\frac{\ddot{a}}{a}\right) = H^2(\varphi)[1 - \epsilon_{\rm H}] \,. \tag{1.37}$$

Hence, inflation ($\ddot{a} > 0$) occurs if the Hubble slow-roll parameter satisfies

$$\epsilon_{\rm H} < 1 \,. \tag{1.38}$$

The inflationary dynamics described by Eq. (1.33) and Eq. (1.34) are valid even in a regime where the slow-roll approximation given by Eq. (1.30) is violated.

To summarise, slow-roll inflation occurs if the conditions given by Eq. (1.30) are valid with the inflationary dynamics being described by Eq. (1.28) and Eq. (1.29). However inflation (not necessarily of the slow-roll variety) occurs if the condition given by Eq. (1.38) is valid with the inflationary dynamics being described by Eq. (1.33) and Eq. (1.34) [28].

The potential slow-roll parameters $\epsilon_{\rm V}$ and $\eta_{\rm V}$ are in fact the limiting case of the Hubble slow-roll parameters $\epsilon_{\rm H}$ and $\eta_{\rm H}$ where, in the slow-roll limit, $\epsilon_{\rm H} \longrightarrow \epsilon_{\rm V}$ and $\eta_{\rm H} \longrightarrow \eta_{\rm V} - \epsilon_{\rm V}$.

It has been shown that Eq. (1.35) and Eq. (1.36) are the first two terms in an infinite hierarchy of slow-roll parameters [27]. Higher order terms are given by

$$^l\lambda_{\rm H} \equiv \left(\frac{m_{\rm Pl}^2}{4\pi}\right)^l \frac{(H')^{l-1}}{H^l} \frac{{\rm d}^{(l+1)}H}{{\rm d}\varphi^{(l+1)}} \quad ; \qquad l \geq 1 \,, \tag{1.39}$$

where the slow-roll parameter $\eta_{\rm H}$ is reproduced by Eq. (1.39) for $l = 1$.

It can be seen that if the Hubble slow-roll parameters are specified to infinite order, this is equivalent to specifying all the derivatives of the Hubble parameter (or equivalently the potential) to infinite order. This would amount to fully describing the form for the potential along which any particular model of inflation evolves.

1.9 Power spectrum

In Sec. 1.6 we reviewed inflation as a possible method for the generation of perturbations in the early Universe. In order to formalise the nature of these perturbations one needs to consider their statistical properties.

It is well known that a wave or perturbation $f(\mathbf{x})$ at any instant, no matter how complicated, can be decomposed into a superposition of different wave vectors $\mathbf{k}$

$$f(\mathbf{k}) = \int f(\mathbf{x})e^{-i\mathbf{k.x}}\mathrm{d}^3x \ , \tag{1.40}$$

where wavenumbers are given by $k = |\mathbf{k}|$, and each k is inversely proportional to the physical size of the corresponding perturbation of wavelength λ or comoving size R where $R \equiv \lambda/a(t)$. Hence, a perturbation of wavelength λ in an expanding Universe has a corresponding comoving wavenumber k defined by

$$k \propto \frac{a(t)}{\lambda} \ . \tag{1.41}$$

During inflation one is usually concerned with perturbations at horizon crossing. This is the scale below which causality can operate, and subsequently, the evolution of perturbations can occur. Hence, perturbations with physical wavelengths equal to the horizon, $\lambda = H^{-1}$, have a corresponding comoving wavenumber given by

$$k = aH \ . \tag{1.42}$$

Perturbations with comoving wavenumber $k < aH$ are said to be outside of the horizon or super-horizon. Those with $k > aH$ are said to be within the horizon or sub-horizon.

In cosmology the scalar perturbation of most interest is the primordial comoving curvature perturbation $\mathcal{R}$. We continue this section working in terms of this quantity and review $\mathcal{R}$ in more detail in Sec. 2.4. A commonly used measure of distribution of perturbations on any given comoving scale k is the power spectrum, $\mathrm{P}_{\mathcal{R}}(k)$. The power spectrum for gaussian perturbations is defined by the two-point correlation function:

$$\langle \mathcal{R}(\mathbf{k_1})\mathcal{R}^*(\mathbf{k_2}) \rangle = (2\pi)^3 \mathrm{P}_{\mathcal{R}}(k)\delta^3(\mathbf{k_1} - \mathbf{k_2}) \ , \tag{1.43}$$

where the angular brackets denote an ensemble average, $\mathcal{R}^*$ is the complex conjugate of $\mathcal{R}$ and $\delta^3(\mathbf{k_1} - \mathbf{k_2})$ is a Dirac delta function which constrains $\mathbf{k_1} = \mathbf{k_2}$. It is common

to define a dimensionless quantity $\mathcal{P}$ also known as the power spectrum

$$\mathcal{P}_\mathcal{R}(k) \equiv \left(\frac{k^3}{2\pi^2}\right) P_\mathcal{R}(k) \ . \tag{1.44}$$

Hence,

$$\mathcal{P}_\mathcal{R}(k) \equiv \left(\frac{k^3}{2\pi^2}\right) \langle|\mathcal{R}|^2\rangle \ . \tag{1.45}$$

Qualitatively the power spectrum tells us how the amplitude of perturbations varies on different scales. If the Universe has lots of overdense and underdense regions on a particular scale, the resulting power spectrum on this scale will be large.

For a particular given model of inflation the power spectrum can be approximated by [29, 30]

$$\mathcal{P}_\mathcal{R}^{1/2}(k) \approx \left(\frac{1}{2\pi}\right) \left(\frac{H^2}{|\dot{\varphi}|}\right) \Big|_{k=aH} \ , \tag{1.46}$$

where the inflation model dependency of the power spectrum enters the $\dot{\varphi}$ term through either Eq. (1.29) or Eq. (1.34). We shall review a more accurate expression for the power spectrum in Sec. 5.4.

Here we have concentrated on the relatively simple case of scalar curvature perturbations as these are responsible for density fluctuations which lead to structure formation in the Universe. We shall investigate scalar perturbations in more depth in the next chapter, however, we now describe another type of perturbation which can be treated independently from scalar perturbations known as tensor perturbations, or gravity waves. Tensor perturbations can produce detectable distortions in the CMB, hence, it is useful to define the power spectrum of tensor perturbations $P_\mathcal{T}$ in a similar fashion to Eq.(1.43):

$$\langle h(\mathbf{k_1}, \tau)h^*(\mathbf{k_2}, \tau)\rangle = (2\pi)^3 P_\mathcal{T}(k)\delta^3(\mathbf{k_1} - \mathbf{k_2}) \ , \tag{1.47}$$

where h represents tensor perturbations to the metric $g_{\mu\nu}$ and where τ is conformal time and is related to proper time t by

$$d\tau = \frac{dt}{a} \ . \tag{1.48}$$

One can also redefine the power spectrum of tensor perturbations as

$$\mathcal{P}_\mathcal{T}(k) \equiv \left(\frac{k^3}{2\pi^2}\right) P_\mathcal{T}(k) \ . \tag{1.49}$$

1.10   Cosmological observables

It is common to take the form of the power spectrum to be a power-law:

$$\mathcal{P}_{\mathcal{R}}(k) = \mathcal{P}_{\mathcal{R}}(k_0) \left(\frac{k}{k_0}\right)^{n_s-1} , \tag{1.50}$$

where k_0 is a pivot point usually taken to be the scale where observations of the power spectrum are most accurate and n_s is the scalar spectral index quantifying the 'tilt' of the power spectrum. In a Universe which has more structure on large scales than on small scales, the spectral index is $n_s < 1$. The opposite is true for $n_s > 1$. For the case of $n_s = 1$ the power spectrum is the same on all scales and is known as a scale-invariant (or Harrison-Zeldovich) spectrum.

From Eq. (1.50) the spectral index is

$$n_s - 1 \equiv \frac{\mathrm{dln}\mathcal{P}_{\mathcal{R}}(k)}{\mathrm{dln}k} . \tag{1.51}$$

From the WMAP 7 year data [9]

$$\mathcal{P}_{\mathcal{R}}(k_0) = (2.43 \pm 0.11) \times 10^{-9} , \tag{1.52}$$

where $k_0 = 0.002\mathrm{Mpc}^{-1}$. In the case of a power-law power spectrum given by Eq. (1.50), the WMAP 7 year data has constrained the spectral index to be [9]

$$n_s = 0.963 \pm 0.014 . \tag{1.53}$$

However, a constant spectral index in Eq. (1.50) is an assumption only valid for a pure power-law. In general the power spectrum can be parameterised by a Taylor expansion about the pivot point

$$\mathcal{P}_{\mathcal{R}}(k) = \mathcal{P}_{\mathcal{R}}(k_0) \left(\frac{k}{k_0}\right)^{n_s(k_0)-1+\frac{1}{2}\left(\frac{\mathrm{d}n_s}{\mathrm{dln}k}\right)\ln\left(\frac{k}{k_0}\right)+\dots} . \tag{1.54}$$

Now considering the first 2 terms in the Taylor expansion, (the spectral index n_s and the running of the spectral index $\mathrm{d}n_s/\mathrm{dln}k$) the observational constraints on n_s become significantly less constrained [9]

$$n_s(k_0) = 1.027^{+0.050}_{-0.051} , \tag{1.55}$$

$$\frac{\mathrm{d}n_s}{\mathrm{dln}k} = -0.034 \pm 0.026 . \tag{1.56}$$

where the running of the spectral index is

$$\frac{\mathrm{d}n_s}{\mathrm{d}\ln k} \equiv \frac{\mathrm{d}^2\ln\mathcal{P}_{\mathcal{R}}(k)}{\mathrm{d}\ln k^2} \ . \tag{1.57}$$

We see that to one sigma, the negative running in Eq. (1.56) suggests that small-scale structure cannot not form in any significant abundance. This is only true if the higher order terms in the Taylor expansion are zero. However, higher order terms in the Taylor expansion are poorly constrained by the limited range of current observations. We shall discuss this further in chapter 5.

One can define the scalar to tensor ratio

$$r \equiv \frac{\mathcal{P}_{\mathcal{R}}}{\mathcal{P}_{\mathcal{T}}} \ , \tag{1.58}$$

From WMAP 7 year data [19]

$$r < 0.36 \quad (95\% \ \mathrm{CL}) \ . \tag{1.59}$$

1.11 Number of e-foldings of inflation

The amount of inflationary expansion from some initial time t to the end of inflation t_{end} is given by the number of e-foldings N defined as

$$N(t) \equiv \ln\left[\frac{a(t_{\mathrm{end}})}{a(t)}\right] = \int_t^{t_{\mathrm{end}}} H\mathrm{d}t \ , \tag{1.60}$$

where N decreases as a function of time until the end of inflation defined as $N = 0$. The initial time is usually taken to be when the current Hubble scale left the horizon during inflation. Current observations probe a range of scales corresponding to approximately 10-15 e-foldings of inflation [31, 32].

The total number of e-foldings which elapsed between our currently observable scales exiting the horizon during inflation and the end of inflation N_{cos} is an important quantity which we use in Sec. 5. To determine this one must assume a model for the history of the Universe. A common assumption is that following inflation there is a period of reheating. Subsequent to this there is a period of radiation domination which gives way to matter domination and finally to the current dark energy dominated epoch. Here we assume the recent expansion due to dark energy has a negligible effect on the

final results and so take the final epoch to be matter dominated. From this one can write [28, 31]

$$\frac{k}{a_0 H_0} = \frac{a_k H_k}{a_0 H_0} = \frac{a_k}{a_{\text{end}}} \frac{a_{\text{end}}}{a_{\text{reh}}} \frac{a_{\text{reh}}}{a_{\text{eq}}} \frac{a_{\text{eq}}}{a_0} \frac{H_k}{H_{\text{eq}}} \frac{H_{\text{eq}}}{H_0} . \tag{1.61}$$

where 'end' is the end of inflation, 'reh' is the end of reheating and 'eq' is the era of matter-radiation equality. Hence, using Eq. (1.60)

$$\frac{k}{a_0 H_0} = e^{-N} \frac{a_{\text{end}}}{a_{\text{reh}}} \frac{a_{\text{reh}}}{a_{\text{eq}}} \frac{a_{\text{eq}}}{a_0} \frac{H_k}{H_{\text{eq}}} \frac{H_{\text{eq}}}{H_0} . \tag{1.62}$$

Using the relations $\rho_{\text{m}} \propto a^{-3}$ and $\rho_{\text{r}} \propto a^{-4}$ for the matter and radiation dominated epochs respectively, one finds [31]

$$\begin{aligned} N(k) &= -\ln\left(\frac{k}{a_0 H_0}\right) + \frac{1}{3}\ln\left(\frac{\rho_{\text{reh}}}{\rho_{\text{end}}}\right) + \frac{1}{4}\ln\left(\frac{\rho_{\text{eq}}}{\rho_{\text{reh}}}\right) \\ &\quad + \ln\left(\frac{H_k}{H_{\text{eq}}}\right) + \ln\left(\frac{a_{\text{eq}} H_{\text{eq}}}{a_0 H_0}\right) . \end{aligned} \tag{1.63}$$

An upper bound to the number of e-foldings before the end of inflation that cosmological scales exited the horizon is given by maximizing Eq. (1.63). Assuming instant reheating ($\rho_{\text{reh}} = \rho_{\text{end}}$) and substituting in measured values [31]; $a_{\text{eq}} H_{\text{eq}}/a_0 H_0 = 219\Omega_0 h$, $H_{\text{eq}} = 5.25 \times 10^6 h^3 \Omega_0^2 H_0$, $H_0 = 1.75 \times 10^{-61} h m_{\text{Pl}}$, $h \approx 0.7$ and using the slow-roll approximation given by Eq. (1.28), one can write [31]

$$N_{\text{cos}} = 68.5 + \frac{1}{4}\ln\frac{V_0}{m_{\text{Pl}}^4} . \tag{1.64}$$

Using Eq. (1.28) and Eq. (1.31), the power spectrum given by Eq. (1.46) can be rewritten in terms of the potential slow-roll parameters as [28]

$$\mathcal{P}_{\mathcal{R}}(k_0) \approx \frac{8V_0}{3m_{\text{Pl}}^4} \frac{1}{\epsilon_{\text{V}}} . \tag{1.65}$$

Using Eq. (1.52) this then gives [31]

$$N_{\text{cos}} \approx 63.3 + \frac{1}{4}\ln\epsilon_{\text{V}} . \tag{1.66}$$

The potential slow-roll parameter ϵ_{V} is expected to be small for most of the duration of inflation except towards the end. Eq. (1.66), therefore, provides an estimate for an upper bound on the number of e-foldings of inflation corresponding to observable scales:

$$N_{\text{cos}} \approx 63 . \tag{1.67}$$

Relaxing the assumption of instant reheating reduces $N_{\rm cos}$. However, the physics of reheating is poorly understood. We use this calculation to estimate the number of e-foldings of inflation for many inflationary models in chapter 5.

In this chapter we have reviewed the 'standard cosmology' with a brief description of the Big Bang and inflation theory. We have outline slow-roll inflation and the Hamilton-Jacobi formalism which we will use in chapter 5 to constrain models of inflation. The tightest constraints on the observable quantities outlined in Sec. 1.10 come from WMAP and large-scale structure as discussed. We allude to the possibility that these observational constraints may be significantly weakened if some assumptions about the form of the power spectrum are relaxed. In particular, on scales much smaller than those probed by current observations, large departures from the observed value of the power spectrum given by Eq. (1.52) may be possible. This may result in significant formation of small-scale structure such as primordial black holes and ultra compact minihalos. In this thesis we discuss the possible formation of these objects along with constraints on models of inflation. We begin the next chapter by reviewing cosmological perturbation theory which is essential in relating perturbations from inflation to density perturbations.

Chapter 2

Primordial Perturbations

2.1 Introduction

The dynamics of an expanding FRW spacetime can be neatly described by the Einstein equations (see Sec. 1.2). This provides a mathematical description for the evolution of an homogeneous and isotropic Universe from the Big Bang followed by radiation domination through to matter domination. Inflation was proposed as a way of solving key problems with the Big Bang, notably, the generation of homogeneity on extremely large-scales. However, it is evident that our Universe is not exactly homogeneous or isotropic. Rather there exist anisotropies as observed in the CMB and inhomogeneities such as galaxy clusters, voids, solar systems and planets. Any successful theory of the early Universe must explain how these inhomogeneities came about. Whilst there are several competing theories [33, 34, 35], inflation has proved to be the most popular. This is largely because it predicts the generation of inhomogeneities or primordial perturbations in the early Universe .

According to quantum field theory empty space is not actually empty but filled with virtual particles and anti-particle pairs. The pairs appear and almost instantaneously annihilate setting up quantum fluctuations of the spacetime that they fill. These fluctuations can be thought of as physical waves or fields. On macroscopic scales these fluctuations average to zero and so we perceive space to be an empty vacuum. Inflation is defined as a period of accelerating expansion driven by an inflaton field (see

Sec. 1.6). During inflation, a small patch of the Universe filled by quantum vacuum fluctuations of the inflaton field is stretched to beyond the Hubble radius. In the process the quantum fluctuations become classical perturbations. As the space expands, new vacuum fluctuations are also generated and stretched creating classical perturbations of all wavelengths. These classical perturbations in the field generate fluctuations in the curvature of spacetime known as primordial curvature perturbations. These curvature perturbations, in turn, seed perturbations in the matter density of the Universe. Through gravitational infall, these regions eventually go on to form the structure that we observe in the Universe today.

In the following chapter we briefly review cosmological linear perturbation theory. Much of this topic was introduced and developed by Bardeen [36]. We concentrate on scalar perturbations as these are largely responsible for structure formation in the Universe. For a more detailed description of linear perturbation theory there are numerous reviews [28, 37, 38, 39].

2.2   Metric perturbations

In order to produce a mathematical description of perturbations in an expanding Universe we start with a spatially homogeneous and isotropic FRW background spacetime metric $g_{\mu\nu}^{(0)}$. First order perturbations $\delta g_{\mu\nu}$ are introduced to this background so that

$$g_{\mu\nu} = g_{\mu\nu}^{(0)} + \delta g_{\mu\nu} \ , \tag{2.1}$$

where

$$g_{\mu\nu}^{(0)} = a^2(\tau) \begin{pmatrix} -1 & 0 \\ 0 & \gamma_{ij} \end{pmatrix} \ , \tag{2.2}$$

and where $\gamma_{ij} = \mathrm{diag}(1,1,1)$ is the spatially flat Euclidean metric. The unperturbed background FRW line element in Cartesian coordinates is therefore given by

$$\mathrm{d}s^2 = a^2(\tau)(-\mathrm{d}\tau^2 + \mathrm{d}x^2 + \mathrm{d}y^2 + \mathrm{d}z^2) \ , \tag{2.3}$$

The most general form for the perturbed metric line element is

$$\mathrm{d}s^2 = a^2(\tau)\{-(1+2\phi)\mathrm{d}\tau^2 + 2B_i\mathrm{d}\tau\mathrm{d}x^i + [(1-2\psi)\delta_{ij} + 2E_{ij}]\mathrm{d}x^i\mathrm{d}x^j\} \ , \tag{2.4}$$

where ϕ and ψ are scalar perturbations, B_i is a vector perturbation and E_{ij} a tensor perturbation. One can decompose any vector or tensor quantity into components, which, in linear theory, evolve independently of each other. In the following, ';' represents covariant spatial derivatives with respect to γ_{ij}. Hence, one can decompose any vector perturbation X_i into the sum of two components: a component constructed from the gradient of a scalar quantity, $A_{;i}$, and so is necessarily curl-free, $A_{;[ij]} = 0$, and a component constructed from an intrinsically vector quantity which we notate $X_i^{(\mathrm{v})}$ and is therefore divergence-free $X_{i;j}^{(\mathrm{v})} = 0$. In an alternative notation commonly used in the literature, any vector quantity can be decomposed as

$$X_i = X_i^{(\|)} + X_i^{(\perp)} = A_{;i} + X_i^{(\mathrm{v})} \ . \tag{2.5}$$

The parallel and perpendicular notation arises because in Fourier space, $X_i^{(\|)}$ is identified as a component which is parallel (or longitudinal) to the comoving wavevector $\mathbf{k}$. Similarly, $X_i^{(\perp)}$ is a component which is perpendicular (or transverse) to the $\mathbf{k}$ direction.

From Eq. (2.4), one can apply this decomposition to the metric variable B_i:

$$B_i = B_i^{(\|)} + B_i^{(\perp)} = B_{;i} + B_i^{(\mathrm{v})} \ , \tag{2.6}$$

where the curl-free (parallel) part is given by $B_{;i}$ and is written as the gradient of a scalar potential B, and the divergence-free (perpendicular) part is written as $B_i^{(\mathrm{v})}$. We follow closely the notation used by Liddle and Lyth [28] and perform a Fourier transformation. The curl-free part can then be written as

$$B_i^{(\|)} = -\frac{ik_i}{k} B_{\mathbf{k}} \ , \tag{2.7}$$

where $B_{\mathbf{k}}$ is the amplitude of the scalar potential B for a given wave vector $\mathbf{k}$. The divergence-free property of $B_i^{(\perp)}$ can be written as

$$k_i B_i^{(\perp)} = 0 \ . \tag{2.8}$$

Similar to the vector case, the tensor metric variable E_{ij} can be decomposed. This results in a scalar constructed curl-free component, an intrinsically vector divergence-free component and an intrinsically tensor divergence-free component. Again, in

Fourier space, one can decompose and write the independent components of E_{ij} as

$$E_{ij}^{(\parallel)} = \left(-\frac{k_i k_j}{k^2} + \frac{1}{3}\delta_{ij}\right) E_{\mathbf{k}} \,, \tag{2.9}$$

$$k_i E_i^{(\perp)} = 0 \,, \tag{2.10}$$

$$k_i E_{ij}^{(\mathrm{T})} = 0 \,, \tag{2.11}$$

where $E_{\mathbf{k}}$ is the amplitude of the scalar potential E for a given wave vector $\mathbf{k}$.

This decomposition proves to be very useful when investigating perturbations by reducing the number of free parameters. One can isolate intrinsically tensor perturbations to investigate gravitational wave production or intrinsically vector perturbations to study vorticity. In the following, we consider only first order scalar perturbations in order to investigate curvature perturbations produced during inflation.

2.2.1 Coordinate change

The introduction of perturbations to a homogeneous flat FRW background leads to ambiguity in the choice of coordinates. In general relativity there is no preferred coordinate system, so to obtain useful results that can be compared to existing literature, we must be able to transform from one coordinate system to another. To do this it is usual to introduce a first order change in the coordinates:

$$\tilde{\tau} = \tau + \xi^0 \,, \qquad\qquad \tilde{x}^i = x^i + \xi^i \,, \tag{2.12}$$

where a tilde denotes a new coordinate system and $\xi^0 = \xi^0(\tau, x^i)$ and $\xi^i = \xi^i(\tau, x^i)$ are small arbitrary scalar and vector functions respectively. As discussed previously, we can decompose $\xi^i = \xi^i(\tau, x^i)$ into the sum of curl-free and divergence-free components:

$$\xi^i = \xi^{i(\parallel)} + \xi^{i(\perp)} = \xi^i_; + \xi^{i(\mathrm{v})} \,. \tag{2.13}$$

Writing in terms of a Fourier expansion in comoving wave numbers, k, the curl-free component is

$$\xi^{i(\parallel)} = -\frac{ik^i}{k}\xi_{\mathbf{k}} \,. \tag{2.14}$$

and the divergence-free component is $k^i \xi^{i(\perp)} = 0$. Perturbations to the flat FRW background are, therefore, given by the following 4-vector coordinate shift

$$\xi^\alpha \equiv \left(\xi^0, (\xi^i_; + \xi^{i(\mathrm{v})})\right) \,. \tag{2.15}$$

We now consider the effect of a first order change of coordinates on the metric line element, Eq. (2.4), and obtain expressions for the metric variables in any new coordinate system indicated by a tilde. We begin by considering a change in coordinates for an arbitrary scalar quantity q:

$$\widetilde{q}(\widetilde{x}^{\alpha}) = \widetilde{q}(x^{\alpha} + \xi^{\alpha}) \approx \widetilde{q}(x^{\alpha}) + q_{;\alpha}\xi^{\alpha} \ , \tag{2.16}$$

where we have used the Taylor approximation,

$$f(x + a) \approx f(x) + af'(x) \ . \tag{2.17}$$

For any scalar quantity

$$\widetilde{q}(\widetilde{x}^{\alpha}) = q(x^{\alpha}) \ . \tag{2.18}$$

Equating this with Eq. (2.16), the resulting scalar quantity in the new coordinate frame is

$$\widetilde{q}(x^{\alpha}) = q(x^{\alpha}) - q_{;\alpha}\xi^{\alpha} \ . \tag{2.19}$$

Omitting the coordinate labels, the perturbation in a scalar quantity in a new coordinate reference frame is given in terms of the old reference frame by

$$\widetilde{\delta q} = \delta q - q_{;\alpha}\xi^{\alpha} \ . \tag{2.20}$$

Similarly for vector quantities, V_{β}, a change in coordinates results in the following transformation

$$\widetilde{V}_{\beta}(\widetilde{x}^{\beta}) = \widetilde{V}_{\beta}(x^{\beta} + \xi^{\beta}) \approx \widetilde{V}_{\beta}(x^{\beta}) + V_{\beta;\eta}\xi^{\eta} \ . \tag{2.21}$$

Also for vector quantities

$$\widetilde{V}_{\beta}(\widetilde{x}^{\beta}) = \frac{\partial x^{\eta}}{\partial \widetilde{x}^{\beta}}V_{\eta}(x^{\beta}) = (\delta^{\eta}_{\beta} - \xi^{\eta}_{;\beta})V_{\eta}(x^{\beta}) = V_{\beta}(x^{\beta}) - V_{\eta}\xi^{\eta}_{;\beta} \ . \tag{2.22}$$

Equating with Eq. (2.21) gives

$$\widetilde{V}_{\beta}(x^{\beta}) = V_{\beta}(x^{\beta}) - V_{\eta}\xi^{\eta}_{;\beta} - V_{\beta;\eta}\xi^{\eta} \ , \tag{2.23}$$

hence,

$$\widetilde{\delta V}_{\beta} = \delta V_{\beta} - V_{\eta}\xi^{\eta}_{;\beta} - V_{\beta;\eta}\xi^{\eta} \ . \tag{2.24}$$

For tensor quantities, $g_{\mu\nu}$, a change in coordinates results in the following transformation

$$\widetilde{g}_{\mu\nu}(\widetilde{x}^{\gamma}) = \widetilde{g}_{\mu\nu}(x^{\gamma} + \xi^{\gamma}) \approx \widetilde{g}_{\mu\nu}(x^{\gamma}) + g_{\mu\nu;\gamma}\xi^{\gamma} \ , \tag{2.25}$$

and

$$\widetilde{g}_{\mu\nu}(\tilde{x}^{\gamma}) = \frac{\partial x^{\lambda}}{\partial \tilde{x}^{\mu}}\frac{\partial x^{\rho}}{\partial \tilde{x}^{\nu}}g_{\lambda\rho}(x^{\gamma}) = (\delta_{\mu}^{\lambda} - \xi_{;\mu}^{\lambda})(\delta_{\nu}^{\rho} - \xi_{;\nu}^{\rho})g_{\lambda\rho}(x^{\gamma}) \ , \qquad (2.26)$$

so that to first order in perturbations

$$\widetilde{g}_{\mu\nu}(\tilde{x}^{\gamma}) = (\delta_{\mu}^{\lambda}\delta_{\nu}^{\rho} - \xi_{;\mu}^{\lambda}\delta_{\nu}^{\rho} - \xi_{;\nu}^{\rho}\delta_{\mu}^{\lambda})g_{\lambda\rho}(x^{\gamma}) = g_{\mu\nu}(x^{\gamma}) - g_{\lambda\nu}\xi_{;\mu}^{\lambda} - g_{\mu\rho}\xi_{;\nu}^{\rho} \ . \qquad (2.27)$$

Equating this with Eq. (2.25) and changing dummy indices gives

$$\widetilde{\delta g}_{\mu\nu} = \delta g_{\mu\nu} - g_{\gamma\nu}\xi_{;\mu}^{\gamma} - g_{\mu\gamma}\xi_{;\nu}^{\gamma} - g_{\mu\nu;\gamma}\xi^{\gamma} \ . \qquad (2.28)$$

For perturbations about a FRW spacetime we can deal with the 00, $0i$ and ij components separately (n.b. on a flat space background $\xi_{;i} \equiv \xi_{;}^{i}$)

$$\widetilde{\delta g}_{00} = \delta g_{00} + 2a(a\xi^{0})' \ , \qquad (2.29)$$

$$\widetilde{\delta g}_{0i} = \delta g_{0i} - a^{2}(\xi'_{;i} + \xi^{i(\mathrm{v})'}) + a^{2}\xi_{;i}^{0} \ , \qquad (2.30)$$

$$\widetilde{\delta g}_{ij} = \delta g_{ij} - 2aa'\xi^{0}\delta_{ij} - a^{2}[\xi_{;j}^{i(\mathrm{v})} + \xi_{;i}^{j(\mathrm{v})} + 2\xi_{;ij}] \ , \qquad (2.31)$$

where primes are derivatives with respect to conformal time $\partial/\partial\tau$. By inspection of the general perturbed metric, Eq. (2.4), we see that

$$\delta g_{00} = -2a^{2}\phi \ . \qquad (2.32)$$

Using Eq. (2.29), the coordinate transformation relation for the metric variable ϕ is

$$\tilde{\phi} = \phi - \xi^{0'} - \mathcal{H}\xi^{0} \ , \qquad (2.33)$$

where $\mathcal{H} = aH = a'/a$ is the conformal Hubble parameter. By inspection of Eq. (2.4)

$$\delta g_{0i} = a^{2}B_{i} \ . \qquad (2.34)$$

Using Eq. (2.30) the coordinate transformation relation for the metric variable B_{i} is given by

$$\widetilde{B}_{i} = B_{i} - (\xi'_{;i} + \xi^{i(\mathrm{v})'}) + \xi_{;i}^{0} \ . \qquad (2.35)$$

Similarly, by inspection of Eq. (2.4),

$$\delta g_{ij} = a^{2}[-2\psi\delta_{ij} + 2E_{ij}] \ . \qquad (2.36)$$

Using Eq. (2.31), ignoring divergence-free vector components, we can split the equations into two parts: the first dependent on δ_{ij}, and the other dependent on '$_{;ij}$'. The part dependent on δ_{ij} yields

$$\widetilde{\psi} = \psi + \mathcal{H}\xi^0 \, , \tag{2.37}$$

and the part dependent on '$_{;ij}$' gives

$$\widetilde{E}_{ij} = E_{ij} - \xi_{;ij} \, . \tag{2.38}$$

The general metric line element, given by Eq. (2.4), under a coordinate transformation can be written

$$\mathrm{d}s^2 = a^2(\mathrm{d}\tilde{\tau})\{-(1 + 2\tilde{\phi})\mathrm{d}\tilde{\tau}^2 + 2\tilde{B}_i\mathrm{d}\tilde{\tau}\mathrm{d}\tilde{x}^i + [(1 - 2\tilde{\psi})\delta_{ij} + 2\tilde{E}_{ij}]\mathrm{d}\tilde{x}^i\mathrm{d}\tilde{x}^j\} \, . \tag{2.39}$$

Using Eq. (2.7), Eq. (2.9) and Eq. (2.14) one can perform an expansion in Fourier modes of Eq. (2.33), Eq. (2.35), Eq. (2.37) and Eq. (2.38). Ignoring all divergence-free vector or tensor components, the resulting scalar metric perturbations in any new coordinate frame are given by

$$\tilde{\phi} = \phi - \xi^{0\prime} - \mathcal{H}\xi^0 \, , \tag{2.40}$$

$$\tilde{B} = B - \xi' + k\xi^0 \, , \tag{2.41}$$

$$\tilde{\psi} = \psi + \mathcal{H}\xi^0 \, , \tag{2.42}$$

$$\tilde{E} = E - k\xi \tag{2.43}$$

where we have omitted the subscript **k** labels.

In order to obtain useful information about the evolution of matter and radiation perturbations, we now consider the effects of a coordinate transformation on the density and velocity perturbations of a single fluid within this perturbed FRW background. For a perfect fluid with density ρ, pressure P and 4-velocity u^μ, the energy-momentum tensor is given by

$$T^\mu_\nu = (\rho + P)u^\mu u_\nu + P\delta^\mu_\nu + \pi^\mu_\nu \, , \tag{2.44}$$

where π^μ_ν is the anisotropic stress tensor and the scalar quantity ρ can be written in terms of a background homogeneous part ρ_0 plus a small density perturbation

$$\rho(\tau, x^i) = \rho_0(\tau) + \delta\rho(\tau, \mathrm{x}^i) \, . \tag{2.45}$$

The perturbation in the density then transforms under a coordinate change according to Eq. (2.19)

$$\widetilde{\delta\rho} = \delta\rho - \rho'\xi^0 \ . \tag{2.46}$$

Similarly, the inflaton field φ can be decomposed into a background part and a perturbed part:

$$\varphi(\tau) = \varphi_0(\tau) + \delta\varphi(\tau, \mathrm{x}^i) \ , \tag{2.47}$$

where the inflaton perturbation transforms as

$$\widetilde{\delta\varphi} = \delta\varphi - \varphi'\xi^0 \ . \tag{2.48}$$

Using the energy conservation equation, $\partial_\mu T^{\mu 0} = 0$, one can obtain, from Eq. (2.44), the continuity equation

$$\rho' = -3\mathcal{H}(\rho + P) \ . \tag{2.49}$$

Substituting this into Eq. (2.46) gives

$$\tilde{\delta} = \delta + 3\mathcal{H}(1 + w)\xi^0 \ , \tag{2.50}$$

where $\omega \equiv P/\rho$ is the equation of state and δ is the density contrast which, using Eq. (2.45), is defined as

$$\delta = \frac{\delta\rho}{\rho} \equiv \frac{\rho - \rho_0}{\rho_0} \ . \tag{2.51}$$

The 3-velocity, v^i, given by the spatial part of the 4-velocity, u^μ, can be decomposed into curl-free and divergence-free components, as described previously. The curl-free part $v^{i(\|)}$ can be expanded into Fourier wave modes:

$$v^{i(\|)} = -\frac{ik^i}{k}V_{\mathbf{k}} \ , \tag{2.52}$$

where $V_{\mathbf{k}}$ is the amplitude of the velocity potential (or peculiar velocity) for a given wave vector $\mathbf{k}$. Since the flow is irrotational for scalar perturbations [38, 28], we need only consider the curl-free part. Using Eq. (2.12) and omitting the subscript $\mathbf{k}$ labels, the velocity potential transforms as

$$\tilde{V} = V + \xi' \ . \tag{2.53}$$

Eqs. (2.40)-(2.43) along with Eq. (2.50) and Eq. (2.53) are important equations which allow us to work in any convenient coordinate system and transform to another coordinate system by choosing appropriate values for ξ and ξ^0. This is known as a gauge transformation.

2.3   Choice of gauge

For an unperturbed Universe the comoving gauge represents a unique choice of coordinates. Here, a comoving observer is simply one which is 'carried' by the expansion of the Universe. In this gauge the threading (hypersurfaces of constant spatial coordinates) of comoving observers are free-falling (vanishing 4-velocity) and the slicing (hypersurfaces of constant time) is orthogonal to the threading [28]. As these properties are true everywhere in an unperturbed Universe, the comoving observer is a preferred coordinate system. For a perturbed Universe, however, there exists no preferred coordinate system. The introduction of perturbations means that different observers in the Universe will measure different properties. One must therefore work with equations in a particular coordinate system and require that the equations must reduce to those of flat space in the limit of vanishing perturbations. A particular set of coordinates which satisfies this condition is called a **gauge** [36]. Alternatively, one may work in a coordinate system in which quantities are gauge-invariant by construction (this is discussed further in Sec. 2.4).

The choice of gauge is equivalent to fixing ξ and ξ^0 and is largely dependent on the most convenient choice for any given problem. Gauge choice is only relevant for perturbations outside the horizon. On sub-horizon scales the differences between gauges becomes negligible. There are several commonly used gauges in the literature but we focus on two in particular; the conformal Newtonian gauge, where the evolution equations take on a particularly simple form, and the comoving total-matter gauge which is a specific example of a comoving gauge.

2.3.1   Conformal Newtonian gauge

The conformal Newtonian or Longitudinal gauge [36, 40] is a convenient and mathematically simple choice of gauge. In this gauge, fixed time hypersurfaces (slicing) are orthogonal to fixed spatial hypersurfaces (threading). Also, anisotropy in the expansion rate on spatial hypersurfaces (shear) vanishes. The metric line element in the conformal Newtonian gauge is given by setting the following metric variables in Eq. (2.39)

to zero:

$$\tilde{B} = \tilde{E} = 0 \; . \tag{2.54}$$

The metric line element in the conformal Newtonian gauge is then given by

$$ds^2 = a^2(\tau) \left[-(1 + 2\phi_{\mathrm{N}})d\tau^2 + (1 - 2\psi_{\mathrm{N}})\delta_{ij}dx^i dx^j \right] \; , \tag{2.55}$$

where a subscript 'N' denotes the conformal Newtonian gauge. In this gauge the metric variables coincide with the gauge-invariant Bardeen potentials [36] $\phi_{\mathrm{N}} \equiv \Phi_{\mathrm{A}}$ and $\psi_{\mathrm{N}} \equiv -\Psi_{\mathrm{H}}$.

For a fluid with energy density ρ, pressure P and four velocity u^μ, the components of the energy-momentum tensor are given by Eq. (2.44). The Einstein equations, given by Eq. (1.6), can be solved to first order in perturbations for a radiation dominated Universe ($\omega = 1/3$) giving the energy and momentum constraints as

$$-k^2\psi_{\mathrm{N}} - 3\mathcal{H}\psi_{\mathrm{N}}' - 3\mathcal{H}^2\phi_{\mathrm{N}} = \frac{3}{2}\mathcal{H}^2\delta_{\mathrm{N}} \; , \tag{2.56}$$

$$-k(\psi_{\mathrm{N}}' + \mathcal{H}\phi_{\mathrm{N}}) = \frac{3}{2}\mathcal{H}^2(1 + \omega)V_{\mathrm{N}} \; , \tag{2.57}$$

where we have used the background solution to the Einstein equations:

$$\mathcal{H}^2 - \mathcal{H}' = 4\pi G a^2(\rho + P) \equiv \frac{3}{2}\mathcal{H}^2(1 + \omega) \; . \tag{2.58}$$

Substituting Eq. (2.56) into Eq. (2.57), the density contrast for modes well inside the horizon ($k \gg \mathcal{H}$) is given by the familiar Newtonian Poisson equation:

$$\delta = -\frac{2}{3}\left(\frac{k}{\mathcal{H}}\right)^2 \psi \; . \tag{2.59}$$

The spatial component of the Einstein equations is

$$\psi_{\mathrm{N}}'' + 2\mathcal{H}\psi_{\mathrm{N}}' + \mathcal{H}\phi_{\mathrm{N}}' + (2\mathcal{H}' + \mathcal{H}^2)\phi_{\mathrm{N}} = 4\pi G a^2(\delta P_{\mathrm{N}} - \frac{2}{3}k^2\Pi_{\mathrm{N}}) \; , \tag{2.60}$$

where Π_{N} is the scalar part of the decomposed anisotropic stress tensor. The pressure perturbation δP_{N} can be split into an adiabatic and a non-adiabatic part δP_{nad}:

$$\delta P_{\mathrm{N}} = \frac{P'}{\rho'}\delta\rho + \delta P_{\mathrm{nad}} \; . \tag{2.61}$$

The spatial off-diagonal Einstein equation is

$$k^2(\psi_{\mathrm{N}} - \phi_{\mathrm{N}}) = 3\mathcal{H}^2(1 + \omega)\Pi_{\mathrm{N}} \; . \tag{2.62}$$

For isotropic fluids $\Pi_N = 0$ and so $\psi_N = \phi_N$. This implies that in the conformal Newtonian gauge, ϕ_N corresponds to the familiar Newtonian gravitational potential.

Finally the continuity and Euler equations are given respectively by

$$\frac{3}{4}\delta'_N = kV_N + 3\psi'_N, \tag{2.63}$$

$$V'_N = -\frac{1}{4}k\delta_N - k\phi_N + \frac{2}{3}k\Pi_N. \tag{2.64}$$

2.3.2 Comoving orthogonal gauge

A natural choice of gauge is that of a comoving observer. Comoving gauges are a class of gauges in which an observer moves with the expansion and any perturbations within the Universe. A subclass of this type of gauge is called the comoving orthogonal gauge in which spatial coordinates are chosen so that the 3-velocity of a single fluid vanishes, $\tilde{v}^i = 0$. Orthogonality of the constant time hypersurfaces to the 4-velocity, u^μ, demands that the momentum vanishes also. To show this the 4-velocity is written as

$$u^\mu = \frac{d\tau}{dt}\frac{dx^\mu}{d\tau} = \frac{1}{a}(1, v^i). \tag{2.65}$$

Using $u_\mu \equiv g_{\mu\nu}u^\nu$ and Eq. (2.4) gives

$$u_\mu = a\left[-1, (\tilde{B}_i^{(\parallel)} + \tilde{v}_i^{(\parallel)})\right], \tag{2.66}$$

to first order in perturbations. From Eq. (2.65) a vanishing 3-velocity and orthogonality of the constant time hypersurfaces to the 4-velocity then implies

$$u^\mu = u_\mu = 0. \tag{2.67}$$

From Eq. (2.66) along with Eq. (2.7) and Eq. (2.52), the comoving orthogonal gauge is then given by setting

$$\tilde{B} + \tilde{V} = 0. \tag{2.68}$$

2.3.3 Comoving total matter gauge

A convenient multi-fluid extension to the comoving orthogonal gauge, as described above, is to use the rest frame of the total matter where the total 4-momentum is orthogonal to the constant time hypersurfaces [39, 28]. We move to the Total-Matter

gauge (TM) by displacing the slicing of the conformal Newtonian gauge so that it becomes comoving but leave the threading and the spatial coordinates unchanged. This is done by imposing the following conditions: from Eq. (2.53), we see that in order to prevent a relabelling of the threading we must set $\xi = 0$. Also, the condition for a comoving slicing given above is $\tilde{B} + \tilde{V} = 0$. From Eq. (2.41) and Eq. (2.53), we can therefore write

$$\tilde{B}_{\mathrm{TM}} + \tilde{V}_{\mathrm{TM}} = B + V + k\xi^0 = 0 , \tag{2.69}$$

Hence,

$$\xi^0 = -\frac{1}{k}(B + V) . \tag{2.70}$$

The conditions imposed in order to perform a gauge transformation from the conformal Newtonian gauge to the Total-Matter gauge are

$$\xi = 0, \qquad \xi^0 = -\frac{V_{\mathrm{N}}}{k} . \tag{2.71}$$

Substituting Eq. (2.71) into Eqs. (2.40)-(2.43), the transformation equations are then given by the following relations:

$$\tilde{\phi}_{\mathrm{TM}} = \phi_{\mathrm{N}} + \frac{\mathcal{H}}{k}V_{\mathrm{N}} , \tag{2.72}$$

$$\tilde{B}_{\mathrm{TM}} = B_{\mathrm{N}} - V_{\mathrm{N}} = -V_{\mathrm{N}} , \tag{2.73}$$

$$\mathcal{R} \equiv \tilde{\psi}_{\mathrm{TM}} = \psi_{\mathrm{N}} - \frac{\mathcal{H}}{k}V_{\mathrm{N}} , \tag{2.74}$$

$$\tilde{E}_{\mathrm{TM}} = E_{\mathrm{N}} = 0 . \tag{2.75}$$

Substituting Eq. (2.71) into Eq. (2.50) and Eq. (2.53), the density and velocity potential transformation equations are

$$\tilde{\delta}_{\mathrm{TM}} = \delta_{\mathrm{N}} - \frac{3\mathcal{H}V_{\mathrm{N}}}{k}(1 + \omega) , \tag{2.76}$$

$$\tilde{V}_{\mathrm{TM}} = V_{\mathrm{N}} . \tag{2.77}$$

2.3.4 Uniform curvature gauge

The uniform curvature gauge [39, 41] is one in which spatial hypersurfaces are chosen so that the spatial part of the metric perturbation is zero. This requires $\tilde{\psi} = \tilde{E} = 0$. Eq. (2.42) and Eq. (2.43) then gives

$$\xi = \frac{E}{k} , \qquad \xi^0 = -\frac{\psi}{\mathcal{H}} . \tag{2.78}$$

In any comoving gauge $\widetilde{\delta\varphi} = 0$ [42]. From Eq. (2.48) one then finds for the comoving gauge:

$$\xi^0 = \frac{\delta\varphi}{\varphi'} \ . \tag{2.79}$$

Using Eq. (2.42) one can then write

$$\mathcal{R} \equiv \tilde{\psi}_{\text{com}} = \psi + \mathcal{H}\frac{\delta\varphi}{\varphi'} \ , \tag{2.80}$$

where the subscript 'com' denotes the comoving gauge. Here ψ and $\delta\varphi$ can be defined in any particular gauge. From Eq. (2.80) it is evident that $\mathcal{R}$ represents the gravitational potential on comoving hypersurfaces

$$\mathcal{R} = \psi|_{\delta\varphi=0} \ . \tag{2.81}$$

Substituting Eq. (2.78) into Eq. (2.48), perturbations in the inflaton field in the uniform curvature gauge are given by

$$\widetilde{\delta\varphi}_{\text{uniform}} = \delta\varphi + \varphi'\frac{\psi}{\mathcal{H}} \ , \tag{2.82}$$

where a subscript 'uniform' denotes the uniform curvature gauge. Using Eq. (2.81) perturbations in the inflaton field on uniform curvature hypersurfaces in terms of the comoving curvature perturbation are given by

$$\widetilde{\delta\varphi}_{\text{uniform}} = \frac{\dot{\varphi}}{H}\mathcal{R} \ . \tag{2.83}$$

2.4   Curvature perturbation

The spatial metric tensor at a given fixed conformal time slicing τ is given by the coefficient of $dx^i dx^j$ in Eq. (2.4). The spatial curvature scalar $R^{(3)} = g^{ij}R_{ij}$ is given by a contraction of the spatial part of the Ricci tensor R_{ij} with the spatial part of the metric. Similarly the spatial Ricci tensor is constructed from the spatial Riemann curvature tensor $R_{ij} \equiv R^k_{ikj}$ where the Riemann tensor is defined as

$$R^i_{jkm} = \partial_k\Gamma^i_{jm} - \partial_m\Gamma^i_{jk} + \Gamma^i_{nk}\Gamma^n_{jm} - \Gamma^i_{nm}\Gamma^n_{jk} \tag{2.84}$$

and the Christoffel symbols are dependent on the metric:

$$\Gamma^i_{jk} = \frac{1}{2}g^{mi}\left(\partial_k g_{mj} + \partial_j g_{mk} - \partial_m g_{jk}\right) \ . \tag{2.85}$$

The resulting spatial curvature on constant conformal time hypersurfaces for a flat FRW background Universe is [36, 39]

$$R^{(3)} = -4\frac{k^2}{a^2}\psi \; . \tag{2.86}$$

We recall that ψ is a gauge dependent variable which under a change of coordinates transforms according to Eq. (2.42). In any comoving gauge it can be defined by Eq. (2.80). We see from Eq. (2.80) that although $\mathcal{R}$ is defined as the curvature perturbation in the comoving gauge, it can be constructed from variables which have not yet been defined in any particular gauge. As such $\mathcal{R}$ is often rather confusingly called a gauge-invariant variable. To put it more accurately, $\mathcal{R}$ is a gauge-dependent variable (comoving gauge) which is constructed from gauge-invariant quantities and so can be described as *gauge-invariant by construction* [42].

We now wish to relate comoving curvature perturbations to metric perturbations in the conformal Newtonian gauge. Using Eq. (2.57) along with Eq. (2.74) we can write

$$\mathcal{R} = \psi_{\mathrm{N}} + \frac{2}{3}\mathcal{H}\frac{\psi'_{\mathrm{N}} + \mathcal{H}\phi_{\mathrm{N}}}{(1+\omega)} \; . \tag{2.87}$$

For an isotropic fluid ($\psi_{\mathrm{N}} = \phi_{\mathrm{N}}$), Eq. (2.87) has the growing solution for any epoch where ω is constant [28, 42]:

$$\phi_{\mathrm{N}} = \frac{(3+3w)}{(5+3w)}\mathcal{R} \; . \tag{2.88}$$

It can be shown by taking the first derivative of Eq. (2.87) and using the Einstein gravitational field equations that the comoving curvature perturbation $\mathcal{R}$ is constant on superhorizon scales [29, 43]. This can also be shown without using the gravitational field equations by simply invoking the local conservation of energy-momentum [44] [1]. The constancy of $\mathcal{R}$ on superhorizon scales makes this quantity ideal as a tool for investigating perturbations generated by inflation.

Using Eq. (2.59) for an isotropic fluid we can find a relationship between the density contrast and the curvature perturbation on comoving hypersurfaces:

$$\delta(k,t) = -\frac{2(1+w)}{(5+3w)}\left(\frac{k}{aH}\right)^2 \mathcal{R}(k) \; . \tag{2.89}$$

---

[1]The curvature perturbation on comoving hypersurfaces is related to that on uniform density hypersurfaces by $\mathcal{R} = -\zeta$.

Using Eq. (1.45) the power spectrum of density perturbations is then simply related to the power spectrum of comoving curvature perturbations by

$$\mathcal{P}_\delta(k,t) = \frac{4(1+w)^2}{(5+3w)^2}\left(\frac{k}{aH}\right)^4 \mathcal{P}_\mathcal{R}(k) \;, \tag{2.90}$$

where

$$\mathcal{P}_\delta(k) \equiv \left(\frac{k^3}{2\pi^2}\right)\langle|\delta_{\mathbf{k}}|^2\rangle \;. \tag{2.91}$$

As we can see from Eq. (2.89), the density perturbation is proportional to the comoving curvature perturbation multiplied by $(k/aH)^2$. Previous authors [45, 28] have treated this by setting $k/aH = 1$ so that $\delta \propto \mathcal{R}$. This is an approximation which does not take into account the evolution of density perturbations prior to and post horizon crossing. It simply equates the value at horizon crossing ($k = aH$) to the entire evolution. As we shall later see, this has important consequences for the study of structure formation in the Universe. We therefore do not make this approximation but instead retain the time dependent $(k/aH)^2$ term in order to more accurately trace the evolution of density perturbations away from horizon crossing.

Fig. 2.1 shows the ratio of the density to the comoving curvature perturbation as a function of k/aH. The dotted red line shows the case where, for each comoving wavemode, prior to and post horizon crossing, the ratio $\delta/\mathcal{R}$ given by Eq. (2.89) is evaluated with the k/aH prefactor set to unity throughout its evolution. The dashed blue line shows the case where, for each comoving wavemode, the ratio $\delta/\mathcal{R}$ is evaluated using Eq. (2.89) retaining the time dependent $(k/aH)^2$ term.

From Fig. 2.1, retaining the $(k/aH)^2$ term in Eq. (2.89) results in an initial growth in the ratio $\delta/\mathcal{R}$ prior to horizon entry. However, as we see from Fig. 2.1, this ratio continues to grow quadratically as the perturbation evolves in the sub-horizon limit ($k \gg aH$). This would imply that density perturbations grow indefinitely at late times. Clearly Eq. (2.89) does not completely specify the evolution of the density perturbation on all scales. We therefore find a more accurate relationship between the density contrast and comoving curvature perturbation in the next section.
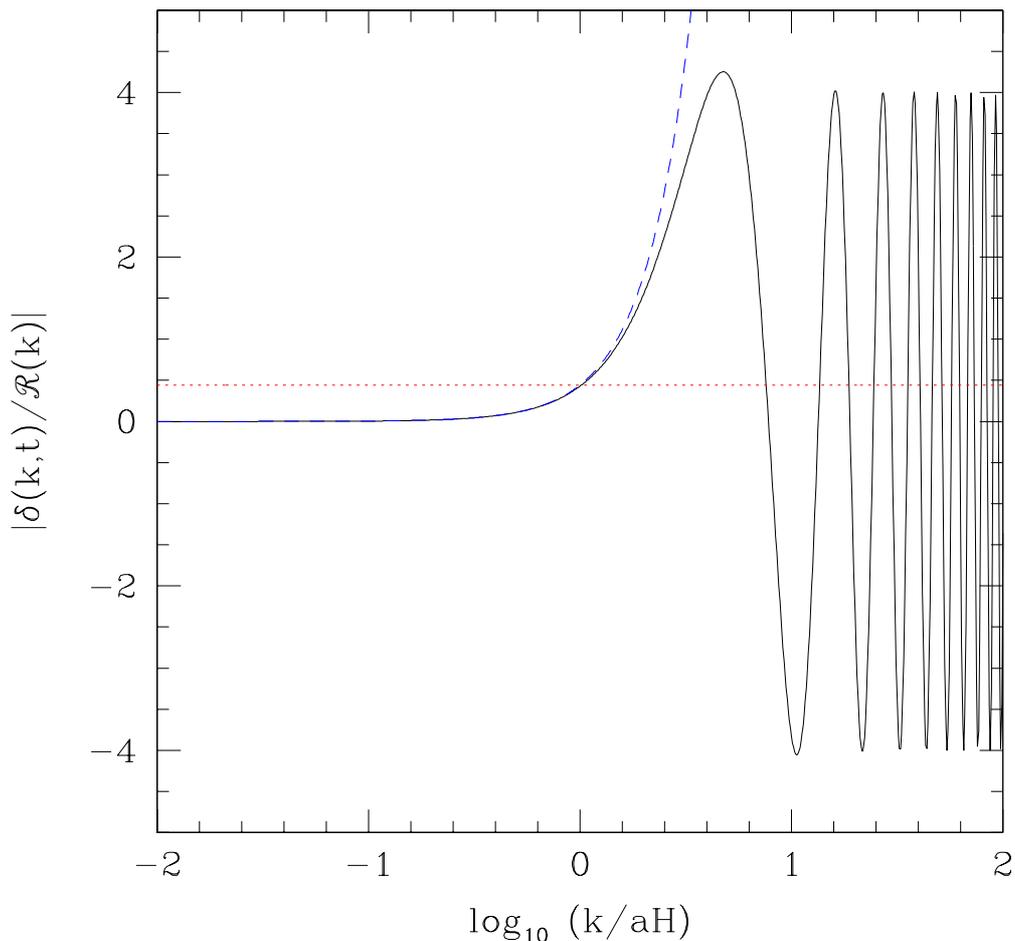
Figure 2.1: The ratio of the density perturbation to the comoving curvature perturbation as a function of k/aH. The dotted red line shows the relationship given by Eq. (2.89) evaluated with the k/aH prefactor set to unity. The blue dashed line shows the ratio given by Eq. (2.89) retaining the $(k/aH)^2$ term. The black solid line shows the ratio given by Eq. (2.100).

2.5 Density perturbation evolution

Green, Hofmann & Schwarz [46] studied the density contrast on sub-horizon scales. We use their analysis in order to derive expressions for primordial perturbations valid on all scales during radiation domination. We first work in the conformal Newtonian gauge using Eq. (2.55) and then perform a gauge transformation to the comoving total matter gauge as described in Sec. 2.3.3. Using Eq. (2.56) and Eq. (2.57) along with Eqs. (2.60)-(2.64) for an isotropic fluid in a radiation dominated Universe, we find the differential equation

$$\phi_{\mathrm{N}}'' + \frac{4}{x}\phi_{\mathrm{N}}' + \frac{1}{3}\phi_{\mathrm{N}} = 0 \ , \tag{2.92}$$

where $x \equiv k\tau = k/aH$ and we have redefined primes $' \equiv d/dx$. The solution to this equation can be written in terms of spherical Bessel functions:

$$\phi_{\mathrm{N}} = \psi_{\mathrm{N}} = C\frac{j_1(\kappa)}{\sqrt{3}\kappa} \; , \tag{2.93}$$

$$\delta_{\mathrm{N}} = \frac{2}{\sqrt{3}}\left(2\frac{j_1(\kappa)}{\kappa} - j_0(\kappa) - \kappa j_1(\kappa)\right)C \; , \tag{2.94}$$

$$V_{\mathrm{N}} = \left(j_1(\kappa) - \frac{\kappa}{2}j_0(\kappa)\right)C \; , \tag{2.95}$$

where C is a normalisation constant and $\kappa \equiv x/\sqrt{3}$. We normalise these expressions using the curvature perturbation on comoving hypersurfaces $\mathcal{R}$ which in terms of the gauge-dependent curvature perturbation, ψ, is defined by Eq. (2.74). Using Eq.(2.94) and Eq. (2.95) we find

$$\mathcal{R} = \frac{1}{2\sqrt{3}}j_0(\kappa)C \; . \tag{2.96}$$

Taking the superhorizon limit ($k \ll aH$) we find

$$\mathcal{R}(\kappa \ll 1) \approx \frac{1}{2\sqrt{3}}C \equiv \mathcal{R}_0 \; , \tag{2.97}$$

where $\mathcal{R}_0$ is defined as the value of $\mathcal{R}$ in the superhorizon limit. We substitute this normalisation into Eqs.(2.93)-(2.95) and using Eqs. (2.76)-(2.77) for a radiation dominated Universe, we find the density and velocity perturbations in the Total-Matter gauge:

$$\delta_{\mathrm{TM}} = -4\kappa j_1(\kappa)\mathcal{R}_0 \; , \tag{2.98}$$

$$V_{\mathrm{TM}} = -\sqrt{3}[\kappa j_0(\kappa) - 2j_1(\kappa)]\mathcal{R}_0 \; . \tag{2.99}$$

Substituting for $\kappa \equiv x/\sqrt{3}$ and normalising the comoving curvature perturbation in the super-horizon limit $\mathcal{R}_0$ to the value found by WMAP (given by $\mathcal{R}$ in Sec. 1.10), Eq. (2.98) can be rewritten as

$$\delta_{\mathrm{TM}} = -\frac{4}{\sqrt{3}}\left(\frac{k}{aH}\right)j_1(\frac{k}{\sqrt{3}aH})\mathcal{R} \; . \tag{2.100}$$

In the super-horizon limit $j_1(\kappa) \approx \sqrt{3}/9x$ and so

$$\delta_{\mathrm{TM}} \approx -\frac{4}{9}\left(\frac{k}{aH}\right)^2 \mathcal{R} \; , \tag{2.101}$$

in agreement with Eq. (2.89) for $\omega = 1/3$. In the sub-horizon limit we now find

$$\delta_{\mathrm{TM}} \approx 4\cos\left(\frac{k}{\sqrt{3}aH}\right)\mathcal{R} \; . \tag{2.102}$$

The solid black line in Fig. 2.1 shows the density to comoving curvature perturbation ratio given by Eq. (2.100). As can be seen, all three coincide at horizon crossing $k = aH$ as expected, however, large departures prior to and post horizon crossing are evident. In particular, using Eq. (2.100), we have an initial growth in the ratio $\delta/\mathcal{R}$ prior to horizon entry but no longer have an indefinite increase in this ratio after horizon crossing. Rather $\delta/\mathcal{R}$ has an oscillatory nature in the sub-horizon regime. This agrees with the current understanding of structure formation, whereby, on sub-horizon scales, density perturbations grow through gravitational attraction. This eventually leads to a rise in radiation pressure and a subsequent expansion. The result is an oscillatory behaviour of perturbations on sub-horizon scales. Fig. 2.1 reflects this oscillatory property.

Using Eq. (2.100) we can write the power spectrum of density perturbations in terms of the power spectrum of comoving curvature perturbations as

$$\mathcal{P}_\delta(k,t) = \frac{16}{3} \left(\frac{k}{aH} \right)^2 j_1^2(k/\sqrt{3}aH)\mathcal{P}_\mathcal{R}(k) \ . \tag{2.103}$$

The above equation is a new, more accurate expression, which takes into account the full time evolution of perturbations. As expected, it reduces to Eq. (2.90) in the super-horizon limit, however, it also takes into account the evolution of perturbations in the sub-horizon regime. We emphasize that to accurately relate the power spectrum of density perturbations to the power spectrum of comoving curvature perturbations, one should use our new expression given by Eq. (2.103) rather than the approximate expression given by Eq. (2.90). This new expression will become relevant in later sections where we will use it to calculate constraints on the power spectrum of comoving curvature perturbations from observational bounds on the abundance of primordial black holes and ultra compact mini halos.

Chapter 3

Primordial Black Holes

3.1 Introduction

The Universe contains inhomogeneities, as observed by the presence of galaxy clusters and large-scale structure. This along with the discovery of an expanding Universe suggests that the structure observed today evolved from some initial inhomogeneities early in the history of the Universe. This theory was supported by the later discovery of the CMB. This prompted Zeldovich & Novikov [47] and Hawking & Carr [48, 49] to consider the possibility that very large amplitude inhomogeneities, or density perturbations, may also have existed in the early dense Universe and may have been sufficiently large to collapse and form black holes. These early Universe black holes formed from initial perturbations are known as **Primordial Black Holes** (PBHs).

Of particular interest in this thesis are PBH formation from perturbations generated by inflation. There are many scenarios in which large amplitude perturbations on small-scales may arise. These include a simple power-law power spectrum of perturbations with a blue tilted spectral index ($n_s > 1$) (see Sec. 3.4 for further discussion) or a more complicated form for the power spectrum of perturbations incorporating a running of the spectral index (and possibly higher terms, see Sec. 1.10). PBHs may also form from sharp peaks in the power spectrum on small-scales. These will be discussed in more detail in chapter 5.

PBHs may also form via alternative mechanisms to inflation such as a softening of

the equation of state [50, 51], the collapse of cosmic strings [52, 53], collapse of domain walls [54, 55] or bubble collisions [56, 57]. For a review of PBH formation see Refs. [58, 59, 5, 60]. We do not consider these possibilities here.

Since the formation of PBHs was suggested, thorough searches have been undertaken to find these objects. These involve possible detection of gamma-ray emissions [61, 62, 63, 64, 65] and other approaches such as gravitational lensing effects [66, 67, 68, 69]. PBHs have also been suggested as a possible candidate for dark matter [70].

As PBHs form from large amplitude, small-scale primordial perturbations, the abundance of PBHs in the Universe reveals information about the distribution of these perturbations. Although searches have so far found no evidence for the existence of PBHs, important information about the early Universe can still be obtained from them. Specifically, that their abundance in the Universe must be relatively small in order to evade detection. Constraints on PBH abundance [71, 6, 5] (see Ref. [5] for a recent review) can then be translated into constraints on the primordial density or curvature perturbations. Indeed, before detailed observations of the CMB from WMAP, PBHs provided the strongest upper limits on the spectral index [72, 73, 74].

In the following work we review PBH formation and evaporation. We compile constraints on PBH abundance and use these to find constraints on the power spectrum of primordial curvature perturbation.

3.2   Formation of PBHs

A PBH is formed if an overdense region is large enough to overcome the pressure force resisting gravitational collapse. The criteria for PBH formation can be given in terms of the density contrast defined in Eq. (2.51). A PBH will form at horizon crossing if the smoothed density contrast in the comoving gauge is [49]

$$\delta_c \leq \delta_{\text{hor}}(R) \leq 1 \ , \tag{3.1}$$

where δ_c is a critical density contrast which can be estimated by the requirement that the radius of the overdense region at maximum expansion must be larger than the Jeans

length in a radiation dominated Universe [49, 75]. A simple calculation finds

$$\delta_c \sim \omega = \frac{1}{3} \ . \tag{3.2}$$

The upper limit in Eq. (3.1) arises as perturbations exceeding this would form a separate closed Universe [49, 75, 76]. The resulting mass of the PBH formed is usually taken to be a fixed fraction $f_M = \omega^{3/2}$ of the horizon mass [75, 73]:

$$
\begin{aligned}
M_{\mathrm{PBH}} &= f_M M_{\mathrm{H}} \ , &\tag{3.3}\\
&= \frac{f_M}{\sqrt{g_\star^i}} \left(\frac{t}{t_{\mathrm{Pl}}} \right) m_{\mathrm{Pl}} \ , &\tag{3.4}
\end{aligned}
$$

where $g_\star$ is the total number of effectively massless degrees of freedom.

With increasingly more sophisticated numerical hydrodynamical studies the value of the fraction in Eq. (3.2) has fluctuated over the years (see [77] for a review). More recent numerical simulations investigating near critical phenomena in gravitational collapse [78, 79, 80] have suggested that the PBH mass may depend on the size of the fluctuation from which it forms [81, 82, 77]. We discuss the possible effects of this in Sec. 3.6. Shibata & Sasaki [83] used an alternative method for studying PBH formation using metric perturbations rather than focusing on density perturbations. Green et al. [45] subsequently used this result to obtain the corresponding density perturbations for PBH formation using peaks theory [84] rather than Press-Schechter theory. They found that the critical density contrast is closest to $\delta_c \sim 1/3$ as originally found by Carr [49]. Therefore, throughout, we use the critical value given by Eq. (3.2).

From Eq. (3.4) we see that PBHs can form with a wide range of masses, with those that formed at the Planck time having a mass of the order $M_{\mathrm{PBH}} \sim 10^{-2} m_{\mathrm{Pl}}$ (where we have used $g_\star^i \approx 100$). In contrast black holes which form at the present epoch, from the collapse of a stellar core, cannot have a mass less than $\sim 1 M_\odot$.

3.3   PBH lifetime

The possible existence of PBHs led Hawking to study their quantum mechanical properties. This lead to the discovery that black holes radiate thermally with a temperature [85, 86]:

$$T_{\mathrm{PBH}} = \frac{\hbar c^3}{8\pi G M_{\mathrm{PBH}} k_{\mathrm{B}}} \approx 1.06 \left(\frac{10^{13}\,\mathrm{g}}{M_{\mathrm{PBH}}} \right) \mathrm{GeV} \ . \tag{3.5}$$

The current understanding of PBH evaporation [87] is that PBHs directly emit all particles which appear elementary at the energy scale of the PBH and have rest mass less than the black hole temperature. Thus if the black hole temperature exceeds the QCD confinement scale, quark and gluon jets are emitted directly. The quark and gluon jets then fragment and decay producing astrophysically stable particles: photons, neutrinos, electrons, protons and their anti-particles. Using conservation of energy and taking into account the number of emitted species the mass loss rate can be written as [88]

$$\frac{\mathrm{d}M_{\mathrm{PBH}}}{\mathrm{d}t} = -5.34 \times 10^{25} \phi(M_{\mathrm{PBH}}) M_{\mathrm{PBH}}^{-2} \ \mathrm{g\,s^{-1}}, \tag{3.6}$$

where $\phi(M_{\mathrm{PBH}})$ takes into account the number of directly emitted species ($\phi(M_{\mathrm{PBH}}) = 0.267g_0 + 0.147g_{1/2} + 0.06g_1 + 0.02g_{3/2} + 0.007g_2$ where g_s is the number of degrees of freedom with spin s) and is normalized to one for PBHs with mass $M_{\mathrm{PBH}} \gg 10^{17}$ g which can only emit photons and neutrinos. For lighter PBHs $\phi(5 \times 10^{14} \ \mathrm{g} < M_{\mathrm{PBH}} < 10^{17} \ \mathrm{g}) = 1.569$. Integrating Eq. (3.6) the PBH lifetime is then given by [88]

$$\tau \approx 6.24 \times 10^{-27} M_{\mathrm{PBH}}^3 \phi(M_{\mathrm{PBH}})^{-1} \,\mathrm{s}. \tag{3.7}$$

From the WMAP 5 year data [89] the present age of the Universe is $t_0 = 13.69 \pm 0.13$ Gyr [1]. The initial mass of a PBHs which is evaporating today is therefore [90]

$$M_{\mathrm{PBH}} \approx 5 \times 10^{14} \mathrm{g}, \tag{3.8}$$

while less massive PBHs will have evaporated by the present day.

3.4 Inflation and PBHs

Inflation provides a mechanism for the generation of density perturbations. If PBHs form from these density perturbations, one can place limits on the spectrum of perturbations by requiring that PBHs are not over-produced. Observational limits on the PBH abundance can be translated into constraints on the primordial curvature perturbation. This can then be used to constrain models of inflation which predict large amplitude perturbations on small scales (see Chapter 5).

---

[1]Using the more recent WMAP 7 year data ($t_0 = 13.75 \pm 0.13$) does not change the results significantly.

The power spectrum of the primordial curvature perturbation, $\mathcal{P}_{\mathcal{R}}(k)$, on cosmological scales is now accurately measured by observations of the cosmic microwave background (CMB) [89, 9] (see Sec. 1.9) and large-scale structure [91, 92]. These measurements can be used to constrain, and in some cases exclude, inflation models (c.f. Ref. [93]). Cosmological observations span a relatively small range of scales (comoving wavenumbers between $k \sim 1\,\mathrm{Mpc}^{-1}$ and $k \sim 10^{-3}\,\mathrm{Mpc}^{-1}$), and hence probe a limited region of the inflaton potential. The PBH constraints on the curvature power spectrum are fairly weak; the upper limit is many orders of magnitude larger than the measurements on cosmological scales. They do, however, apply over a very wide range of scales (from $k \sim 10^{-2}\,\mathrm{Mpc}^{-1}$ to $k \sim 10^{23}\,\mathrm{Mpc}^{-1}$) and therefore provide a useful constraint on models of inflation [94]. The simplest assumption for the power spectrum is a scale-free power-law with constant spectral index n_s as given by Eq. (1.50). In this case the PBH abundance constraints require $n_s < 1.25 - 1.30$ [72, 73, 95, 96]. The spectral index on cosmological scales is, however, now accurately measured: $n_s = 0.963^{+0.014}_{-0.015}$ [89]. In other words, if the power spectrum is a pure power-law then the number of PBHs formed will be completely negligible. However, if the primordial perturbations are produced by inflation then the power spectrum is not expected to be an exact power-law over all scales [97]. This realises the possibility that on small-scales the amplitude of perturbations may be large resulting in the significant formation of PBHs.

We focus in the following on the standard case of PBH formation, which applies to scales which have left the horizon at the end of inflation. It has recently been shown [98, 99, 100] that PBHs can also form on scales which never leave the horizon during inflation, and therefore never become classical. We also only consider gaussian perturbations and a trivial initial radial density profile, and refer to Ref. [101] for the effects of non-gaussian perturbations and to Refs. [83, 102] for estimates on the effect of deviations from a trivial initial density profile.

3.5 Initial PBH abundance

Before we outline the observational constraints on PBH abundance to constrain properties of the early Universe, we must relate current PBH abundances to initial abundances. Taking into account the cosmological expansion, the initial PBH mass fraction, $\beta(M_{\mathrm{PBH}})$, is related to the present day PBH density, Ω^0_{PBH}, by

$$\beta(M_{\mathrm{PBH}}) \equiv \frac{\rho^{\mathrm{i}}_{\mathrm{PBH}}}{\rho^{\mathrm{i}}_{\mathrm{crit}}} = \frac{\rho^{\mathrm{eq}}_{\mathrm{PBH}}}{\rho^{\mathrm{eq}}_{\mathrm{crit}}} \left(\frac{a_{\mathrm{i}}}{a_{\mathrm{eq}}}\right) \approx \Omega^0_{\mathrm{PBH}} \left(\frac{a_{\mathrm{i}}}{a_{\mathrm{eq}}}\right) , \tag{3.9}$$

where 'eq' refers to the epoch of matter-radiation equality and ρ_{crit} is the critical energy density defined in Eq. (1.12). The entropy in a comoving volume, s, is given by

$$s = g_{*s} a^3 T^3 , \tag{3.10}$$

where $g_{\star s}$ refers to the number of entropy degrees of freedom and T is the temperature of the Universe. In an isotropic Universe the entropy is constant [18] and so

$$a \propto g_{\star s}^{-1/3} T^{-1} . \tag{3.11}$$

Using the radiation density, $\rho = \frac{\pi^2}{30} g_\star T^4$, and horizon mass, $M_{\mathrm{H}} = \frac{4\pi}{3} \rho H^{-3}$, we obtain

$$\beta(M_{\mathrm{PBH}}) = \Omega^0_{\mathrm{PBH}} \left(\frac{g^{\mathrm{eq}}_\star}{g^{\mathrm{i}}_\star}\right)^{1/12} \left(\frac{M_{\mathrm{H}}}{M^{\mathrm{eq}}_{\mathrm{H}}}\right)^{1/2} , \tag{3.12}$$

where we have taken $g_{\star s} \approx g_\star$. The horizon mass at matter-radiation equality is given by (c.f. Ref. [45])

$$M^{\mathrm{eq}}_{\mathrm{H}} = \frac{4\pi}{3} \rho_{\mathrm{eq}} H^{-3}_{\mathrm{eq}} = \frac{8\pi}{3} \frac{\rho^0_{\mathrm{rad}}}{a_{\mathrm{eq}} k^3_{\mathrm{eq}}} . \tag{3.13}$$

Inserting numerical values given by Ref. [89]

$$\Omega^0_{\mathrm{rad}} h^2 = 4.17 \times 10^{-5} , \tag{3.14}$$

$$\rho_{\mathrm{crit}} = 1.88 \times 10^{-29} h^2 \, \mathrm{g \, cm}^{-3} , \tag{3.15}$$

$$k_{\mathrm{eq}} = 0.07 \, \Omega^0_{\mathrm{m}} h^2 \, \mathrm{Mpc}^{-1} , \tag{3.16}$$

$$a^{-1}_{\mathrm{eq}} = 24000 \, \Omega^0_{\mathrm{m}} h^2 , \tag{3.17}$$

$$\Omega^0_{\mathrm{m}} h^2 = 0.1326 \pm 0.0063 , \tag{3.18}$$

and using $g^{\mathrm{i}}_\star \approx 100$ and $g^{\mathrm{eq}}_\star \approx 3$ [103] gives

$$M^{\mathrm{eq}}_{\mathrm{H}} = 1.3 \times 10^{49} (\Omega_{\mathrm{m}} h^2)^{-2} \, \mathrm{g} . \tag{3.19}$$

Using Eq. (3.3) we find

$$\beta(M_{\mathrm{PBH}}) = 6.4 \times 10^{-19} \, \Omega^0_{\mathrm{PBH}} \frac{1}{f_M^{\frac{1}{2}}} \left(\frac{M_{\mathrm{PBH}}}{5 \times 10^{14} \, \mathrm{g}}\right)^{1/2} . \tag{3.20}$$

3.6 PBH abundance constraints

PBH constraints can, broadly, be split into two classes: those that arise from their present day gravitational consequences and those that arise from the products of their evaporation. In both cases, in order to constrain the primordial density, we need to translate the constraints into limits on the initial PBH mass fraction.

Throughout we will assume that the PBHs form at a single epoch and their mass is a fixed fraction of the horizon mass $M_{\mathrm{PBH}} = f_M M_{\mathrm{H}}$, where $f_M \approx (1/3)^{3/2}$ [75]. A scale-invariant power spectrum produces an extended PBH mass function [104, 64]:

$$\frac{\mathrm{d}n_{\mathrm{PBH}}}{\mathrm{d}M_{\mathrm{PBH}}} \propto M_{\mathrm{PBH}}^{-5/2} \ . \tag{3.21}$$

However, as discussed previously, in this case the number density of PBHs would be completely negligible [94, 105]. For scale-dependent power spectra which produce an interesting PBH abundance it can be assumed that all PBHs form at a single epoch [106]. As a consequence of near critical phenomena in gravitational collapse [78, 79, 80] the PBH mass may, however, depend on the size of the fluctuation from which it forms [81, 82, 77, 107] in which case the mass function has finite width. Most of the constraints that we discuss below effectively apply to the mass function integrated over a range of masses. The range of applicability is usually significantly larger than the width of the mass function produced by critical collapse, so in the absence of a concrete prediction or model for the primordial power spectrum in most cases it is reasonable to approximate the mass function as a delta-function. The constraints from cosmic-rays and gamma-rays produced by recently evaporating PBHs are an exception to this [108]. These constraints depend significantly on the PBH mass function and therefore need to be calculated on a case by case basis [109, 110, 111, 112, 113, 5]. We therefore do not include these constraints in our calculation of generalised constraints on the curvature perturbation power spectrum.

We now compile, and where relevant update, the PBH abundance constraints. We divide the constraints into two classes: those, for PBHs with $M_{\mathrm{PBH}} > 5 \times 10^{14}$g, arising from their gravitational consequences (Sec. 3.6.1) and those for $M_{\mathrm{PBH}} < 5 \times 10^{14}$g arising from their evaporation (Sec. 3.6.2).

3.6.1 Gravitational constraints

3.6.1.1 Present day density

The present day density of PBHs with $M_{\mathrm{PBH}} > 5 \times 10^{14}\,\mathrm{g}$ which haven't evaporated by today must be less than the upper limit on the present day cold dark matter (CDM) density. Using the 5 year WMAP measurements [89], $\Omega^0_{\mathrm{CDM}} h^2 = 0.1099 \pm 0.0062$, $h = 0.719^{+0.026}_{-0.027}$, gives (95% upper confidence limit) [2]

$$\Omega^0_{\mathrm{PBH}} < 0.25 \,, \tag{3.22}$$

which, using Eq. (3.20), leads to

$$\beta(M_{\mathrm{PBH}}) < 1.6 \times 10^{-19} \frac{1}{f_M^{\frac{1}{2}}} \left(\frac{M_{\mathrm{PBH}}}{5 \times 10^{14}\,\mathrm{g}} \right)^{1/2} \quad \text{for} \ \ M_{\mathrm{PBH}} > 5 \times 10^{14}\,\mathrm{g}\,. \tag{3.23}$$

3.6.1.2 Lensing of cosmological sources

If there is a cosmologically significant density of compact objects then the probability that a distant point source is lensed is high. This possibility was first investigated by Press & Gunn [114] and has led to an extensive search for lensing signatures from compact objects. Non-detection allows limits to be placed on the abundance of such objects. The limits as given below have been calculated assuming an Einstein de Sitter Universe, $\Omega_{\mathrm{m}} = 1$, and a uniform density of compact objects. The recalculation of the constraints for a Λ dominated Universe would be non-trivial. The constraints would, however, be tighter (due to the increased path length and the larger optical depth to a given red-shift) [115], and the constraints given below are therefore conservative and valid to within a factor of order unity.

Gamma-ray bursts

Light compact objects can femtolens distant gamma-ray bursts (GRBs). The time delay induced by such a lens is such that a characteristic interference pattern may be

---

[2]Using WMAP 7 year data results in a small change to this result finding $\Omega^0_{\mathrm{PBH}} < \Omega_{\mathrm{CDM}} = 0.26$ (95% upper confidence limit).

produced [66]. A null search using BATSE data leads to a constraint [116]:

$$\Omega_c < 0.2 \quad \text{for} \quad 10^{-16} M_\odot < M_{\text{PBH}} < 10^{-13} M_\odot \; , \tag{3.24}$$

where Ω_c is the density of compact objects, assuming a mean GRB red-shift of one.

Quasars

Compact objects with mass $10^{-3} M_\odot < M_{\text{PBH}} < 300 M_\odot$ can microlens quasars, amplifying the continuum emission without significantly changing the line emission [67]. Limits on an increase in the number of small equivalent width quasars with red-shift lead to the constraint [115]:

$$\Omega_c < 0.2 \quad \text{for} \quad 0.001 M_\odot < M_{\text{PBH}} < 60 M_\odot \; , \tag{3.25}$$

assuming $\Omega_{\text{tot}} = \Omega_c$.

Radio sources

Massive compact objects, $10^6 M_\odot < M_{\text{PBH}} < 10^8 M_\odot$, can millilens radios sources producing multiple sources with milliarcsec separation [68]. Using Very Long Baseline Interferometry (VLBI) a null search of a sample of 300 compact radio sources places a constraint [117]:

$$\Omega_c < 0.013 \quad \text{for} \quad 10^6 M_\odot < M_{\text{PBH}} < 10^8 M_\odot \; . \tag{3.26}$$

3.6.1.3 Halo fraction constraints

There are also constraints from the gravitational consequences of PBHs within the Milky Way halo. They are typically expressed in terms of the fraction of the mass of the Milky Way halo in compact objects:

$$f_{\text{h}} = \frac{M_{\text{PBH}}^{\text{MW}}}{M_{\text{tot}}^{\text{MW}}} \; . \tag{3.27}$$

These constraints require some modeling of the Milky Way halo (typically the density and/or velocity distribution of the halo objects). Consequently there is a factor of a few uncertainty in the precise values of the constraints.

Assuming that PBHs make up the same fraction of the dark matter halo as they do of the cosmological cold dark matter, and ignoring the uncertainties in the CDM density (since this is negligible compared with the uncertainties in halo fraction limit calculations), we can relate the halo fraction to the PBH cosmological density:

$$f_h \equiv \frac{M_{\mathrm{PBH}}^{\mathrm{MW}}}{M_{\mathrm{CDM}}^{\mathrm{MW}}} \approx \frac{\rho_{\mathrm{PBH}}^0}{\rho_{\mathrm{CDM}}^0} = \frac{\Omega_{\mathrm{PBH}}^0 h^2}{\Omega_{\mathrm{CDM}}^0 h^2} \approx 5\Omega_{\mathrm{PBH}}^0 \ . \tag{3.28}$$

Microlensing

Solar and planetary mass compact objects in the Milky Way halo can microlens stars in the Magellanic Clouds, causing a temporary one-off brightening of the microlensed star [118]. The relationship between the observed optical depth to gravitational microlensing, τ, (the probability that a given star is amplified by more than a factor of 1.34) and the fraction of the halo in MACHOs depends on the distribution of MACHOS in the MW halo. For the 'standard' halo model used by the microlensing community (a spherical cored isothermal sphere) $\tau \approx 5 \times 10^{-7} f_h$ [119, 120, 121], with the derived value of limits on f_h varying by factors of order unity for other halo models.

The EROS collaboration find a 95% upper confidence limit $\tau < 0.36 \times 10^{-7}$ which they translate into limits on the halo fraction [121]:

$$f_h < 0.04 \quad \text{for} \quad 10^{-3} M_\odot < M_{\mathrm{PBH}} < 10^{-1} M_\odot \,, \tag{3.29}$$

or

$$f_h < 0.1 \quad \text{for} \quad 10^{-6} M_\odot < M_{\mathrm{PBH}} < M_\odot \,. \tag{3.30}$$

Combined EROS and MACHO collaboration limits on short duration events constrain the abundance of light MACHOs [122]:

$$f_h < 0.25 \quad \text{for} \quad 10^{-7} M_\odot < M_{\mathrm{PBH}} < 10^{-3} M_\odot \,, \tag{3.31}$$

while a dedicated search by the MACHO collaboration for long (> 150 days) duration events leads to limits on more massive MACHOs [69]:

$$f_h < 1.0 \quad \text{for} \quad 0.3 M_\odot < M_{\mathrm{PBH}} < 30 M_\odot \,, \tag{3.32}$$

or

$$f_h < 0.4 \quad \text{for} \quad M_{\mathrm{PBH}} < 10 M_\odot \,. \tag{3.33}$$

Combined, these limits give

$$f_h \quad < \quad 0.25 \quad \text{for} \quad 10^{-7} M_\odot < M_{\text{PBH}} < 10^{-6} M_\odot \,, \tag{3.34}$$

$$f_h \quad < \quad 0.1 \quad \text{for} \quad 10^{-6} M_\odot < M_{\text{PBH}} < M_\odot \,, \tag{3.35}$$

$$f_h \quad < \quad 0.4 \quad \text{for} \quad M_\odot < M_{\text{PBH}} < 10 M_\odot \,. \tag{3.36}$$

Wide binary disruption

Binary star systems are abundant in the solar system [123, 124]. Binaries with wide separations are particularly susceptible to perturbations by galactic objects. More massive compact objects would affect the orbital parameters of wide binaries [125, 126]. Comparison of the separations of observed halo binaries [127] with simulations of encounters between compact objects and wide binaries lead to a constraint [128]:

$$f_h < 0.2 \quad \text{for} \quad 10^3 M_\odot < M_{\text{PBH}} < 10^8 M_\odot \,. \tag{3.37}$$

Recently Quinn et al. [129] have re-analysed the radial velocity measurements of wide binary systems sampled by Chaname & Gould [127] and used by Yoo, Chaname & Gould [128]. They find that three of the candidate systems are genuine binaries. However, one candidate is spurious at the 5-sigma level. Omitting this spurious candidate leads to the somewhat weaker limit [129]:

$$f_h \lesssim 0.4 \quad \text{for} \quad 10^3 M_\odot < M_{\text{PBH}} < 10^8 M_\odot \,. \tag{3.38}$$

Disk heating

Massive halo objects traversing the Galactic disk will heat the disk, increasing the velocity dispersion of the disk stars [130]. This leads to a limit, from the observed stellar velocity dispersions, on the halo fraction in massive objects [131]

$$f_h < \frac{M_{\text{disk,lim}}}{M_{\text{PBH}}} \,, \tag{3.39}$$

where $M_{\text{disk,lim}}$ is the maximum mass of halo objects which can dominate the disk and is given by [131]

$$M_{\text{disk,lim}} = 3 \times 10^6 \left(\frac{\rho_h}{0.01 M_\odot \text{pc}^{-3}} \right)^{-1} \left(\frac{\sigma_{\text{obs}}}{60 \, \text{km s}^{-1}} \right)^2 \left(\frac{t_s}{10^{10} \, \text{yr}} \right)^{-1} M_\odot \,, \tag{3.40}$$

where ρ_h is the local halo density and $\sigma_{\rm obs}$ and $t_{\rm s}$ are the velocity dispersion and age of the halo stars, respectively.

3.6.2 Evaporation constraints

3.6.2.1 Diffuse gamma-ray background

PBHs with masses in the range $2 \times 10^{13}\,{\rm g} < M_{\rm PBH} < 5 \times 10^{14}\,{\rm g}$ evaporate between $z \approx 700$ and the present day and can contribute to the diffuse gamma-ray background [105, 132, 62, 64, 133, 109]. As discussed in Sec. 3.6, these constraints depend significantly on the PBH mass function [108] and hence we will not consider them further.

3.6.2.2 Cosmic-rays

The abundance of PBHs evaporating around the present day can also be constrained by limits on the abundance of cosmic-rays (in particular positrons and antiprotons) [64, 134]. The constraints from anti-protons have been calculated for several mass functions and are essentially equivalent to those from the diffuse gamma-ray background [135, 112].

3.6.2.3 Neutrinos

Neutrinos produced by PBH evaporation contribute to the diffuse neutrino background. The neutrino spectrum, and hence the resulting PBH abundance constraints, depend strongly on the PBH mass function, but the constraints are typically weaker than those from the diffuse gamma-ray background [110, 111].

3.6.2.4 Hadron injection

Using Eq. (3.7), PBHs with mass $M_{\rm PBH} < 10^{10}\,{\rm g}$ have a lifetime $\tau \lesssim 10^3\,{\rm s}$ and evaporate before the end of nucleosynthesis. This can therefore affect the light element abundances [136, 137, 138, 139]. In particular emitted quarks or gluons fragment into hadrons which can interact with ambient protons and neutrons. This can increase

the neutron abundance which, in turn, alters the abundance of Deuterium and ^{4}He. Constraints can be obtained by comparing predictions with observed light element abundances.

The constraints from hadron injection have been re-evaluated (see Ref. [140]), taking into account the emission of fundamental particles [61] and using more up to date measurements of the Deuterium and ^{4}He abundances ($D/H \leq 4.0 \times 10^{-5}, Y_p \leq 0.252$ respectively):

$$\beta(M_{\mathrm{PBH}}) < 10^{-20} \quad \text{for} \quad 10^8 \mathrm{g} < M_{\mathrm{PBH}} < 10^{10} \mathrm{g} , \tag{3.41}$$

$$\beta(M_{\mathrm{PBH}}) < 10^{-22} \quad \text{for} \quad 10^{10} \mathrm{g} < M_{\mathrm{PBH}} < 3 \times 10^{10} \mathrm{g} . \tag{3.42}$$

3.6.2.5 Photodissociation of deuterium

The photons produced by PBHs which evaporate between the end of nucleosynthesis and recombination can photodissociate deuterium [141]. The resulting constraints on the PBH abundance have been updated, in the context of braneworld cosmology in Ref. [142]. They find that the PBH fraction at the time of evaporation β_{evap} is given by

$$\beta_{\mathrm{evap}} \lesssim 0.1 \left(\frac{t_{\mathrm{evap}}}{t_{\mathrm{eq}}} \right)^{\frac{1}{2}} . \tag{3.43}$$

Using the constancy of entropy given by Eq. (3.11) and the radiation density, $\rho = \frac{\pi^2}{30} g_\star T^4$, and horizon mass, $M_{\mathrm{H}} = \frac{4\pi}{3} \rho H^{-3}$, we find (using Eq. (3.19))

$$\beta(M_{\mathrm{PBH}}) < 3 \times 10^{-22} \frac{1}{f_M^{\frac{1}{2}}} \left(\frac{M_{\mathrm{PBH}}}{10^{10} \mathrm{g}} \right)^{1/2} \quad \text{for} \quad 10^{10} \mathrm{g} < M_{\mathrm{PBH}} < 10^{13} \mathrm{g} . \tag{3.44}$$

3.6.2.6 CMB distortion

Photons emitted by PBHs which evaporate between $z \sim 10^6$ and recombination at $z \sim 10^3$ can produce distortions in the cosmic microwave background radiation [143]. Using the COBE/FIRAS limits on spectral distortions of the CMB from a black body spectrum [144], Ref. [145] finds

$$\beta(M_{\mathrm{PBH}}) < 10^{-21} , \quad \text{for} \quad 10^{11} \mathrm{g} < M_{\mathrm{PBH}} < 10^{13} \mathrm{g} . \tag{3.45}$$

3.6.2.7 (Quasi-)stable massive particles

In extensions of the standard model there are generically stable or long lived massive ($\mathcal{O}(100\,\mathrm{GeV})$) particles. Light PBHs with mass $M_{\mathrm{PBH}} \lesssim 10^{11}\,\mathrm{g}$ can emit these particles and their abundance is hence limited by the present day abundance of stable massive particles [146] and the decay of long-lived particles [147, 148][3].

Gravitinos in supergravity theories and moduli in string theories are generically quasi-stable and decay after nucleosynthesis, potentially altering the light element abundances. The effect of their decay on the products of nucleosynthesis leads to a constraint on the initial PBH fraction [147]:

$$
\begin{aligned}
\beta(M_{\mathrm{PBH}}) \;<\; & 5 \times 10^{-19} \left(\frac{g_\star^{\mathrm{i}}}{200} \right)^{1/4} \left(\frac{\alpha}{3} \right) \left(\frac{x_\phi}{6 \times 10^{-3}} \right)^{-1} \\
& \times \; \frac{1}{f_M{}^{\frac{1}{2}}} \left(\frac{M_{\mathrm{PBH}}}{10^9\,\mathrm{g}} \right)^{-1/2} \left(\frac{\bar{Y}_\phi}{10^{-14}} \right) \\
& \qquad \text{for } M_{\mathrm{PBH}} < 10^9\,\mathrm{g} ,
\end{aligned}
\tag{3.46}
$$

where x_ϕ is the fraction of the luminosity going into quasi-stable massive particles, $g_\star^{\mathrm{i}}$ is the initial number of degrees of freedom (taking into account supersymmetric particles), α is the mean energy of the particles emitted in units of the PBH temperature and $\bar{Y}_\phi$ is the limit on the quasi-stable massive particle number density to entropy density ratio.

In supersymmetric models, in order to avoid the decay of the proton, there is often a conserved quantum number R-parity, which renders the Lightest Supersymmetric Particle (LSP) stable and the present day density of such stable particles produced via PBH evaporation must not exceed the upper limit on the present day CDM density [146]. This leads to a constraint on the initial PBH fraction (c.f. Ref. [147]):

$$
\begin{aligned}
\beta(M_{\mathrm{PBH}}) \;<\; & 6 \times 10^{-19} h^2 \left(\frac{g_\star^{\mathrm{i}}}{200} \right)^{1/4} \left(\frac{\alpha}{3} \right) \left(\frac{x_{\mathrm{LSP}}}{0.6} \right)^{-1} \\
& \times \; \frac{1}{f_M{}^{\frac{1}{2}}} \left(\frac{M_{\mathrm{PBH}}}{10^{11}\,\mathrm{g}} \right)^{-1/2} \left(\frac{m_{\mathrm{LSP}}}{100\,\mathrm{GeV}} \right)^{-1} \\
& \qquad \text{for } M_{\mathrm{PBH}} < 10^{11}\,\mathrm{g} \left(\frac{100\,\mathrm{GeV}}{m_{\mathrm{LSP}}} \right) ,
\end{aligned}
\tag{3.47}
$$

---

[3]More massive PBHs can also emit these particles in the late stages of their evaporation, when their mass drops below $\sim 10^9\,\mathrm{g}$. However the resulting constraints are substantially weaker than those from hadron injection during nucleosynthesis.

where m_{LSP} is the mass of the LSP and x_{LSP} is the fraction of the luminosity carried away by the LSP.

These constraints depend on the (uncertain) details of physics beyond the standard model, and we therefore summarise them conservatively as

$$\beta(M_{\mathrm{PBH}}) \lesssim 10^{-18} \frac{1}{f_M^{\frac{1}{2}}} \left(\frac{M_{\mathrm{PBH}}}{10^{11}\mathrm{g}} \right)^{-1/2} \qquad \text{for} \quad M_{\mathrm{PBH}} < 10^{11}\,\mathrm{g}\,. \tag{3.48}$$

3.6.2.8 Present day relic density

It was first suggested by MacGibbon [149] that black hole evaporation could leave a stable Planck mass relic [150, 151, 149], in which case the present day density of relics must not exceed the upper limit on the CDM density:

$$\Omega_{\mathrm{rel}}^0 < 0.25\,. \tag{3.49}$$

Assuming

$$\Omega_{\mathrm{PBH}} = \frac{M_{\mathrm{PBH}}}{M_{\mathrm{rel}}} \Omega_{\mathrm{rel}}\,, \tag{3.50}$$

where the relic mass is written as a fraction of the Planck mass $M_{\mathrm{rel}} = f_{\mathrm{rel}} m_{\mathrm{Pl}}$ and using Eq. (3.20), this gives a tentative constraint [4]

$$\beta(M_{\mathrm{PBH}}) < 4 \frac{1}{f_M^{1/2} f_{\mathrm{rel}}} \left(\frac{M_{\mathrm{PBH}}}{5 \times 10^{14}\,\mathrm{g}} \right)^{3/2} \qquad \text{for} \quad M_{\mathrm{PBH}} < 5 \times 10^{14}\,\mathrm{g}\,. \tag{3.51}$$

The constraints described above are summarised in table 3.1 and are displayed in Fig. 3.1. As can be seen from Fig. 3.1 the constraints probe a very large range of scales and in some cases several constraints overlap across particular mass ranges. The solid black line indicates the strongest constraints for each mass scale and we consider only these when constraining the primordial power spectrum.

---

[4]It has been suggested by Carr et al [5] that the upper mass limit of validity for the present day relic constraint is lower than the value given here. This is because larger PBHs would come to dominate the total energy density of the Universe before evaporating. Consequently, the associated PBH emission would affect the observed baryon asymmetry. This correction would not affect our results as several other constraints, discussed previously, overlap with a large portion of the relic density constraints. In the following we only consider present relic constraints for low mass PBHs.
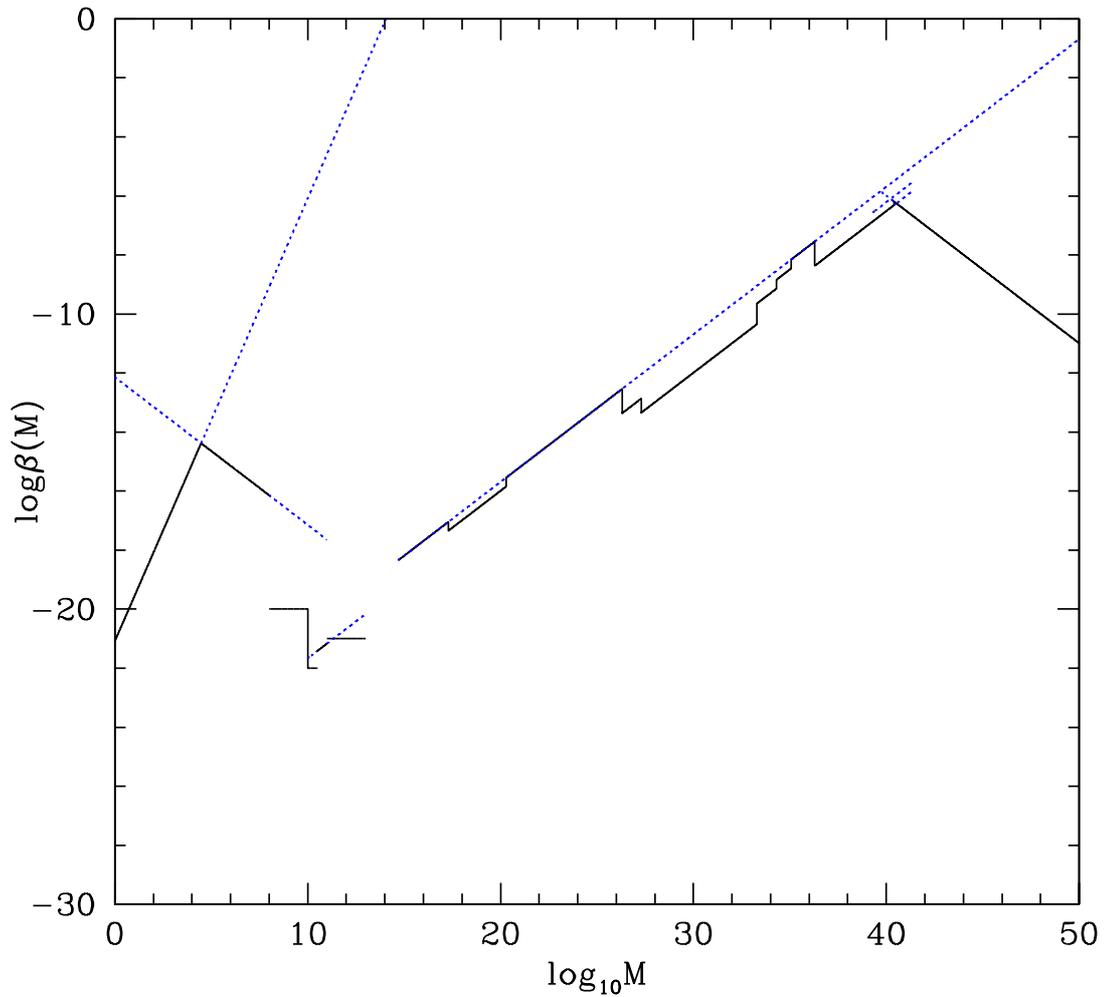
Figure 3.1: The limits on the initial mass fraction of PBHs as a function of PBH mass (in grams). The solid black lines represent the tightest limits for each mass range and the dotted blue lines are the weaker limits where there is an overlap between constraints. As discussed in Sec. 3.6 we have not considered the diffuse gamma-ray background constraint which applies for 2×10^{13} g $< M_{\mathrm{PBH}} < 5 \times 10^{14}$ g as it depends significantly on the PBH mass function.

Table 3.1: Summary of constraints on the initial PBH abundance, $\beta(M_{\mathrm{PBH}})$.

description	mass range	constraint on $\beta(M_{\mathrm{PBH}})$
Gravitational constraints		
present day PBH density	$M_{\mathrm{PBH}} > 5 \times 10^{14}\,\mathrm{g}$	$< 2 \times 10^{-19} \frac{1}{f_M^{\frac{1}{2}}} \left(\frac{M_{\mathrm{PBH}}}{5 \times 10^{14}\,\mathrm{g}} \right)^{1/2}$
GRB femtolensing	$10^{-16} M_\odot < M_{\mathrm{PBH}} < 10^{-13} M_\odot$	$< 1 \times 10^{-19} \frac{1}{f_M^{\frac{1}{2}}} \left(\frac{M_{\mathrm{PBH}}}{5 \times 10^{14}\,\mathrm{g}} \right)^{1/2}$
Quasar microlensing	$0.001 M_\odot < M_{\mathrm{PBH}} < 60 M_\odot$	$< 1 \times 10^{-19} \frac{1}{f_M^{\frac{1}{2}}} \left(\frac{M_{\mathrm{PBH}}}{5 \times 10^{14}\,\mathrm{g}} \right)^{1/2}$
Radio source microlensing	$10^6 M_\odot < M_{\mathrm{PBH}} < 10^8 M_\odot$	$< 6 \times 10^{-20} \frac{1}{f_M^{\frac{1}{2}}} \left(\frac{M_{\mathrm{PBH}}}{5 \times 10^{14}\,\mathrm{g}} \right)^{1/2}$
Halo density		
LMC Microlensing	$10^{-7} M_\odot < M_{\mathrm{PBH}} < 10^{-6} M_\odot$	$< 3 \times 10^{-20} \frac{1}{f_M^{\frac{1}{2}}} \left(\frac{M_{\mathrm{PBH}}}{5 \times 10^{14}\,\mathrm{g}} \right)^{1/2}$
	$10^{-6} M_\odot < M_{\mathrm{PBH}} < M_\odot$	$< 1 \times 10^{-20} \frac{1}{f_M^{\frac{1}{2}}} \left(\frac{M_{\mathrm{PBH}}}{5 \times 10^{14}\,\mathrm{g}} \right)^{1/2}$
	$M_\odot < M_{\mathrm{PBH}} < 10 M_\odot$	$< 5 \times 10^{-20} \frac{1}{f_M^{\frac{1}{2}}} \left(\frac{M_{\mathrm{PBH}}}{5 \times 10^{14}\,\mathrm{g}} \right)^{1/2}$
Wide binary disruption	$10^3 M_\odot < M_{\mathrm{PBH}} < 10^8 M_\odot$	$< 3 \times 10^{-20} \frac{1}{f_M^{\frac{1}{2}}} \left(\frac{M_{\mathrm{PBH}}}{5 \times 10^{14}\,\mathrm{g}} \right)^{1/2}$
Disk heating	$M_{\mathrm{PBH}} > 3 \times 10^6 M_\odot$	$< 2 \times 10^6 \frac{1}{f_M^{1/2}} \left(\frac{M_{\mathrm{PBH}}}{5 \times 10^{14}\,\mathrm{g}} \right)^{-1/2}$
Evaporation		
diffuse gamma-ray background	$2 \times 10^{13}\,\mathrm{g} < M_{\mathrm{PBH}} < 5 \times 10^{14}\,\mathrm{g}$	*depends on PBH mass function*
cosmic-rays	similar to DGRB	*depends on PBH mass function*
neutrinos	similar to DGRB	*depends on PBH mass function*
hadron injection	$10^8\,\mathrm{g} < M_{\mathrm{PBH}} < 10^{10}\,\mathrm{g}$	$< 10^{-20}$
	$10^{10}\,\mathrm{g} < M_{\mathrm{PBH}} < 3 \times 10^{10}\,\mathrm{g}$	$< 10^{-22}$
photodissociation of deuterium	$10^{10}\,\mathrm{g} < M_{PBH} < 10^{13}\,\mathrm{g}$	$< 3 \times 10^{-22} \frac{1}{f_M^{\frac{1}{2}}} \left(\frac{M_{PBH}}{10^{10} g} \right)^{1/2}$
CMB distortion	$10^{11}\,\mathrm{g} < M_{\mathrm{PBH}} < 10^{13}\,\mathrm{g}$	$< 10^{-21}$
(Quasi-)stable massive particles	$M_{\mathrm{PBH}} < 10^{11}\,\mathrm{g}$	$<\sim 10^{-18} \frac{1}{f_M^{\frac{1}{2}}} \left(\frac{M_{\mathrm{PBH}}}{10^{11}\,\mathrm{g}} \right)^{-1/2}$
present day relic density	$M_{\mathrm{PBH}} < 5 \times 10^{14}\,\mathrm{g}$	$< 4 \frac{1}{f_M^{1/2} f_{\mathrm{rel}}} \left(\frac{M_{\mathrm{PBH}}}{5 \times 10^{14}\,\mathrm{g}} \right)^{3/2}$

A recent detailed review and update of PBH abundance constraints is given by Carr et al. [5]. Here, evaporation constraints have been updated using the more modern view of PBH evaporation into fundamental quark-gluon jets. PBH constraints have also been calculated using the most recent data on the light element abundances [152, 153, 154, 155, 156, 157]. Ref. [5] also revise constraints arising from the most recent observational data on the diffuse γ-ray background [158, 159, 160, 161] assuming that all PBHs initially form with the same mass (i.e. approximate the PBH mass function as a delta-function). The resulting limits over the mass range $M_{\mathrm{PBH}} = 10^9 - 10^{17}\mathrm{g}$ given in Ref. [5] are stronger than those outlined in this work (with the exception of constraints from CMB distortion).

3.7 Press-Schechter theory

The fraction of the energy density of the Universe contained in regions dense enough to form PBHs is given, as in Press-Schechter theory [162], by

$$\beta(M_{\mathrm{PBH}}) = 2\frac{M_{\mathrm{PBH}}}{M_H}\int_{\delta_{\mathrm{c}}}^{1} P(\delta_{\mathrm{hor}}(R))\,\mathrm{d}\delta_{\mathrm{hor}}(R)\,, \tag{3.52}$$

where the factor of 2 takes into account that on any smoothing scale half of the Universe is in the form of under-dense regions which will never exceed the threshold for collapse into bound objects. This 'ad-hoc' factor of 2 agrees well with N-body simulations [163, 164] and allows for the fact that these under-dense regions may be a part of a larger over-dense region [28].

The horizon mass is related to the comoving smoothing scale, R, by [45]

$$M_{\mathrm{H}} = M_{\mathrm{H}}^{\mathrm{eq}}(k_{\mathrm{eq}}R)^2\left(\frac{g_{\star,\mathrm{eq}}}{g_{\star}}\right)^{1/3}\,, \tag{3.53}$$

where the horizon mass at matter-radiation equality $M_{\mathrm{H}}^{\mathrm{eq}}$ is given by Eq. (3.19). Taking the initial perturbations to be Gaussian, the probability distribution of the smoothed density contrast, $P(\delta_{\mathrm{hor}}(R))$, is given by (e.g. Ref. [28])

$$P(\delta_{\mathrm{hor}}(R)) = \frac{1}{\sqrt{2\pi}\sigma_{\mathrm{hor}}(R)}\exp\left(-\frac{\delta_{\mathrm{hor}}^2(R)}{2\sigma_{\mathrm{hor}}^2(R)}\right)\,, \tag{3.54}$$

where $\sigma(R)$ is the mass variance

$$\sigma^2(R) = \int_0^{\infty} W^2(kR)\mathcal{P}_{\delta}(k,t)\frac{\mathrm{d}k}{k}\,, \tag{3.55}$$

and $W(kR)$ is the Fourier transform of the window function used to smooth the density contrast. We assume a Gaussian window function for which $W(kR) = \exp\left(-k^2R^2/2\right)$. This leads to a relationship between the PBH initial mass fraction and the mass variance,

$$
\begin{aligned}
\beta(M_{\mathrm{PBH}}) &= \frac{2f_{\mathrm{M}}}{\sqrt{2\pi}\sigma_{\mathrm{hor}}(R)} \int_{\delta_{\mathrm{c}}}^{\infty} \exp\left(-\frac{\delta_{\mathrm{hor}}^2(R)}{2\sigma_{\mathrm{hor}}^2(R)}\right) \mathrm{d}\delta_{\mathrm{hor}}(R) \;, \\
&\approx f_M \mathrm{erfc}\left(\frac{\delta_{\mathrm{c}}}{\sqrt{2}\sigma_{\mathrm{hor}}(R)}\right) \;,
\end{aligned}
\tag{3.56}
$$

where we have used the fact that the probability distribution is a rapidly decreasing function of $\delta_{\mathrm{hor}}(R)$ so that the upper limit of integration is not important and can be taken to infinity.

Constraints on the PBH initial mass fraction can therefore be translated into constraints on the mass variance by simply inverting Eq. (3.56).

3.8 Constraints on the curvature perturbation power spectrum

In order to calculate the constraints on the curvature perturbation power spectrum we use the results of Sec. 2.5. Eq. (2.103) relates the density perturbation power spectrum to the power spectrum of curvature perturbation accurately taking into account the full time evolution of perturbations prior to and post horizon entry. Substituting this into Eq. (3.55), and setting the comoving scale to correspond the the size of the horizon $R = (aH)^{-1}$, gives

$$
\sigma_{\mathrm{hor}}^2(R) = \frac{16}{3} \int_0^{\infty} (kR)^2 \, j_1^2(kR/\sqrt{3}) \exp(-k^2R^2) \mathcal{P}_{\mathcal{R}}(k) \frac{\mathrm{d}k}{k} \;.
\tag{3.57}
$$

Since the integral is dominated by scales $k \sim 1/R$ we assume that, *over the scales probed by a specific PBH abundance constraint*, the curvature power spectrum can be written as a power-law given by Eq. (1.50). This assumption is valid for general slow-roll inflation models such as those considered in Refs. [165, 166, 32]. Using Eqs. (3.56) & (3.57), we translate the PBH abundance constraints compiled in Sec. 3.6 into constraints on the amplitude of the power spectrum of curvature perturbation.

For each constraint we take the pivot point, k_0, to correspond to the scale of interest, $k_0 = 1/R$, and consider a range of values for $n_s(k_0)$ consistent with slow-roll inflation, $0.9 < n_s(k_0) < 1.1$. The resulting constraints for $n_s(k_0) = 1$ are displayed in Fig. 3.2. For $n_s(k_0) = 0.9$ and 1.1 the constraints are weakened or strengthened, respectively, by an amount of the order of 2 percent. This indicates that, for slow-roll inflation models, the constraints are not particularly sensitive to the exact shape of the power spectrum in the vicinity of the scale of interest.

The large scale constraints (small k) come from various astrophysical sources such as Milky Way disk heating, wide binary disruption and a variety of lensing effects. The small scale constraints generally arise from the consequences of PBH evaporation, in particular on nucleosynthesis and the CMB. These evaporation constraints lead to tighter constraints on the abundance of PBHs and therefore the primordial power spectrum is more tightly constrained on these scales. In general the constraints on the amplitude of the primordial power spectrum span the range

$$\mathcal{P}_{\mathcal{R}}(k) < 10^{-2} - 10^{-1} \, , \tag{3.58}$$

with some scale dependence.
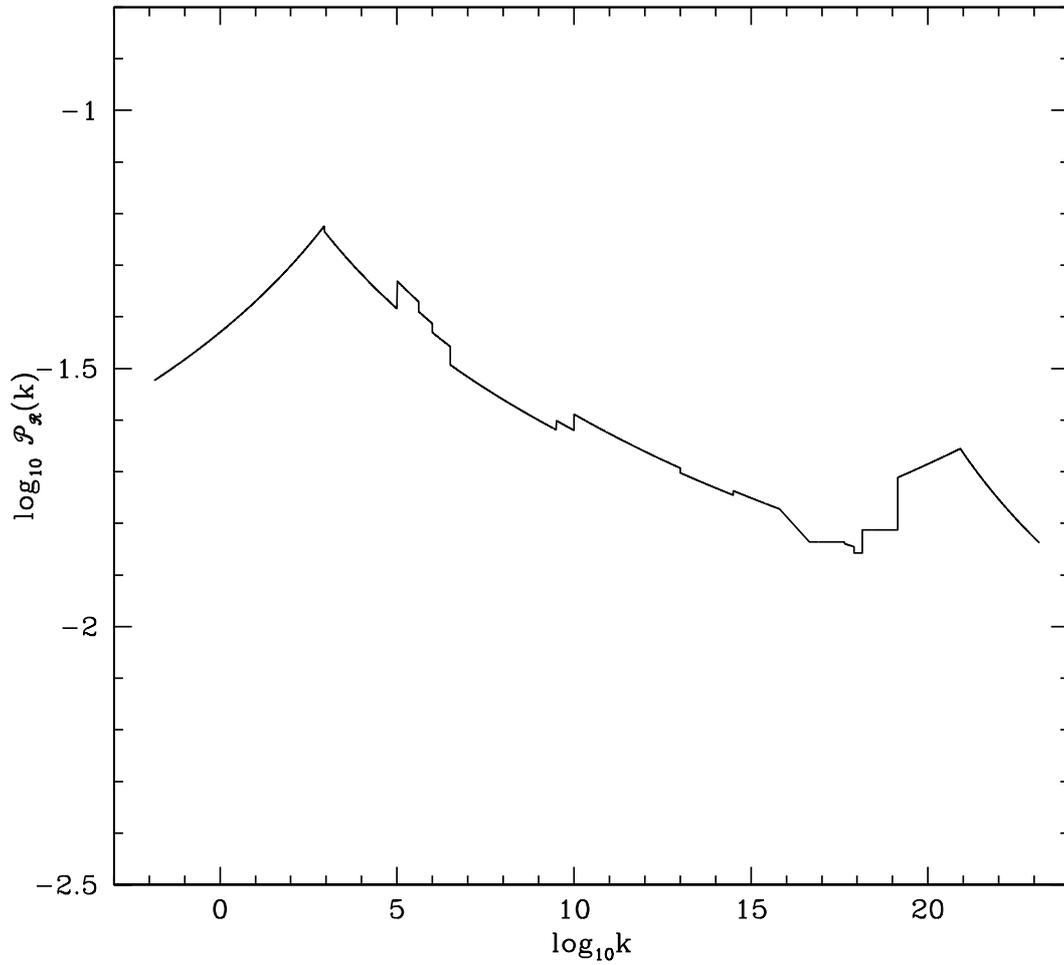
Figure 3.2: Generalised constraints on the amplitude of the power spectrum of the primordial curvature perturbation as a function of comoving wavenumber (in units of Mpc^{-1}). We have assumed that the power spectrum is scale-invariant over the (relatively small) range of scales which contribute to a given constraint. Deviations from scale-invariance consistent with slow-roll inflation lead to small changes in the constraints (see text for further details).

Chapter 4

Ultracompact minihalos

4.1 Introduction

The existence of dark matter was first proposed in 1933 by Fritz Zwicky [167]. Its composition is still unknown and has become one of the fundamental questions in cosmology. In recent years a class of matter known as Weakly Interacting Massive Particles (WIMPs) have become the most popular candidate for dark matter [168, 169, 170]. The weak interaction of WIMPs with baryonic matter explains the difficulty in detection so far. Within this class, a prime candidate which arises within supersymmetry theory is the lightest supersymmetric particle (LSP) [171], usually the lightest neutralino. In the early Universe these supersymmetric WIMPs were created and annihilated at equal rates. Once the Universe expanded and cooled sufficiently, the creation of WIMPs ceased. As the Universe continued to expand, the low cross-section of WIMPs resulted in their abundance 'freezing out' producing a relic density Ω_χ given by [168]

$$\Omega_\chi h^2 \sim \frac{3 \times 10^{-27} \text{cm}^3\text{s}^{-1}}{\langle \sigma v \rangle}\,, \tag{4.1}$$

where $\langle \sigma v \rangle$ is the thermally averaged product of the WIMP annihilation cross-section and speed. Since WIMPs have a very low cross section, the process of self-annihilation that occurred in the early Universe may only occur today in regions of large density.

For PBH formation perturbations must be of the order $\delta_c \geq 1/3$ (see Sec. 3.2). Ricotti & Gould [172] have recently proposed that slightly smaller perturbations can collapse before $z \sim 1000$ and seed the formation of dense dark matter structures called ul-

tracompact minihalos (UCMHs). Due to their early formation, the central regions of UCMHs would have a high dark matter (DM) density. If DM is in the form of Weakly Interacting Massive Particles, WIMP annihilation within UCMHs may lead to an observable gamma-ray signal [172, 173].

Scott & Sivertsson [173] have investigated gamma-ray emission from UCMHs formed from perturbations which enter the horizon at three different epochs in the early Universe: e^+e^- annihilation, and the QCD and electroweak (EW) phase transitions. They find that an UCMH corresponding to the e^+e^- annihilation epoch, which has present day mass $M_{\mathrm{UCMH}}(z = 0) \sim 10^2 M_\odot$, could be detected by the *Fermi* satellite or current Air Cherenkov telescopes (ACTs), at a distance of $100\,\mathrm{pc}$. If 1% of the DM is in the form of UCMHs with this mass there would be ~ 3 UCMHs within $100\,\mathrm{pc}$ of the Earth [173]. UCMHs formed at earlier epochs would be lighter, and hence more challenging to detect.

It has been shown that there are single field models of inflation which are compatible with cosmological observations and where the perturbation amplitude on small-scales is large enough to produce a significant density of PBHs [32, 174] (see also references therein). It is therefore possible that UCMHs may form from perturbations generated by single field slow roll inflation. Phase transitions [172, 173] or features in the inflationary potential [175] could also lead to enhanced perturbations on small scales. We do not fix the UCMH mass or abundance. Instead we calculate the constraints on the UCMH halo fraction which would arise from the detection (or non-detection) of gamma-rays from UCMHs by *Fermi* as a function of UCMH mass. We then translate the UCMH abundance constraints into constraints on the power spectrum of the primordial curvature perturbation, as a function of scale. In Sec. 4.2 we summarize the calculation of the properties of the UCMHs and the resulting gamma-ray flux, following Scott & Sivertsson, in Sec. 4.3. In Sec. 4.4 we calculate the lower bound on the UMCH halo fraction which would result from detection of an UCMH by *Fermi*. We also calculate the upper bound which would result if no UCMHs are detected. Finally, in Sec. 4.5 we translate the potential constraints on the abundance of UCMHs into constraints on the power spectrum of the primordial curvature perturbation.

4.2 UCMH formation

Ricotti & Gould [172] find that a density perturbation with amplitude at horizon cross-
ing $\delta > 10^{-3}$ will grow sufficiently during radiation domination that it collapses at
$z \geq 1000$, seeding the formation a UCMH which then grows via spherical infall. It has
been argued that PBHs can also seed the formation of minihalos [176, 177, 172], and
the resulting gamma-ray emission (assuming that the remainder of the dark matter is
in the form of WIMPs) leads to constraints on the abundance of PBHs [178]. UCMHs
could also conceivably form from the clumping of several PBHs. We do not pursue
these possibilities here. Instead, we consider a simple model of UCMH formation.

At some initial time, z_i, the mass of a region which eventually collapses to form a
UCMH $M(z_i)$ is given by

$$M(z_i) = \frac{\Omega_{\mathrm{DM}}(z_i)}{\Omega_{\mathrm{rad}}(z_i)} M_{\mathrm{H}}(z_i) , \qquad (4.2)$$

where $M_{\mathrm{H}}(z_i) = (4\pi/3)\rho H^{-3}$ is the horizon mass at redshift z_i corresponding to the
epoch when the scale of interest entered the horizon. At matter-radiation equality the
DM mass within a UCMH forming region, $M(z_{\mathrm{eq}})$, is then given by [173]

$$M(z_{\mathrm{eq}}) = f_{\chi} \left(\frac{1 + z_{\mathrm{eq}}}{1 + z_i} \right) M_{\mathrm{H}}(z_i) , \qquad (4.3)$$

where $f_{\chi} = \Omega_{\mathrm{DM}}/\Omega_{\mathrm{m}} = 0.834$ [9] is the dark matter fraction and $\Omega_{\mathrm{m}} = \Omega_{\mathrm{DM}} +
\Omega_{\mathrm{baryons}}$. After matter-radiation equality the UCMH mass, $M_{\mathrm{UCMH}}(z)$, grows, due to
radial infall of matter, as [172]

$$M_{\mathrm{UCMH}}(z) = M(z_{\mathrm{eq}}) \left(\frac{1 + z_{\mathrm{eq}}}{1 + z} \right) . \qquad (4.4)$$

Following Scott & Sivertsson [173] we assume that UCMHs stop growing at $z \approx 10$
as the onset of structure formation prevents further matter infall. Using the constancy
of the entropy given by Eq. (3.11) and the the radiation density, $\rho = (\pi^2/30)g_{\star}T^4$, the
horizon mass can be written as

$$M_{\mathrm{H}}(T) = M_{\mathrm{H}}(T_{\mathrm{eq}}) \left(\frac{g_{\star}^{\mathrm{eq}}}{g_{\star}} \right)^{1/2} \left(\frac{T_{\mathrm{eq}}}{T} \right)^2 . \qquad (4.5)$$

Using

$$T \propto g_{\star s}^{-1/3}(1 + z) , \qquad (4.6)$$

the horizon mass as a function of redshift is

$$M_{\mathrm{H}}(z_{\mathrm{i}}) = M_{\mathrm{H}}(z_{\mathrm{eq}}) \left(\frac{g_{\star}^{\mathrm{i}}}{g_{\star}^{\mathrm{eq}}} \right)^{1/6} \left(\frac{1 + z_{\mathrm{eq}}}{1 + z_{\mathrm{i}}} \right)^2 , \quad (4.7)$$

where we have taken $g_{\star s} \approx g_{\star}$.

The UCMH dark matter density profile is by [172, 173]

$$\rho_{\mathrm{UCMH}}(r, z) = \frac{3 f_{\chi} M_{\mathrm{UCMH}}(z)}{16\pi R_{\mathrm{UCMH}}^{\frac{3}{4}}(z) r^{\frac{9}{4}}} , \quad (4.8)$$

where $R_{\mathrm{UCMH}}(z)$ is the radius of the UCMH at redshift z, given by

$$\left(\frac{R_{\mathrm{UCMH}}(z)}{\mathrm{pc}} \right) = 0.019 \left(\frac{1000}{1 + z} \right) \left(\frac{M_{\mathrm{UCMH}}(z)}{M_{\odot}} \right)^{\frac{1}{3}} , \quad (4.9)$$

where $M_{\odot}$ is the mass of the sun.

Baryonic infall may lead to adiabatic contraction of the UCMH density profile [179]. Scott & Sivertsson considered a variable fraction of the total UCMH mass condensing to form a constant density baryonic core. The dark matter density in the centre of the halo does not rise significantly and hence the change in the resulting gamma-ray flux is relatively small. This is true for dark matter in the form of standard WIMPs, with the canonical annihilation cross-section deduced from the measured dark matter density. Motivated by recent electron data [180, 181], Scott & Sivertsson also considered a model with enhanced annihilation cross-section. In that case WIMP annihilation leads to a larger constant density core and adiabatic contraction then has a larger effect. Given the uncertainties in the calculation we therefore do not consider adiabatic contraction.

4.3 WIMP annihilation within UCMHs

WIMP annihilation reduces the density in the inner regions of the UCMH. We use the standard estimate of the maximum density given by comparing the dynamical infall time with the timescale of WIMP annihilation, ρ_{max}, [182, 173]

$$\rho_{\mathrm{max}} \approx \frac{m_{\chi}}{\langle \sigma v \rangle (t_0 - t_{\mathrm{i}})} , \quad (4.10)$$

where m_{χ} is the WIMP mass, $t_0 \approx 13.7\,\mathrm{Gyr}$ [9] the current age of the Universe and we take the UCMH formation time as $t_{\mathrm{i}}(z = z_{\mathrm{eq}}) \approx 77\,\mathrm{kyr}$ [103]. The UCMH present day

density profile is thus given by $\rho_{\mathrm{UCMH}}(r) = \min\{\rho_{\max}, \rho_{\mathrm{UCMH}}(r, z = 10)\}$, where $\rho_{\mathrm{UCMH}}(r, z = 10)$ is given by Eq. (4.8).

The gamma-ray flux above a threshold energy E_{th}, $\Phi_\gamma(E_{\mathrm{th}})$, from WIMP annihilation within an UCMH at a distance d from the Earth can be written as

$$\Phi_\gamma(E_{\mathrm{th}}) = \frac{\Phi_{\mathrm{astro}}\Phi_{\mathrm{particle}}}{2d^2} . \tag{4.11}$$

The particle physics term, Φ_{particle}, is given by

$$\Phi_{\mathrm{particle}} = \frac{1}{m_\chi^2} \sum_f \int_{E_{\mathrm{th}}}^{m_\chi} \langle \sigma_f v \rangle \frac{\mathrm{d}N_f}{\mathrm{d}E} \mathrm{d}E , \tag{4.12}$$

where σ_f is the annihilation cross-section and $\mathrm{d}N_f/\mathrm{d}E$ the differential photon yield of the fth annihilation channel. We use DarkSUSY [183] to compute Φ_{particle} for a range of models with present day DM densities compatible with the WMAP measurement. When calculating the lower limit on the halo fraction of UCMHs which would arise from a detection by *Fermi* we use the largest value of Φ_{particle}. Conversely when calculating the upper limit which would result if no UCMHs are detected we use the smallest value. The astrophysical factor, Φ_{astro}, is given by

$$\Phi_{\mathrm{astro}} = \int_0^{R_h} r^2 \rho_{\mathrm{UCMH}}^2(r, z = 10) \, \mathrm{d}r . \tag{4.13}$$

4.4 Potential UCMH halo fraction constraints

The *Fermi* point source sensitivity above $100\,\mathrm{MeV}$ is [184]

$$\Phi_\gamma(100\,\mathrm{MeV}) = 6 \times 10^{-9} \mathrm{cm}^{-2}\mathrm{s}^{-1} . \tag{4.14}$$

For a given UCMH mass, $M_{\mathrm{UCMH}}(z = 0)$, we determine the distance d within which a UCMH of this mass would be detectable at threshold sensitivity by *Fermi*. We then calculate the fraction of the Universe in the form of UCMHs if there is a single UCMH within this distance. This is the smallest UCMH halo fraction which could be detected by *Fermi*. To do this we assume that the fraction of the DM in the form of UCMHs is independent of position so that the local and global UCMH fractions are identical

$$\begin{aligned} f_{\mathrm{UCMH}} \equiv \frac{\Omega_{\mathrm{UCMH}}}{\Omega_{\mathrm{DM}}} &= \frac{n_{\mathrm{UCMH,MW}}(r)M_{\mathrm{UCMH}}(z = 0)}{\rho_{\mathrm{DM,MW}}(r)} \\ &= \frac{M_{\mathrm{UCMH}}(z = 0)}{M_{\mathrm{DM,MW}}(< d)}, \end{aligned} \tag{4.15}$$

where $\rho_{\mathrm{DM,MW}}(r)$ is the density profile of the Milky Way halo, $n_{\mathrm{UCMH,MW}}(r)$ the number density of UCMHs and $M_{\mathrm{DM,MW}}(< d)$ the mass of DM within a sphere of radius d centred on the Earth. We assume a Navarro, Frenk & White (NFW) halo density profile [185] for the Milky Way:

$$\rho_{\mathrm{DM,MW}}(r) = \frac{\delta_c \rho_{\mathrm{crit}}^0}{(r/r_s)(1 + (r/r_s))^2} , \tag{4.16}$$

where r is the distance from the galactic centre, $\rho_{\mathrm{crit}}^0 = 1.88 \times 10^{-29} h^2 \mathrm{gcm}^{-3}$ is the present day critical density, r_s is the scale radius,

$$\delta_c = \frac{100 c^2 g(c)}{3} , \tag{4.17}$$

and

$$g(c) = \frac{1}{\ln(1 + c) - \frac{c}{1+c}} , \tag{4.18}$$

where $c = r_{\mathrm{vir}}/r_s$ is the concentration parameter and r_{vir} is the virial radius. For the Milky Way we take $r_{\mathrm{vir}} = 258 \, \mathrm{kpc}$ and $c = 12$ [186]. From this we obtain the mass of DM within a volume centred on the Earth using a numerical analysis.

Fig. 4.1 shows the lower limit (black solid line) on the UCMH halo fraction, as a function of UCMH mass, which would result from the detection of a single UCMH by *Fermi* at threshold sensitivity. It also shows the upper limit (blue dashed line) on the UCMH halo fraction if *Fermi* does not detect gamma-rays from UCMHs, assuming that the DM is in the form of self-annihilating WIMPs.

In order to understand the shape of the plot given in Fig. 4.1, we can analyse Eq. (4.15) at various distances. Using Eq. (4.13) and Eq. (4.8) along with Eq. (4.9), we can approximate the relationship between the mass of an UCMH and Φ_{astro} to be

$$\Phi_{\mathrm{astro}} \propto M_{\mathrm{UCMH}}(z = 0) , \tag{4.19}$$

where we have ignored the constant density core given by Eq. (4.10). Hence, more massive UCMHs have a larger gamma-ray flux. Using Eq. (4.11) more massive UCMHs can therefore be detected at a larger distance:

$$d \propto M_{\mathrm{UCMH}}(z = 0)^{1/2} . \tag{4.20}$$

For $M_{\mathrm{UCMH}}(z = 0) \lesssim 10^3 M_\odot$, $d \lesssim 10 \, \mathrm{kpc}$ so that $M_{\mathrm{DM,MW}}(< d)$, given by integrating Eq. (4.16), increases more rapidly than $M_{\mathrm{UCMH}}(z = 0)$. From Eq. (4.15) this
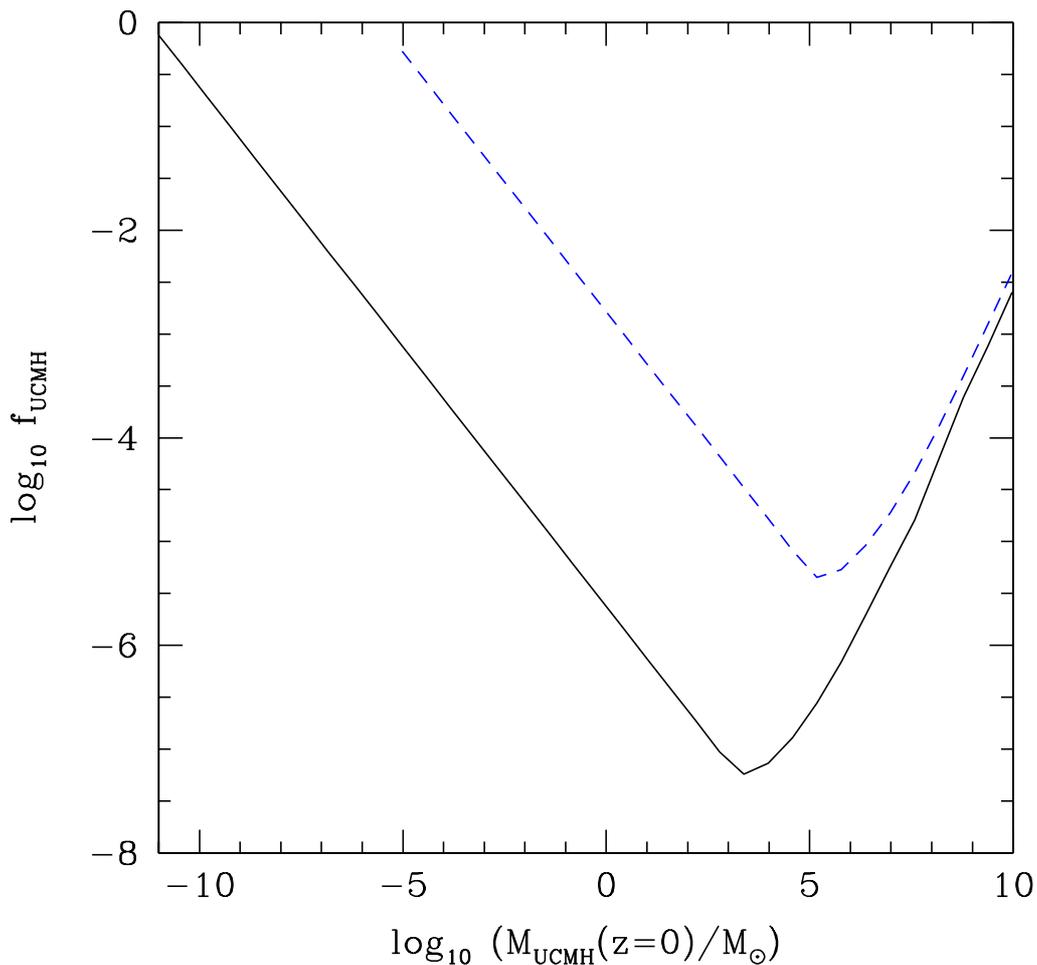
Figure 4.1: Constraints on the UCMH halo fraction, f_{UCMH}, as a function of present day UCMH mass, $M_{\mathrm{UCMH}}(z=0)$. The black solid line shows the lower bound on the halo fraction which would result from the detection of gamma-rays from an UCMH by *Fermi*. The blue dashed line shows the upper limit on the halo fraction if gamma-rays from UCMHs are not detected, assuming DM is in the form of WIMPs.

results in a decreasing limit on the halo fraction as $M_{\mathrm{UCMH}}(z=0)$ is increased. For more massive UCMHs d becomes significantly larger than the scale radius of the Milky Way halo. Integrating Eq. (4.16) for large distances and using Eq. (4.20) gives

$$M_{\mathrm{DM,MW}}(< d) \propto \ln\left[M_{\mathrm{UCMH}}(z=0)\right] . \tag{4.21}$$

From Eq. (4.15) this results in a subsequent increase in the limit on the halo fraction for $M_{\mathrm{UCMH}}(z=0) \gtrsim 10^3 M_\odot$. These features, in particular, the turning point in the halo fraction f_{UCMH}, are evident in Fig. 4.1.

4.5 Potential constraints on $\mathcal{P}_\mathcal{R}$

To translate the limits on the UCMH halo fraction into constraints on the primordial curvature perturbation, we need to relate the present day UCMH halo fraction to the primordial density perturbation distribution. The present day UCMH density, Ω_{UCMH}, is related to the UCMH halo fraction, f_{UCMH}, by Eq. (4.15). Assuming that UCMHs are not destroyed by dynamical processes during structure formation, the present UCMH density is related to the fraction of the Universe at horizon entry which is overdense enough to later form UCMHs, β_{UCMH}, by

$$\Omega_{\mathrm{UCMH}} = \Omega_{\mathrm{DM}} \frac{M_{\mathrm{UCMH}}(z=0)}{M(z_{\mathrm{eq}})} \beta_{\mathrm{UCMH}}(M_{\mathrm{H}}(z_{\mathrm{i}})) \,. \tag{4.22}$$

As UCMHs are far more compact and dense than typical DM halos they will be far less susceptible to disruption. Our lower bounds are conservative; if UCMHs are destroyed, the initial abundance of UCMH forming perturbations, and hence the amplitude of the primordial perturbations, will be under-estimated. The upper limit from non-detection would, however, be weakened.

If the smoothed density contrast, in the comoving gauge, $\delta_{\mathrm{hor}}(R)$, at horizon crossing is in the range $10^{-3} \leq \delta_{\mathrm{hor}}(R) \leq 1/3$, the DM in the region will eventually collapse to form an UCMH [172]. The horizon mass $M_{\mathrm{H}}(z_{\mathrm{i}})$ is related to the smoothing scale, R, by Eq. (3.53) where we use $g_\star^{\mathrm{eq}} \approx 3$ and $g_\star^{\mathrm{i}} \approx 100$ [103].

The fraction of the Universe in regions dense enough to eventually form UCMHs is given by Press-Schechter theory (see Sec. 3.7),

$$\beta_{\mathrm{UCMH}}(M_{\mathrm{H}}(z_{\mathrm{i}})) = 2 \int_{10^{-3}}^{1/3} P(\delta_{\mathrm{hor}}(R)) \mathrm{d}\delta_{\mathrm{hor}}(R) \,, \tag{4.23}$$

where, assuming that the initial perturbations are Gaussian, the probability distribution of the smoothed density contrast, $P(\delta_{\mathrm{hor}}(R))$, is given by Eq. (3.54). The relationship between the present UCMH density and the mass variance is then

$$\Omega_{\mathrm{UCMH}} \approx \frac{2\Omega_{\mathrm{DM}}}{\sqrt{2\pi}\sigma_{\mathrm{hor}}(R)} \frac{M_{\mathrm{UCMH}}(z=0)}{M(z_{\mathrm{eq}})} \int_{10^{-3}}^{1/3} \exp\left(-\frac{\delta_{\mathrm{hor}}^2(R)}{2\sigma_{\mathrm{hor}}^2(R)}\right) \mathrm{d}\delta_{\mathrm{hor}}(R) \,. \tag{4.24}$$

The constraints on the present day UCMH density can therefore be translated into constraints on the mass variance by simply inverting this expression.

The mass variance is given by Eq. (3.57), where we use Eq. (2.103) to relate the power spectrum of density perturbations to the power spectrum of comoving curvature perturbations taking into the full time evolution prior to and post horizon entry. The integral in Eq. (3.57) is dominated by scales $k \sim k_0 = 1/R$. Following Chapter 3, in the context of slow-roll inflation models we can assume that the power spectrum is constant over these scales, $\mathcal{P}_{\mathcal{R}}(k) = \mathcal{P}_{\mathcal{R}}(k_0)$. Relaxing this assumption and assuming a power-law power spectrum with spectral index in the range consistent with slow-roll inflation, $0.9 < n(k_0) < 1.1$, leads to changes by an amount of the order of 3 percent in the power spectrum limits. Using Eq. (4.24) and Eq. (3.57) we can translate the UCMH abundance constraints shown in Fig. 4.1 into constraints on the amplitude of the spectrum of the curvature perturbation. For each UCMH mass considered we take the pivot point, k_0, to correspond to the length scale of the perturbation (see Eq. (3.53)) which eventually forms the UCMH, $k_0 = 1/R$.

Fig. 4.2 shows the resulting constraints on the power spectrum of the primordial curvature perturbation for $n(k_0) = 1$. The potential lower limit on the power spectrum which would arise from the detection of gamma-rays by *Fermi* from a single UCMH is of the order $\mathcal{P}_{\mathcal{R}} \gtrsim 10^{-6.6} - 10^{-5.9}$ on scales $k \sim 10^1 - 10^8 \, \mathrm{Mpc}^{-1}$. If gamma-ray emission from UCMHs are not observed, an upper limit can be placed on the power spectrum of primordial curvature perturbation of the order $\mathcal{P}_{\mathcal{R}} \lesssim 10^{-6.5} - 10^{-6}$ on scales $k \sim 10^1 - 10^6 \, \mathrm{Mpc}^{-1}$. Constraints for larger wavenumbers than those shown in Fig. 4.2 result in $f_{\mathrm{UCMH}} \gtrsim 1$ and so are not considered. The lower bound based on a detection at *Fermi* threshold sensitivity is a conservative limit (provided that the effects of adiabatic contraction are insignificant). The upper limit from non-detection relies on several assumptions, however, most significantly that the DM is in the form of WIMPs and that significant disruption to UCMHs does not occur. If multiple UCMHs were detected by *Fermi* (or ACTs), or the flux was significantly above the detection threshold, then this would imply a larger UCMH halo fraction, and hence the lower limits on the power spectrum of the primordial curvature perturbation would be stronger.

These upper bounds are significantly stronger than those from primordial black hole formation, where we found in Sec. 3.8, $\mathcal{P}_{\mathcal{R}} \lesssim 10^{-1} - 10^{-2}$, and would hence, provide a tighter constraint on models of inflation (c.f. Sec. 5 and Ref. [32]). It does, however,
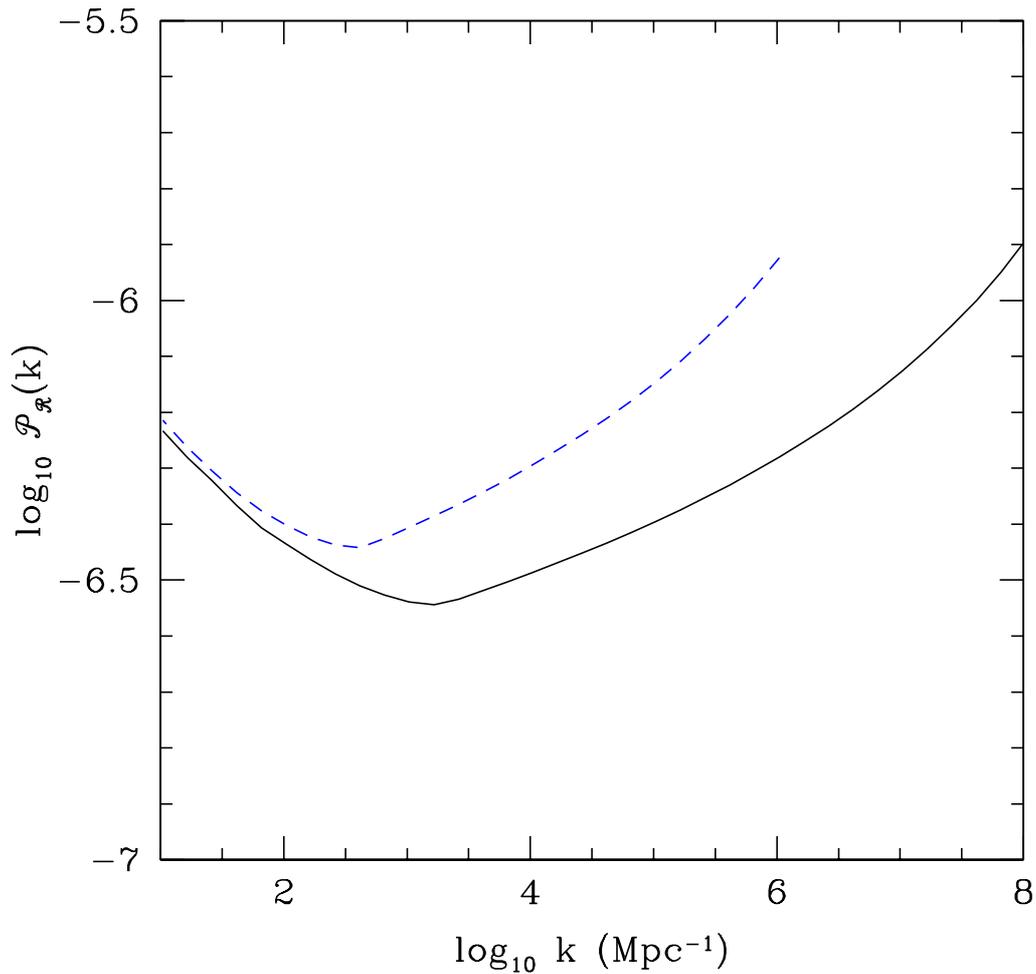
Figure 4.2: Limits on the power spectrum of the primordial curvature perturbation as a function of comoving wavenumber (in units of Mpc^{-1}). The black solid line shows the potential lower bound on the power spectrum resulting from the detection of gamma-rays from an UCMH by *Fermi* at threshold sensitivity. The blue dashed line shows the upper limit on the power spectrum obtained if gamma-rays from UCMHs are not detected by *Fermi*, assuming DM is in the form of WIMPs and UCMHs are not disrupted during structure formation.

rely on the assumptions that dark matter is in the form of WIMPs and UCMHs are not disrupted during the formation of the Milky Way halo.

Chapter 5

Constraining models of inflation

5.1 Introduction

Inflation model building involves assuming an expansion history of the observable Universe and evolving perturbations from the time when current observable scales exit the horizon to the end of inflation. The generation of models of inflation can be approached from two broad methods:

1) on a model case by case basis where one assumes a form for the potential $V(\varphi)$. This is usually motivated by some aspect of particle physics (phenomenological) or by requiring that the potential takes on a simple form. The inflationary dynamics of the model are then given by Eqs. (1.23)-(1.25). The model of inflation must predict values for the observables which are consistent with current data (as given in Sec 1.10).

2) stochastic inflation model building where one uses the Hamilton-Jacobi formalism (Sec. 1.8). Here a particular model of inflation is generated by assigning initial values for the Hubble slow-roll parameters (Eq. (1.35) and Eq. (1.36)) upto an arbitrary order in derivatives of $H(\varphi)$ given by Eq. (1.39). With the Hamilton-Jacobi formalism the condition for inflation is exact and so this model can be numerically evolved to the end of inflation using the flow equations (described in Sec. 5.3). This method has two distinct advantages, firstly a numerical treatment allows one to generate and test many models of inflation simultaneously. Secondly, one is able to test models which cannot be written in a neatly parameterized form. One can therefore, test a larger range of

models not accessible using the more traditional approach described above. Stochastic methods of model testing are therefore very useful in constraining the large range of possible inflation models. Ultimately, however, one would like inflation to be described from some theoretical motivation.

In most cases of inflation model building one is concerned with the properties of perturbations corresponding to current observable scales exiting the horizon during inflation. This is because models are largely tested by their predictions for the observable quantities n_s, r and $\mathrm{d}n_s/\mathrm{dln}k$. The strongest observational constraints we have on these quantities come from WMAP and large-scale structure data (see Sec 1.10). However, these observations only probe a very small range of large scales. A large extrapolation is involved in assuming that a particular model of inflation which satisfies the observational constraints can describe the entire evolution of the Universe. On scales that are beyond current observations, large departures in n_s, r and $\mathrm{d}n_s/\mathrm{dln}k$ are possible. This opens the possibility of large amplitude perturbations on small-scales and therefore a significant formation of PBHs. The running mass model, which was first proposed by Stewart [187, 188], is a specific example of a model which predicts observables compatible with observational data and yet produces a significant PBH abundance. We describe this model in more detail in Sec. 5.2. PBHs are formed on the smallest scales and so are a powerful tool for constraining models of inflation beyond the observable range of scales. Constraints from PBHs can be used in combination with large-scale constraints to effectively constrain models of inflation [32].

In the following chapter we describe the flow equations which are used to evolve the Hubble slow-roll parameters from an initial state to the end of inflation. We compare two methods of calculating the power spectrum of comoving curvature perturbations: the standard analytical calculation using the Stewart-Lyth equation and a numerical calculation using the Mukhanov variable. The difference between these two methods has important implications for the application of PBH constraints. Finally we perform a numerical analysis generating 250,000 inflation models using a stochastic technique [189, 190] finding models consistent with large-scale observations and constraints from PBHs found in Chapter 3.

5.2   Running mass model

The running mass model [187, 188, 191] has been extensively explored within the context of consistency with large-scale data [192, 193, 194, 195] and production of PBHs [165, 166, 196, 197, 113]. The running mass model was proposed to overcome certain problems with models of inflation formulated in supergravity theories [191]. Within supersymmetry, a natural feature that arises is a false vacuum dominated potential given by

$$V(\varphi) = V_0 \pm \frac{1}{2}m^2\varphi^2 \,. \tag{5.1}$$

In the context of supergravity the scale of supersymmetry breaking is such that slow-roll inflation cannot occur [197] since $\eta_V = 1$ on all scales. Stewart [187, 188] proposed a solution to overcome this by including quantum corrections in order to flatten the potential allowing slow-roll inflation to occur over the limited range of scales corresponding to the current observable range. This correction effectively amounts to modifying Eq. (5.1) to include a running mass term $m(\varphi)$.

The relevant aspect here is that while on large-scales the potential is now flat allowing one to recover a near scale-invariant spectrum, on all other scales the slow-roll regime typically breaks down as $\eta_V = 1$. Inflation still continues as $\epsilon_V < 1$ and eventually the potential is dominated by the false vacuum V_0 where it is assumed a secondary mechanism acts to end inflation. In this regime one would expect a significant departure from scale-invariance with a sharp rise in the power spectrum on small scales. PBHs can therefore potentially form in significant numbers in this model.

This example motivates a search for other models which may be consistent with large-scale observational data and result in a significant formation of PBHs on small scales.

5.3   Flow equations

A key quantity required to describe the time evolution of a particular model of inflation is the number of e-foldings of inflation as described in Sec. 1.11. From Eq. (1.34) and Eq. (1.60), the relationship between the evolution of the inflaton field and the number

of e-foldings is

$$N \equiv \int_t^{t_{\text{end}}} H \mathrm{d}t = \int_\varphi^{\varphi_{\text{end}}} \frac{H}{\dot\varphi} \mathrm{d}\varphi = \frac{2\sqrt{\pi}}{m_{\text{Pl}}} \int_{\varphi_{\text{end}}}^\varphi \frac{\mathrm{d}\varphi}{\sqrt{\epsilon_{\text{H}}}} \tag{5.2}$$

therefore,

$$\frac{\mathrm{d}}{\mathrm{d}N} = \frac{m_{\text{Pl}}}{2\sqrt{\pi}} \sqrt{\epsilon_{\text{H}}} \frac{\mathrm{d}}{\mathrm{d}\varphi}. \tag{5.3}$$

From Eq. (1.35) and Eq. (1.39), this allows us to write a set of equations describing the evolution of the Hubble slow-roll parameters in terms of the number of e-foldings of inflation:

$$\frac{\mathrm{d}\epsilon_{\text{H}}}{\mathrm{d}N} = \epsilon_{\text{H}}(\sigma_{\text{H}} + 2\epsilon_{\text{H}}) , \tag{5.4}$$

$$\frac{\mathrm{d}\sigma_{\text{H}}}{\mathrm{d}N} = -5\epsilon_{\text{H}}\sigma_{\text{H}} - 12\epsilon_{\text{H}}^2 + 2(^2\lambda_{\text{H}}) , \tag{5.5}$$

$$\frac{\mathrm{d}(^l\lambda_{\text{H}})}{\mathrm{d}N} = \left[\frac{l-1}{2}\sigma_{\text{H}} + (l-2)\epsilon_{\text{H}} \right] (^l\lambda_{\text{H}}) + {}^{l+1}\lambda_{\text{H}} , \qquad l \geq 2 , \tag{5.6}$$

where

$$\sigma_{\text{H}} \equiv 2(^1\lambda_{\text{H}}) - 4\epsilon_{\text{H}} . \tag{5.7}$$

Eqs. (5.4)-(5.6) together form the **flow equations** of which there is an infinite hierarchy. These were first introduced by Hoffman and Turner [189] and later were generalised by Kinney [190]. They provide a way of evolving the Hubble slow-roll parameters from some specified initial condition (given by a particular inflation model or chosen at random) to the end of inflation or any other required point. If taken to infinite order these equations specify $H(\varphi)$, $H'(\varphi)$, $H''(\varphi)$ etc... to infinite order in derivatives with respect to the inflaton field φ. This is equivalent to completely specifying the form of the potential driving inflation.

The flow equations have been extensively investigated [198, 199, 190, 200, 201, 202, 203, 204, 205, 32]. Although the flow equations do not make any general predictions about inflationary dynamics, they do provide an algorithm which allows one to 'randomly' generate a large number of models to confront with the PBH abundance constraints [198]. This approach can be used to analyse single-field models of inflation. Attempts have been made to develop and use a flow equation formalism for the case of multiple field inflation models [206]. However, due to the large uncertainties in the initial conditions we do not consider this possibility in our work.

5.4 Analytic power spectrum

The standard method of calculating the power spectrum of perturbations has been to use an analytical method formulated by Stewart and Lyth [207]. We briefly outline this calculation closely following the analysis of Ref. [208].

The expression for the inflaton perturbation in uniform curvature gauge, Eq. (2.82), motivates the introduction of a quantity known as the Mukhanov gauge-invariant potential or Mukhanov variable [40, 209, 210] defined by

$$u = a \left[\delta\varphi + \varphi' \frac{\psi}{\mathcal{H}} \right] \; . \tag{5.8}$$

In the comoving gauge this becomes

$$u = z\mathcal{R} \; , \tag{5.9}$$

where

$$z \equiv a\frac{\dot\varphi}{H} \; . \tag{5.10}$$

If u is expanded into comoving Fourier modes u_k, these modes evolve according to a Klein-Gordon equation with a time-varying effective mass:

$$\frac{\mathrm{d}^2 u_k}{\mathrm{d}\tau^2} + \left(k^2 - \frac{1}{z}\frac{\mathrm{d}^2 z}{\mathrm{d}\tau^2} \right) u_k = 0 \; , \tag{5.11}$$

where the effective mass term can be written as a function of the Hubble slow-roll parameters [208]

$$\frac{1}{z}\frac{\mathrm{d}^2 z}{\mathrm{d}\tau^2} = 2a^2 H^2 [1 + \epsilon_{\mathrm{H}} - \frac{3}{2}\eta_{\mathrm{H}} + \epsilon_{\mathrm{H}}^2 - 2\epsilon_{\mathrm{H}}\eta_{\mathrm{H}} + \frac{1}{2}\eta_{\mathrm{H}}^2 + \frac{1}{2}\xi_{\mathrm{H}}] \; , \tag{5.12}$$

where, using Eq. (1.39), $\xi_{\mathrm{H}} \equiv {}^2\lambda_{\mathrm{H}}$.

During inflation comoving wavemodes evolve from sub-horizon to super-horizon scales. The standard choice for the initial conditions in the far sub-horizon limit is that defined by the Bunch-Davies vacuum state [207]:

$$u_k(\tau_{\mathrm{i}}) = \frac{1}{\sqrt{2k}} e^{-ik\tau_{\mathrm{i}}} \; . \tag{5.13}$$

This initial condition is applied when the mode is much smaller than the Hubble radius ($aH/k \to 0$) so that ordinary flat space-time quantum field theory is reproduced and

any spacetime curvature caused by vacuum fluctuations is negligible. In the superhorizon limit, $k^2 \ll z''$, and Eq. (5.11) has a growing mode solution $u_k \propto z$, so that the curvature perturbation $\mathcal{R}_k = |u_k/z|$ 'freezes out' and becomes constant. The power spectrum of curvature perturbation is then (see Sec. 1.9)

$$\mathcal{P}_\mathcal{R}(k) \equiv \frac{k^3}{2\pi^2} |\mathcal{R}_k|^2 = \frac{k^3}{2\pi^2} \left| \frac{u_k}{z} \right|^2 . \tag{5.14}$$

5.4.1 Power-law inflation

Stewart and Lyth [207] investigated the power spectrum for a special case known as power-law inflation [211]. In this model the scale factor evolves as $a(t) \propto t^p$ and the Hubble parameter has the form [208]

$$H(\varphi) \propto \exp\left(\sqrt{\frac{4\pi}{p}} \frac{\varphi}{m_{\text{Pl}}} \right) , \qquad p > 1 , \tag{5.15}$$

where p is a constant. This model is extremely useful as the Hubble slow-roll parameters are constant and given by

$$\epsilon_{\text{H}} = \eta_{\text{H}} = \frac{1}{p} = \text{constant} ,$$
$$^{l+1}\lambda_{\text{H}} = \epsilon_{\text{H}}(^l\lambda_{\text{H}}) \qquad l > 2 . \tag{5.16}$$

This greatly simplifies Eq. (5.11) and using integration by parts, the conformal time is

$$\tau = \int \frac{\mathrm{d}a}{a^2 H} = -\frac{1}{aH} + \int \frac{\epsilon_{\text{H}}\mathrm{d}a}{a^2 H} = -\frac{1}{aH} \frac{1}{1 - \epsilon_{\text{H}}} . \tag{5.17}$$

Eq. (5.11) therefore becomes

$$\left[\frac{\mathrm{d}^2}{\mathrm{d}\tau^2} + k^2 - \frac{\nu^2 - 1/4}{\tau^2} \right] u_k = 0 , \tag{5.18}$$

where

$$\nu \equiv \frac{3}{2} + \frac{1}{p - 1} . \tag{5.19}$$

When modes are in the superhorizon limit ($k/aH \to 0$), Eq. (5.18) has the asymptotic form

$$u_k \to e^{i(\nu-1/2)\pi/2} 2^{\nu-3/2} \frac{\Gamma(\nu)}{\Gamma(3/2)} \frac{1}{\sqrt{2k}} (-k\tau)^{-\nu+1/2} . \tag{5.20}$$

where Γ is the usual gamma function. Substituting this into Eq. (5.14) then gives the power spectrum for the exact case of power-law inflation

$$\mathcal{P}_\mathcal{R}^{1/2}(k) = 2^{\nu-3/2} \frac{\Gamma(\nu)}{\Gamma(3/2)} (\nu - 1/2)^{1/2-\nu} \frac{2}{m_{\text{Pl}}^2} \frac{H^2}{|H'|} \bigg|_{k=aH} . \tag{5.21}$$

5.4.2 Stewart-Lyth equation

Stewart and Lyth [207] obtained a more general solution than Eq. (5.21) by performing an expansion about this exact case. The exact solution for the power-law case is valid as long as $\epsilon_H < 1$ and $\epsilon_H = \eta_H = \sqrt{\xi_H}$. In order to obtain a solution for cases other than power-law inflation one would like to consider $\epsilon_H < 1$ and $\epsilon_H \neq \eta_H \neq \sqrt{\xi_H}$. This is equivalent to the higher order Hubble slow-roll parameters picking up a time dependence. Stewart and Lyth considered a small finite difference between the first two Hubble slow-roll parameters $\zeta_H = \epsilon_H - \eta_H$. If ϵ_H and η_H are slowly varying (valid if they are small [212]) around horizon crossing ($k = aH$) the time dependence is shifted to higher order Hubble slow-roll parameters. One can then follow a similar process to the power-law case writing the conformal time as

$$\tau = -\frac{1}{aH}\frac{1}{1-\epsilon_H} - \frac{2\epsilon_H\zeta_H}{aH} + (\text{expansion in higher order Hubble slow-roll parameters}) \,,$$

$$(5.22)$$

where this is consistent to order $\xi_H \equiv {}^2\lambda_H$. For small and slowly varying ϵ_H and η_H the conformal time can be written

$$\tau \approx -\frac{1}{aH}(1 + \epsilon_H) \,. \tag{5.23}$$

Using Eq. (5.18), this leads to the commonly used Stewart-Lyth equation for the power spectrum of curvature perturbations to lowest order in ϵ_H and η_H:

$$\mathcal{P}_{\mathcal{R}}(k) \approx \frac{[1 - (2C+1)\epsilon_H + C\eta_H]^2}{\pi\epsilon_H} \left(\frac{H}{m_{\mathrm{Pl}}}\right)^2 \Bigg|_{k=aH} \,, \tag{5.24}$$

where $C = -2 + \ln 2 + \gamma \approx -0.729$ and γ is the Euler-Mascheroni constant. Any scale dependence in the power spectrum is contained within the scale dependency of the slow-roll parameters.

There are two crucial points to consider in the derivation of the Stewart-Lyth equation:

1) The expansion around the exact power-law case involves shifting the time dependence of the Hubble slow-roll parameters to higher orders. This requires ϵ_H and η_H to be small and slowly varying around horizon crossing (from the flow Eqs. (5.4)-(5.6), we see that if ϵ_H and η_H are small, this is equivalent to the statement that they are slowly varying).

2) Despite appearances Eq. (5.24) does not give the value of the power spectrum at horizon crossing, rather it gives the value in the asymptotic superhorizon limit written in terms of the values which quantities had at horizon crossing [213]. Therefore for an accurate determination of the power spectrum at a given scale, this asymptotic regime must be reached.

As we will frequently refer to these approximations in the following discussion, we call these two conditions the *Stewart-Lyth conditions*. We discuss these two points and the implications for PBH constraints in Sec. 5.7.

5.5   Numerical power spectrum

We wish to perform a numerical evaluation of the power spectrum of perturbations so that, for the first time, a quantitative comparison can be made with the analytical calculation described above. We ultimately wish to investigate any implications this has for PBH constraints. In this and the following section, we closely follow the work by Chongchitnan and Efstathiou [200]. However, we adopt a different approach to the evolution of the flow equations in Sec. 5.8.3.

A numerical analysis involves tracing the evolution of u_k for each wavemode using Eq. (5.11) from an initial state well inside the horizon to the end of inflation τ_{end}. As Eq. (5.11) has a dependence on the Hubble slow-roll parameters, this evolution is dependent on the model of inflation assumed. This model is chosen by assigning initial values of the Hubble slow-roll parameters. These parameters are then also evolved to the end of inflation using the flow equations Eqs. (5.4)-(5.6).

In summary, analysing Eq. (5.11), the evolution of a given model defined by the Hubble slow-roll parameters is given by the effective mass term and the evolution of perturbations within this model is described through the u_k variable. To perform a numerical analysis, we must specify initial conditions for both u_k and the Hubble slow-roll parameters.

Ideally one would like to initialize modes in the extreme short-wavelength limit by

evaluating Eq. (5.13) in the infinite past i.e.

$$u_k(k/aH \to \infty) = \frac{1}{\sqrt{2k}} e^{-ik\tau} . \tag{5.25}$$

In practise one must set a finite early time limit by imposing a sub-horizon scale in which to set the initial condition. It has been shown that the exact value of this early time limit does not alter the final results significantly as long as k/aH is taken to be sufficiently large [201]. We set the initial conditions, Eq. (5.13), for each mode at an arbitrary sub-horizon scale given by $k/aH = 50$. We have confirmed that using the larger scale limit $k/aH = 100$ does not change the results appreciably.

We change the time variable to the more convenient e-foldings variable (see Sec. 1.11). Eq. (5.11) can then be rewritten as [200]

$$\frac{\mathrm{d}^2 u_k}{\mathrm{d}N^2} + (\epsilon_\mathrm{H} - 1)\frac{\mathrm{d}u_k}{\mathrm{d}N} + \left[\left(\frac{k}{aH}\right)^2 - f(\epsilon_\mathrm{H}, \sigma_\mathrm{H}, \xi_\mathrm{H}) \right] u_k = 0 , \tag{5.26}$$

where

$$f(\epsilon_\mathrm{H}, \sigma_\mathrm{H}, \xi_\mathrm{H}) = 2 - 4\epsilon_\mathrm{H} - \frac{3}{2}\sigma_\mathrm{H} - 2\epsilon_\mathrm{H}^2 + \frac{\sigma_\mathrm{H}^2}{4} + \xi_\mathrm{H} . \tag{5.27}$$

The initial conditions are normalized so that they satisfy the Wronskian condition [208]:

$$u_k^* \frac{\mathrm{d}u_k}{\mathrm{d}\tau} - u_k \frac{\mathrm{d}u_k^*}{\mathrm{d}\tau} = -i . \tag{5.28}$$

The Mukhanov variable is initialized at $k/aH = 50$ to be [214, 200]

$$\begin{aligned} \mathrm{Re}(u_k(\tau_i)) &= \frac{1}{\sqrt{2k}} , & \mathrm{Im}(u_k(\tau_i)) &= 0 , \\ \mathrm{Re}\left(\frac{\mathrm{d}u_k}{\mathrm{d}N}(\tau_i)\right) &= 0 , & \mathrm{Im}\left(\frac{\mathrm{d}u_k}{\mathrm{d}N}(\tau_i)\right) &= -\frac{k}{aH}\frac{1}{\sqrt{2k}} . \end{aligned} \tag{5.29}$$

Each mode is then evolved during inflation from this quantum vacuum ground state through horizon crossing and then to the end of inflation defined by $N = 0$. The power spectrum of curvature perturbations can then be calculated using Eq. (5.14) [200]

$$\mathcal{P}_\mathcal{R}(k) = \mathcal{P}_\mathcal{R}(k_0) \left(\frac{k}{k_0}\right)^3 \left|\frac{u_k}{u_{k_0}}\right|^2_{\mathrm{end}} , \tag{5.30}$$

where k_0 is the scale corresponding to current observable scales. Some further useful relations describing the inflationary evolution are given by

$$\frac{\mathrm{d}(k/aH)}{\mathrm{d}N} = -\frac{k}{aH}(\epsilon_\mathrm{H} - 1) , \tag{5.31}$$

$$\frac{\mathrm{dln}k}{\mathrm{d}N} = (\epsilon_\mathrm{H} - 1) \,, \tag{5.32}$$

$$\frac{\mathrm{d}H}{\mathrm{d}N} = \epsilon_\mathrm{H} H \,. \tag{5.33}$$

We can use the equations reviewed in this section to numerically evolve any given model of inflation to the end of inflation. We can then calculate the power spectrum of perturbations without relying on the Stewart-Lyth equation by using Eq. (5.30).

5.6 Model dependent cosmological observables

Sec. 5.5 provides the necessary equations for calculating the power spectrum of perturbations for any given model of inflation numerically. This then allows us to apply our PBH constraints (see Sec. 3.8) so that models which over-produce PBHs can be eliminated. These models are then plotted according to their predictions for n_s, r and $\mathrm{d}n_s/\mathrm{dln}k$ on large scales to allow comparison to observational data. To apply these large-scale observational constraints we use the Stewart-Lyth equation, Eq. (5.24), to obtain expressions for these observables in terms of the Hubble slow-roll parameters. This is sufficiently accurate as long as the Stewart-Lyth conditions (see Sec. 5.4.2) are obeyed on these scales and for a short time before these scales exited the horizon [215].

Using Eq. (5.24) the cosmological observables n_s and r are given to first order [190]:

$$r \equiv \frac{\mathcal{P}_\mathcal{T}}{\mathcal{P}_\mathcal{R}} = \epsilon_\mathrm{H} \,, \tag{5.34}$$

$$n_s - 1 \equiv \frac{\mathrm{dln}\mathcal{P}_\mathcal{R}}{\mathrm{dln}k} = -4\epsilon_\mathrm{H} + 2\eta_\mathrm{H} \equiv \sigma_\mathrm{H} \,. \tag{5.35}$$

To second order in Hubble slow-roll they are given by [190]

$$r = \epsilon_\mathrm{H}[1 - C_1(\sigma_\mathrm{H} + 2\epsilon_\mathrm{H})] \,, \tag{5.36}$$

$$n_s - 1 = \sigma_\mathrm{H} - (5 - 3C_1)\epsilon_\mathrm{H}^2 - \frac{1}{4}(3 - 5C_1)\sigma_\mathrm{H}\epsilon_\mathrm{H} + \frac{1}{2}(3 - C_1)\xi_\mathrm{H} \,, \tag{5.37}$$

where $C_1 = 4(\ln 2 + \gamma) - 5 \approx 0.0814514$ and $\gamma \approx 0.577$.

The running of the spectral index is defined as the second derivative of the power spectrum. Using the following relationship [190]:

$$\frac{\mathrm{d}}{\mathrm{d}N} = -(1 - \epsilon_H)\frac{\mathrm{d}}{\mathrm{dln}k} \,. \tag{5.38}$$

The running of the spectral index is

$$\frac{\mathrm{d}n_s}{\mathrm{d}\mathrm{ln}k} \equiv \frac{\mathrm{d}^2\mathrm{ln}\mathcal{P}_\mathcal{R}}{\mathrm{d}\mathrm{ln}k^2} = -\left(\frac{1}{1 - \epsilon_\mathrm{H}}\right)\frac{\mathrm{d}n_s}{\mathrm{d}N}, \tag{5.39}$$

which can be evaluated to second order in Hubble slow-roll by using Eq. (5.37) and the flow equations, Eqs. (5.4)-(5.6):

$$\frac{\mathrm{d}n_s}{\mathrm{d}\mathrm{ln}k} \approx -\left(\frac{1}{1 - \epsilon_\mathrm{H}}\right)\left[2\xi_\mathrm{H} - 12\epsilon_\mathrm{H}^2 - 5\epsilon_\mathrm{H}\sigma_\mathrm{H} - \frac{(3 - 5C_1)}{2}\epsilon_\mathrm{H}\xi_\mathrm{H} + \frac{(3 - C_1)}{4}\sigma_\mathrm{H}\xi_\mathrm{H}\right]. \tag{5.40}$$

With our limited knowledge of the inflationary potential based on large-scale observations, it is possible, with some confidence, to constrain the first two Hubble slow-roll parameters, ϵ_H & η_H and to a much lesser extent, the third Hubble slow-roll parameter, ξ_H. As can be seen from Eq. (5.40), ξ_H is the leading order term for the value of the running of the spectral index (see Eq. (1.56)). This uncertainty in the running allows for the possibility that the power spectrum of curvature perturbation, given by Eq. (1.54), may become large on small scales resulting in significant structure such as PBH formation. Higher order Hubble slow-roll parameters are unconstrained by current observations. If these parameters are significant, PBH formation may be even more significant.

5.7 Numerical vs. analytical power spectrum

In the case of simple single-field inflation models, the Stewart-Lyth equation Eq. (5.24), is a good approximation of the power spectrum of perturbations over a large range of scales. However, it can break down any time the Stewart-Lyth conditions (see Sec. 5.4.2) are violated. Specifically, the first condition may be violated if there are features in the inflationary potential causing the Hubble slow-roll parameters to change quickly [213]. The second Stewart-Lyth condition may be violated for modes which exit the horizon close to the end of inflation [212]. These modes do not reach the asymptotic large-scale limit before inflation ends and so can result in an underestimation of the power spectrum at the end of inflation. These can both have important consequences for PBH formation. Fig. 5.1 shows an example model of inflation which shows these features.
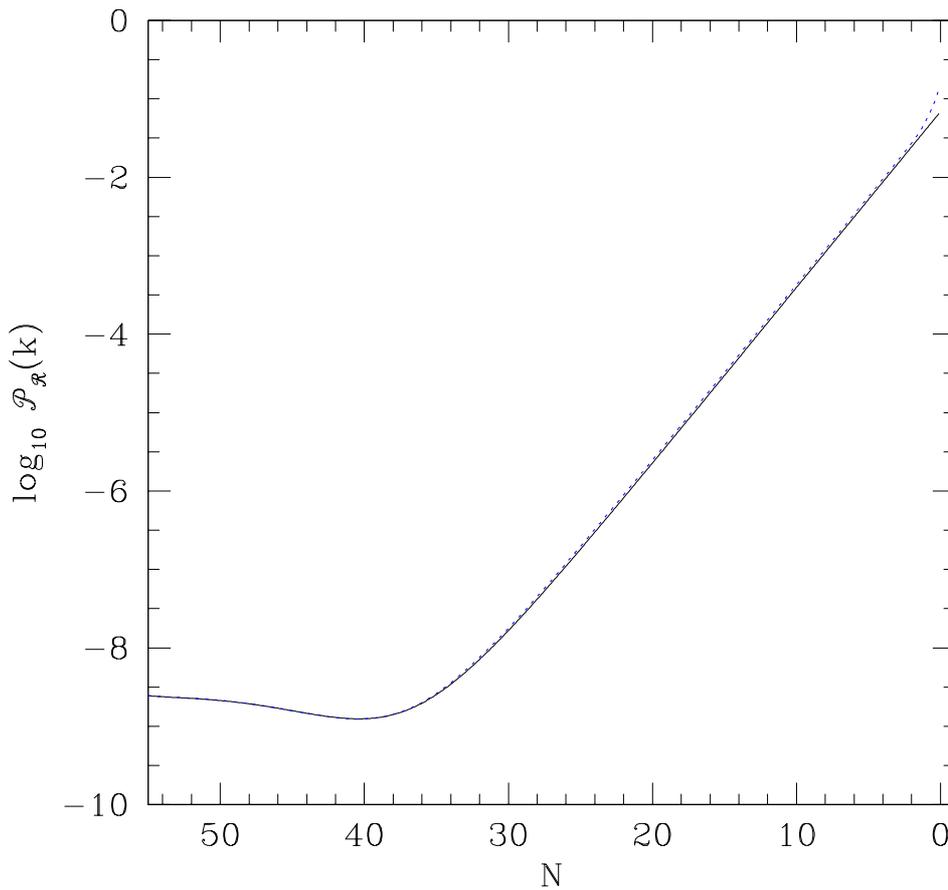
Figure 5.1: The power spectrum of the primordial curvature perturbation generated during the evolution of an example model of inflation as a function of the number of e-foldings. The black solid line shows the power spectrum calculated using the Stewart-Lyth equation while the blue dotted line is the result of a numerical mode by mode calculation.

This model begins with an inflationary expansion which closely follows power-law inflation i.e. has a relatively constant power spectrum of perturbations. Here the Hubble slow-roll parameters vary slowly and the power spectrum of perturbations calculated using the Stewart-lyth equation (solid black line) matches the numerical evaluation (dotted blue line) very well. As the inflationary evolution progresses the Hubble slow-roll parameters begin to differ significantly from each other and the first Stewart-Lyth condition (see Sec. 5.4.2) breaks down. The resulting power spectrum acquires a scale dependency. In this regime the Stewart-Lyth equation tends to under-estimate the power spectrum compared to a numerical evaluation. The effect here is small but may become large for certain inflationary potentials (for instance the model shown in Fig. 5.2) or if there are peaks or features in the inflationary potential [200]. Fig. 5.1
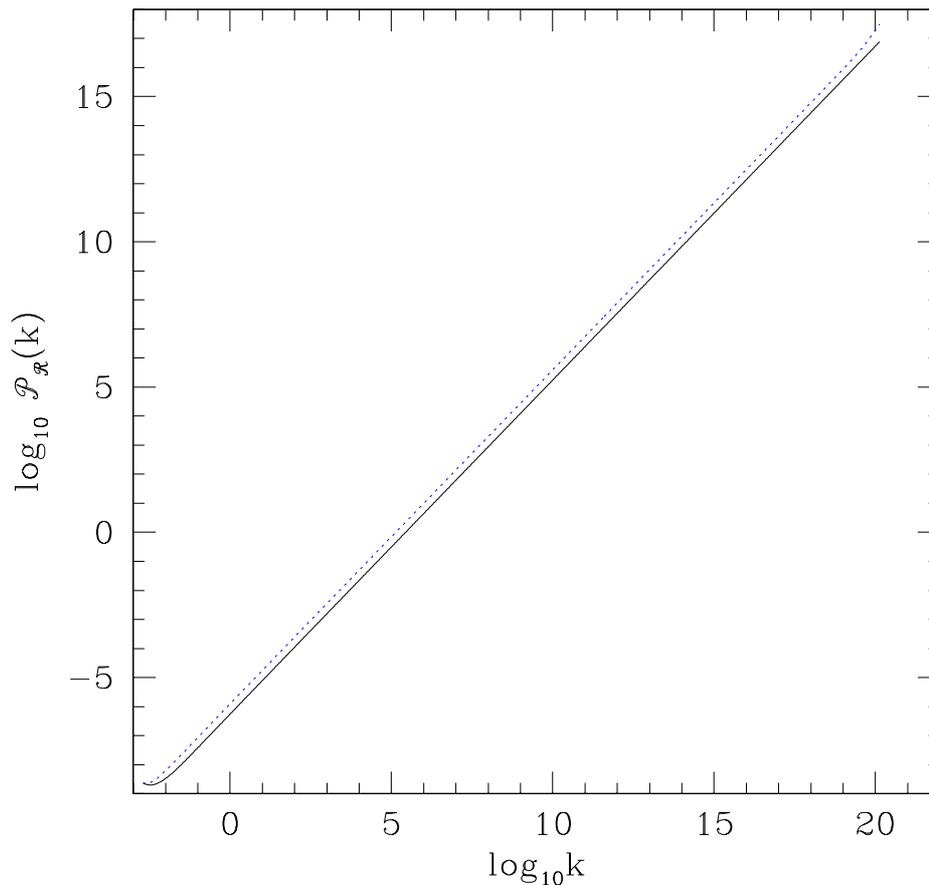
Figure 5.2: The power spectrum of the primordial curvature perturbation generated during the evolution of an example model of inflation as a function of the comoving wavenumber. Here there is a significant difference between an analytical evaluation of the power spectrum (solid black line) from a numerical mode by mode evaluation (blue dotted line)

also shows an enhancement of the power spectrum close to the end of inflation caused by the failure of the second Stewart-Lyth condition.

Fig. 5.3 shows the power spectrum of curvature perturbation as a function of k/aH as perturbations evolve from sub-horizon to super-horizon scales. As discussed previously, the use of the Stewart-Lyth equation requires modes to fully evolve to the asymptotic super-horizon regime where the power spectrum becomes constant. As can be seen in Fig. 5.3, if this asymptotic limit is not reached, such as for modes exiting the horizon close to the end of inflation, the Stewart-Lyth equation leads to an underestimation of the power spectrum. From Fig. 5.3, we can also see that modes which never exit the horizon before the end of inflation have much larger power spectrum amplitudes and could potentially form PBHs on sub-horizon scales. These effects have
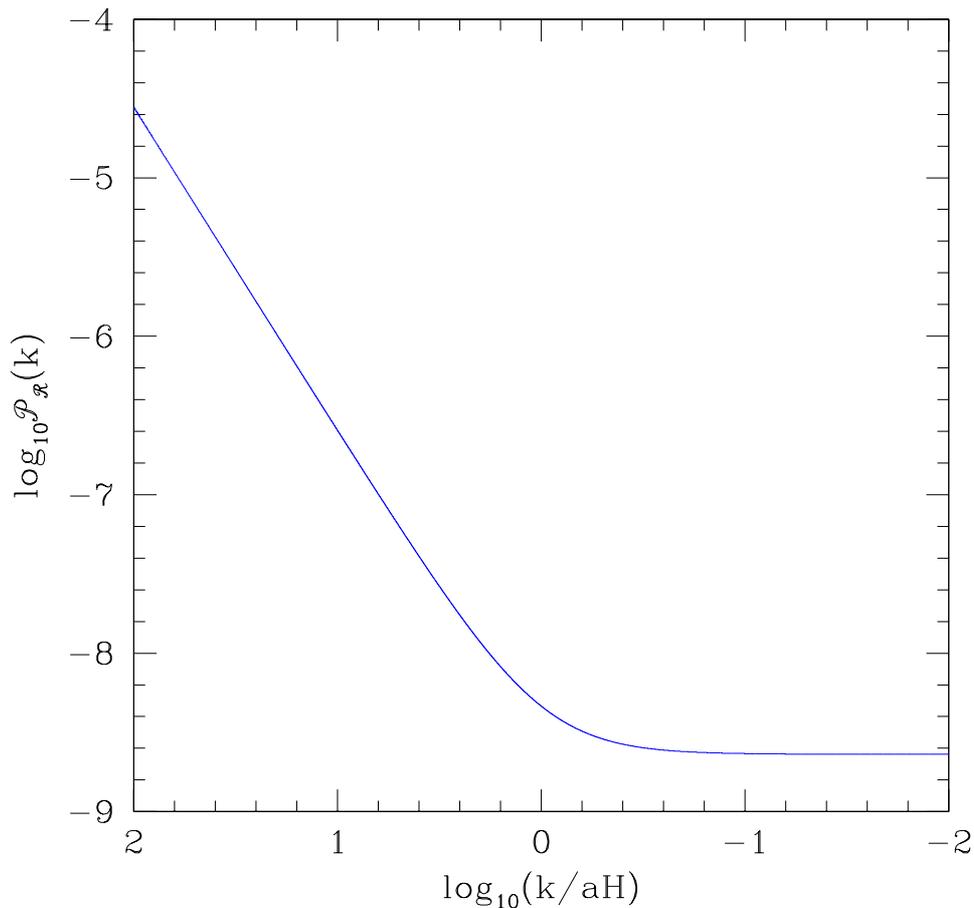
Figure 5.3: The power spectrum of the primordial curvature perturbation as a function of k/aH as perturbations evolve from sub-horizon scales to super-horizon scales for the case of a simple chaotic inflation model ($V(\varphi) \propto m^2 \varphi^2$). The amplitude at horizon crossing ($k = aH$) is larger than that in the asymptotic large-scale limit ($k/aH \to 0$).

been investigated by several authors [98, 99, 100]. Our constraints, however, only consider PBHs formed from perturbations which exited the horizon during inflation. Our constraints on the power spectrum of perturbations are therefore conservative in this respect.

The failure to reach an asymptotic super-horizon limit has been investigated by Leach & Liddle [212]. They numerically calculated the power spectrum generated by a simple quadratic chaotic inflation model and compared the results with an analytical calculation using the Stewart-Lyth equation. Their analysis involved evaluating modes at three different stages; to horizon exit, to the end of inflation, to horizon re-entry for each mode. Their results indicate that the amplitude at horizon exit is typically much greater than the other two cases, both of which are closer to the Stewart-Lyth case.

This is expected as evaluating wave modes to horizon exit would artificially amplify the power spectrum for all modes (except those near the end of inflation) compared to evaluating at the asymptotic limit (see Fig. 5.3). For modes crossing the horizon well away from the end of inflation, there is ample time for the asymptotic limit to be reached and imposing a horizon exit cutoff in the power spectrum evaluation leads to an over-estimation. Each comoving wavemode should, therefore, be evolved at least to the end of inflation defined by $N = 0$.

PBHs form from perturbations which exit and re-enter the horizon close to the end of inflation. Therefore, in order to apply our PBH constraints, it is prudent to calculate the power spectrum numerically on a mode by mode basis as described in Sec. (5.5) in order to account for any enhancement compared to the Stewart-Lyth approximation.

Fig. 5.4 shows an example inflation model selected due its proximity to our PBH bounds and with a power spectrum on large scales that is compatible with the WMAP 7 year data. From Sec. 3.8 we use the more conservative constraint on the power spectrum from PBHs ($\mathcal{P}_\mathcal{R} < 10^{-1}$). We see that the Stewart-Lyth equation leads to an acceptable power spectrum at the end of inflation with the PBH bound not violated. A numerical evaluation of the power spectrum, however, leads to this model of inflation being eliminated due to the overproduction of PBHs.

5.8 Inflation model testing - A stochastic approach

Now that we have demonstrated the virtues of a numerical analysis to predict the power spectrum of perturbations, we examine the ability of our PBH bounds to constrain models of inflation. From Fig. 5.4 we see that our PBH constraint $\mathcal{P}_\mathcal{R} < 10^{-1}$ can be used to eliminate this particular inflation model when the power spectrum is calculated numerically rather than analytically. Rather than performing a case by case model analysis, we now apply our PBH bounds to many inflation models using a stochastic technique. This then allow us to compare the use of the Stewart-Lyth equation to a numerical analysis for a large range of possible models.

Kinney [190] first used the flow equations along with a Monte Carlo approach to stochastically generate 1,000,000 inflation models to compare models of inflation with
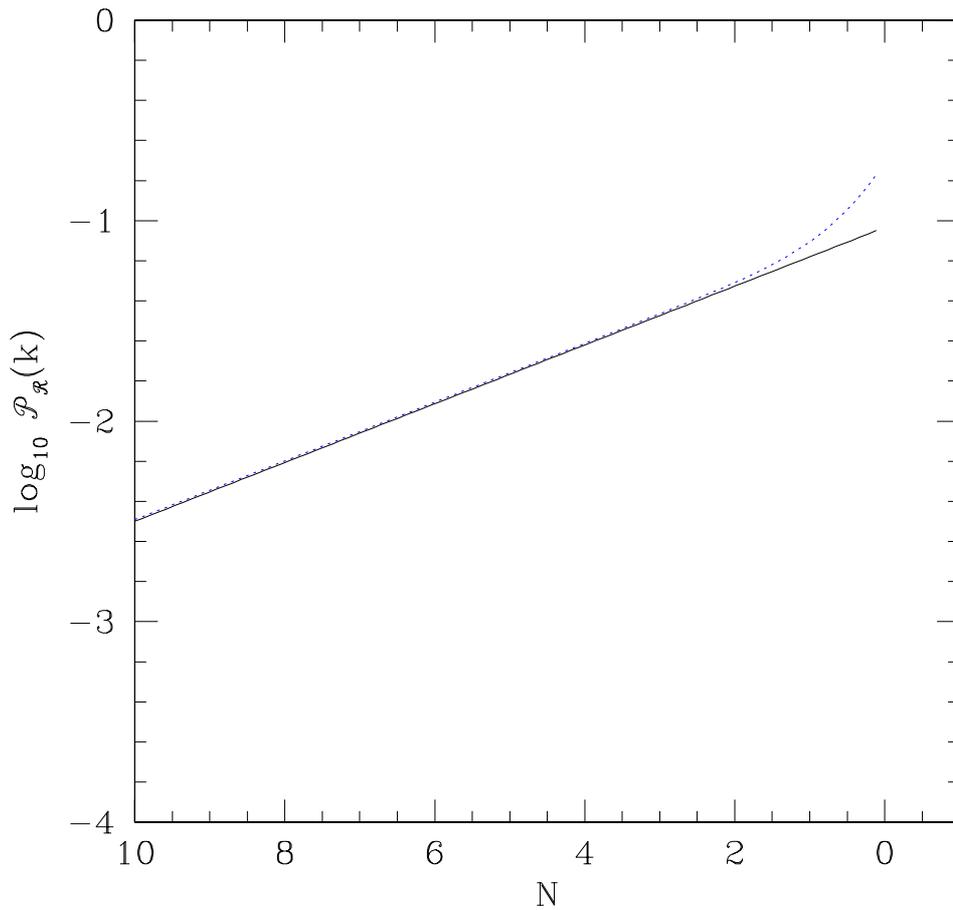
Figure 5.4: The power spectrum of the primordial curvature perturbation generated during the final few e-foldings for an example inflation model. The black solid line shows the power spectrum calculated using the Stewart-Lyth equation while the blue dotted line is the result of a numerical mode by mode calculation.

observational data. In the following we closely follow the method used by Kinney [190] to numerically generate and evolve 250,000 models of inflation. We adopt the following algorithm:

1) Select a point in the parameter space $\epsilon_H, \sigma_H, {}^l\lambda_H$ up to arbitrary order in l and specify the number of e-foldings of inflation from the current Hubble scale crossing the horizon during inflation $N_{\rm cos}$ to the end of inflation $N = 0$ (see Sec. 1.11).

2) Using the flow equations, Eqs. (5.4)-(5.6), evolve the Hubble slow-roll parameters forward in time ($dN < 0$) from the chosen number of e-foldings $N_{\rm cos}$ until either   a) inflation ends *naturally* with $\epsilon_H = 1$,   or   b) inflation ends with $N = 0$

3) If the evolution reaches $N = 0$, calculate the observables r, $n_s - 1$ and $dn_s/d\ln k$

using the values of the Hubble slow-roll parameters chosen initially.

4) If inflation ends with $\epsilon_H = 1$ before $N = 0$ is reached, evolve the Hubble slow-roll parameters, using the flow equations, backward N_{cos} e-foldings and calculate the observables at this new point. These points in the Hubble slow-roll parameter space are equivalent to the class of models Kinney calls *non-trivial points* [190].

5) In the case of inflation ending naturally at late times, $\epsilon_H = 1$ as $dN < 0$, there is the possibility that inflation also ends when evolving backward to early times, $\epsilon_H = 1$ as $dN > 0$. These models are incapable of supporting N_{cos} e-foldings of inflation and so can be discarded.

This process can then be repeated for a large number of inflation models by using a Monte Carlo approach to randomly generate combinations of initial Hubble slow-roll parameters.

5.8.1 Hubble slow-roll hierarchy

The initial Hubble slow-roll parameters are chosen within a range of values collectively known as a *hierarchy*. From Eq. (1.38) the range of ϵ_H is motivated by the requirement for inflation to occur. From Eq. (5.37), the range of σ_H is chosen so as to encompass the observed value of the spectral index. The remaining parameters are chosen within a range of values which decreases by a factor of ten each time so that the hierarchy forms a closed convergent set. This amounts to choosing a finite, albeit large, subset of an infinite number of possible initial conditions. Evolving the hierarchy using the flow equations results in the model following a certain path in the Hubble slow-roll parameter space as a function of N.

Due to the unknown physics behind reheating, the number of e-foldings of inflation between observable scales leaving the horizon during inflation and the end of inflation is somewhat ambiguous (see Sec. 1.11). A range of e-foldings is therefore also considered within the Monte Carlo approach. In our analysis we use the hierarchy suggested

by Kinney [190] along with following range of e-foldings of inflation:

$$
\begin{aligned}
N_{\text{cos}} &= [40, 60]\,, \\
\epsilon_{\text{H}} &= [0, 0.8]\,, \\
\sigma_{\text{H}} &= [-0.5, 0.5]\,, \\
{}^{2}\lambda_{\text{H}} \equiv \xi_{\text{H}} &= [-0.05, 0.05]\,, \\
{}^{3}\lambda_{\text{H}} &= [-0.005, 0.005]\,, \\
&\quad ... \\
{}^{M+1}\lambda_{\text{H}} &= 0\,.
\end{aligned}
\tag{5.41}
$$

In principle, if the hierarchy is taken to infinite order $M = \infty$ we can fully specify the shape of the inflationary potential. In practise one must truncate the hierarchy at some level. We truncate the hierarchy at $M = 6$ so as to encompass a wide variety of models. This is consistent with the work of Ramirez & Liddle [199] who show that small changes in the value of M has negligible impact on the flow analysis predictions. As the flow equations $\mathrm{d}({}^{l}\lambda_{\text{H}})/\mathrm{d}N$ only depend on the Hubble slow-roll parameters upto order $(l+1)$, evaluation of the flow equations is exact within this subset of inflation models [205].

5.8.2 Evolution to late-time asymptotic limit

Our algorithm (Sec. 5.8) differs from that originally proposed by Kinney [190] in how we handle models chosen from the initial hierarchy that are destined to inflate forever, $\epsilon_{\text{H}} \to 0$, but do not reach this limit within N_{cos} e-foldings (i.e. point 2 in the algorithm).

In the original flow algorithm suggested by Kinney the initial hierarchy is assigned at an arbitrarily early point in time $N_{\text{i}} = 1000$ (c.f. our modified algorithm where each model is evolved from N_{cos}). This is then evolved to either a) $\epsilon_{\text{H}} = 1$ where the observables are then calculated at a point N_{cos} e-foldings prior to this point or b) to a late-time attractor characterised by $\epsilon_{\text{H}} \to 0$, $\sigma_{\text{H}} \to \text{constant}$ where the cosmological observables are then calculated at this point i.e. the model is forced to evolve to its asymptotic limit where it is assumed that the entire evolution of the observable Universe lasting N_{cos} e-foldings occurs. This is reasonable if one assumes many e-folds
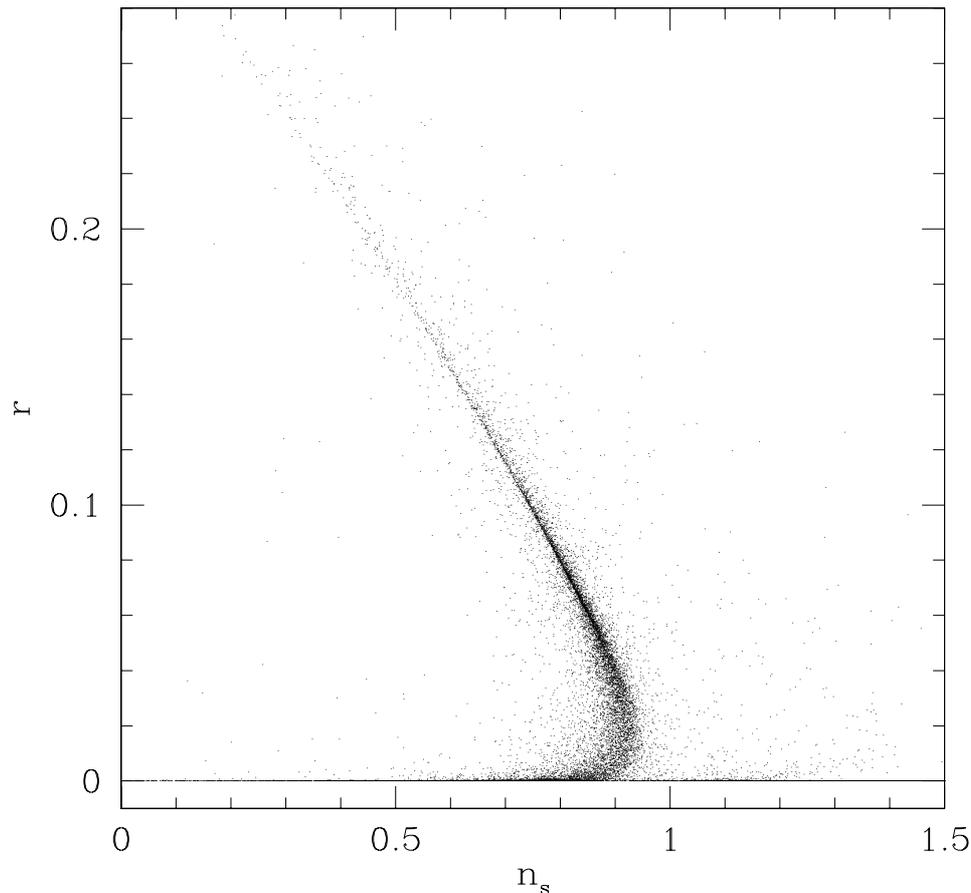
Figure 5.5: The parameter space of observables (n_s, r) obtained from a sample of 250,000 inflation models. Each model is evolved to $\epsilon_H = 1$ or to its asymptotic limit.

of inflation have passed prior to our observable scales leaving the horizon. However, an entire class of models which include those that have not yet reached a late time attractor are excluded with this algorithm. In the following work, we study the original algorithm proposed by Kinney and how this algorithm excludes inflation models which predict a significant formation of PBHs. We also use our new algorithm to include these previously excluded models and apply our PBH constraints.

We stochastically generate and test 250,000 models of inflation using the hierarchy given by Eq. (5.41) and this original algorithm suggested by Kinney [190]. The results agree with those found in Refs. [190, 199, 204] finding the characteristic features shown in Fig. 5.5 and Fig. 5.6.

In Fig. 5.5 two categories of fixed points can broadly be identified. Those resulting from models in which inflation never ends, $\epsilon_H \to 0$, but reaches an asymptotic limit
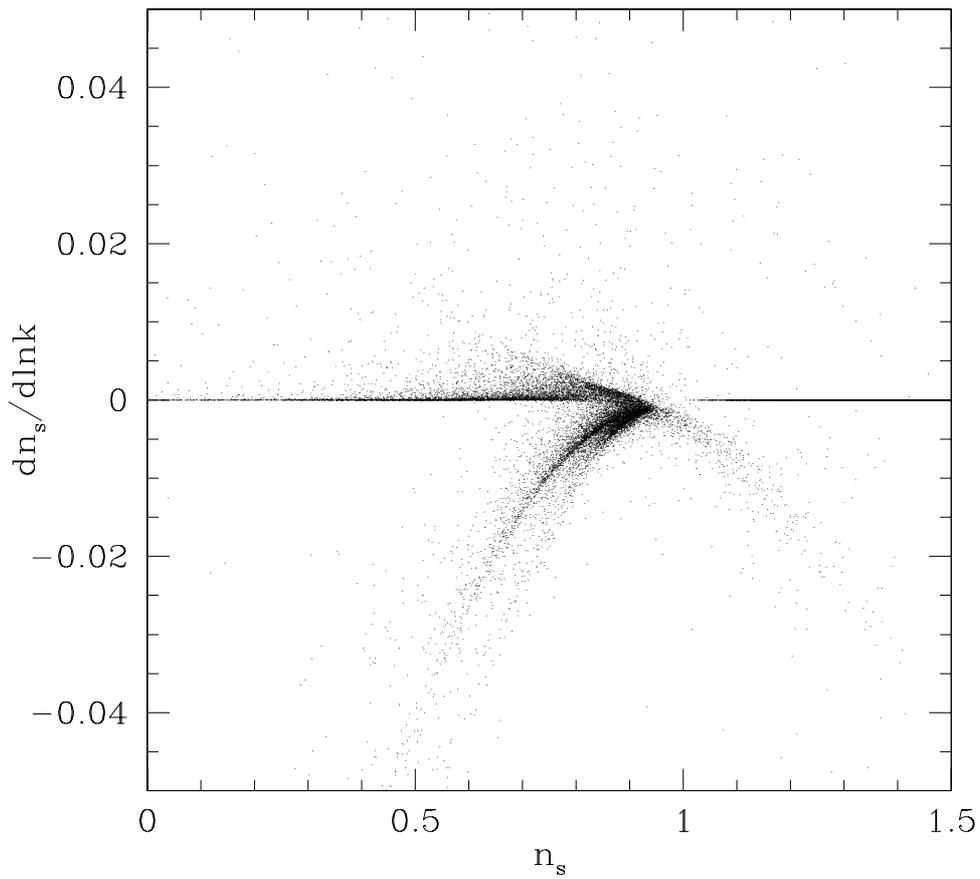
Figure 5.6: The parameter space of observables $(n_s, \mathrm{d}n_s/\mathrm{d}\ln k)$ obtained from the same sample of 250,000 inflation models. Each model is evolved to $\epsilon_\mathrm{H} = 1$ or to its asymptotic limit.

and those in which inflation ends naturally via $\epsilon_\mathrm{H} = 1$

Category 1: Models where inflation never ends, $\epsilon_\mathrm{H} \to 0$. This category accounts for 93 percent of all models tested. An asymptotic limit is identified with the inflaton field being trapped in a local minimum of the potential. Here it is assumed a secondary mechanism, such as hybrid inflation [216], acts to end inflation. The Hubble slow-roll parameters in this asymptotic limit are given by

$$\epsilon_\mathrm{H} \to 0 \,, \qquad \sigma_\mathrm{H} > 0 \,, \qquad (5.42)$$

while the large-scale cosmological observables in this limit are

$$r \to 0 \,, \qquad n_s > 1 \,. \qquad (5.43)$$

In this limit the running of the spectral index as shown in Fig. 5.6 is negligible. There-fore for models which are compatible with the WMAP 7 year measurement of the

spectral index, $n_{\rm s} = 0.963 \pm 0.014$ [9], the amplitude of the curvature perturbations can not be large on any scale and so PBHs are never formed in significant numbers [200].

Category 2: Models where inflation ends naturally, $\epsilon_{\rm H} = 1$. This category accounts for 7 percent of all models tested. The Hubble slow-roll parameters evaluated $N_{\rm cos}$ e-foldings before the end of inflation tend to two possible limiting values:

either 2a)

$$\epsilon_{\rm H} = {}^l\lambda_{\rm H} \to 0 \ , \qquad \sigma_{\rm H} < 0 \ , \tag{5.44}$$

while the large-scale cosmological observables in this limit are

$$r \to 0 \ , \qquad n_s < 1 \ . \tag{5.45}$$

or 2b)

$$\begin{aligned} \epsilon_{\rm H} &= \eta_{\rm H} = \sqrt{\xi_{\rm H}} = \text{constant} \ , \\ \Rightarrow \quad \sigma_{\rm H} &= -2\epsilon_{\rm H} \ , \end{aligned} \tag{5.46}$$

where the large-scale cosmological observables tend towards the diagonal swathe feature given by

$$r \gtrsim 0 \ , \qquad n_s < 1 \ . \tag{5.47}$$

This diagonal swathe is identified as tending towards the the power-law inflation solution (see Sec. 5.4.1).

The models within category 2 generally predict a red tilted spectral index $n_s < 1$ across all scales and so again PBHs are never formed in significant numbers.

The models within category 2 are entirely populated by the *non-trivial* class of models (i.e. models in which $\epsilon_H = 1$ ends inflation and a backwards integration by an amount $N_{\rm cos}$ is performed). The presence of this concentrated swathe of points has invited some speculation as to whether the power-law line represents a general prediction of an attractor solution for many models of inflation. However, as noted by Liddle [198] since the inflationary dynamical equations of motion, Eq. (1.33), never enters into this stochastic method of model testing, no general predictions about inflationary dynamics can be made. Rather the flow equations provide an algorithm which allows us to 'randomly' generate and evolve a large number of models.

However, it does appear from Fig. 5.5 that many models of inflation (specifically the non-trivial points) are able to spend a long time in parts of the parameter space approaching power-law inflation [198]. Although an analytical argument can be found in Ref. [204], a qualitative argument may be presented: The power spectrum, given by the Stewart-Lyth equation, Eq. (5.24), originates from an expansion about the exact case of power-law inflation (see Sec. 5.4.1). In this exact case the Hubble slow-roll parameters have 2 important properties; they are all positive and constant (see Eq. (5.16)). For those models chosen at random with initial parameter values which are all positive, one would expect from the flow equations, Eqs. (5.4)-(5.6), that $\epsilon_H \to 1$. Also for parameters chosen at random with initial values that are close to the power-law values, Eq. (5.16), one can see from the flow equations that each Hubble slow-roll parameter will have only a very small time dependence. These two initial properties, therefore, ensure that the non-trivial points necessarily share conditions which are close to the properties found in power-law inflation. The scatter around the power-law line arises from models which have parameters with a slightly stronger time dependence so that these models reach $\epsilon_H = 1$ more quickly. From our algorithm (Sec. 5.8) on evolving backward by an amount N_{cos} from this point, these models will then have more time to evolve away from the exact power-law line.

In summary, if models start exactly on the power-law line, they will remain there since the Hubble slow-roll parameters are constant and so have no time dependence. However, if the initial configuration is close to, but not exactly power-law, the model is able to remain close to the power-law solution for an amount of time dependent on how far from power-law the initial assigned values are. Hence, the region of Hubble slow-roll parameter space around the power-law line can be viewed as a temporarily stable saddle point in time. The width of the saddle (time spent in this region) depends on how far from exact power-law the initial conditions are. Beyond the saddle point on either side (forward and backward integration in time or e-foldings) the models asymptotes to a stable solution along the $r = 0$ line [190, 198].

The key point to emphasize here is that by using this original algorithm, those models which predict the overproduction of PBHs at the end of inflation are not consistent with WMAP bounds and so can be discounted. This lead Chongchitnan & Efs-

tathiou [200] to conclude that it is unlikely that PBHs would have formed from inflationary dynamics without some ad hoc feature or break in the inflationary potential. This seemed at odds with predictions of the running mass model [187, 188] as described in Sec. 5.2. Here cosmological parameters consistent with observational data are achieved on large-scales and PBHs are over-produced on small-scales. Peiris and Easther [32] have suggested the source of this difference lies in the treatment of models which are destined to inflate forever. We therefore advocate the algorithm as detailed in Sec. 5.8 rather than Kinneys original algorithm as presented in Ref. [190].

5.8.3   Evolution to $N = 0$

Following Peiris and Easther [32], we do not force models which are destined to inflate forever ($\epsilon_H \to 0$) to evolve to their asymptotic limit but instead terminate them once N_{cos} e-foldings of inflation have occurred. At this point it is assumed that another mechanism, for example a second-field such as in hybrid inflation, terminates inflation. Using this approach on the same sample of 250,000 initial conditions, the resulting observables are shown in Fig. 5.7 and Fig. 5.8

From Fig. 5.7 we see that the distinctive swathe (category 2b) of points are still present and again account for around 7 percent of all models tested. These represent the non-trivial points close to the power-law solution for which our treatment is identical to the original algorithm by Kinney [190].

Those points in category 2a still largely lie on the $r = 0$, $n_s < 1$ line. However, some of these models, which would have ended naturally ($n_s = 1$) if evolved further, are now terminated at $N = 0$ before reaching $\epsilon_H = 1$. This results in these points being spread over a larger area of parameter space with observables $r \gtrsim 0, n_s < 1$. Most interestingly however, we now see that those models destined to inflate forever (category 1: 93 percent of models where $\epsilon_H \to 0$) which previously asymptoted to the $r \to 0, n_s > 1$ line in Fig. 5.5, now populate a large region of the parameter space. From Fig. 5.8 many of these models, which in the original algorithm have negligible running in the asymptotic regime (c.f. Fig. 5.6), now have large positive running. A large proportion of these models are now also compatible with the WMAP bounds given in Sec. 1.10.
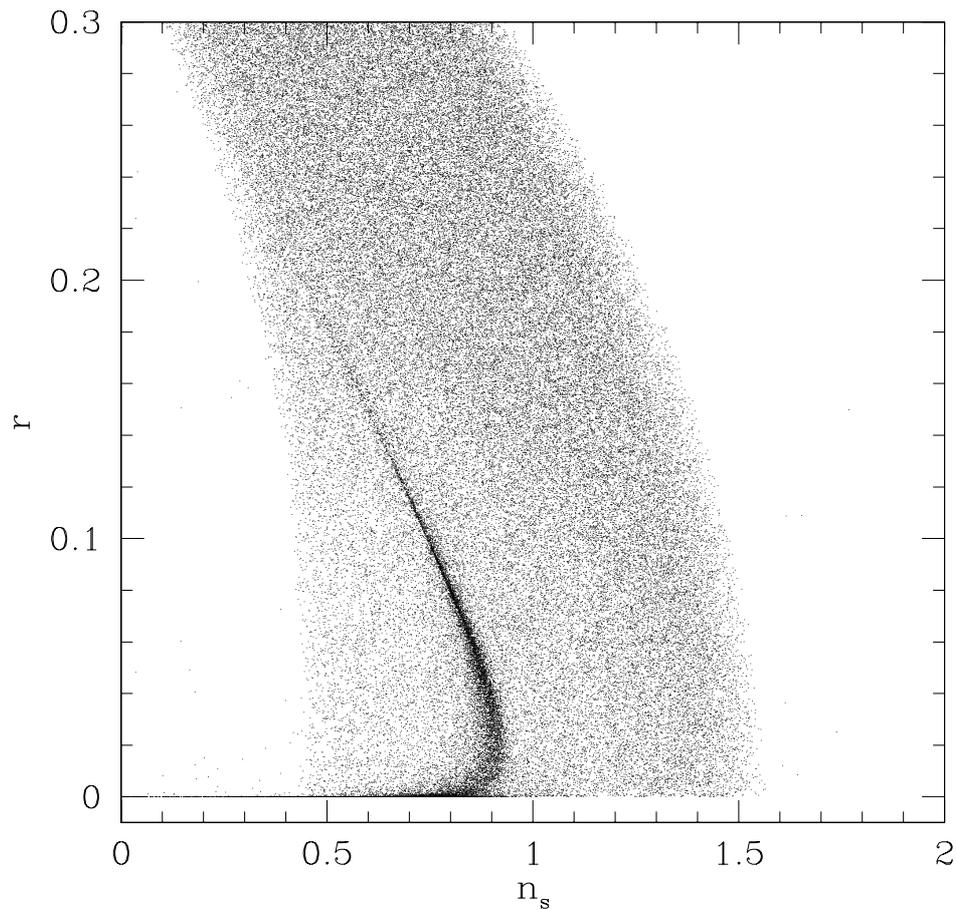
Figure 5.7: The parameter space of observables (n_s, r) obtained from the same sample of 250,000 inflation models. Models are evolved to the end of inflation defined by $N = 0$ or $\epsilon_\mathrm{H} = 1$ as discussed in the text.

Hence, with our algorithm described in Sec. 5.8, we find models which are consistent with the WMAP measurements of the spectral index and its running, but have perturbations on small scales which may be large enough to over-produce PBHs (in agreement with the findings of Ref [32]). This modified algorithm incorporates models such as the running mass model which were missed by the original algorithm.

PBH bounds can significantly constrain the variety of possible inflation models generated by this modified algorithm. Therefore, we proceed by applying our PBH constraint found in Sec. 3.8 and assessing the importance of a numerical evaluation of the power spectrum compared to an analytical assessment.
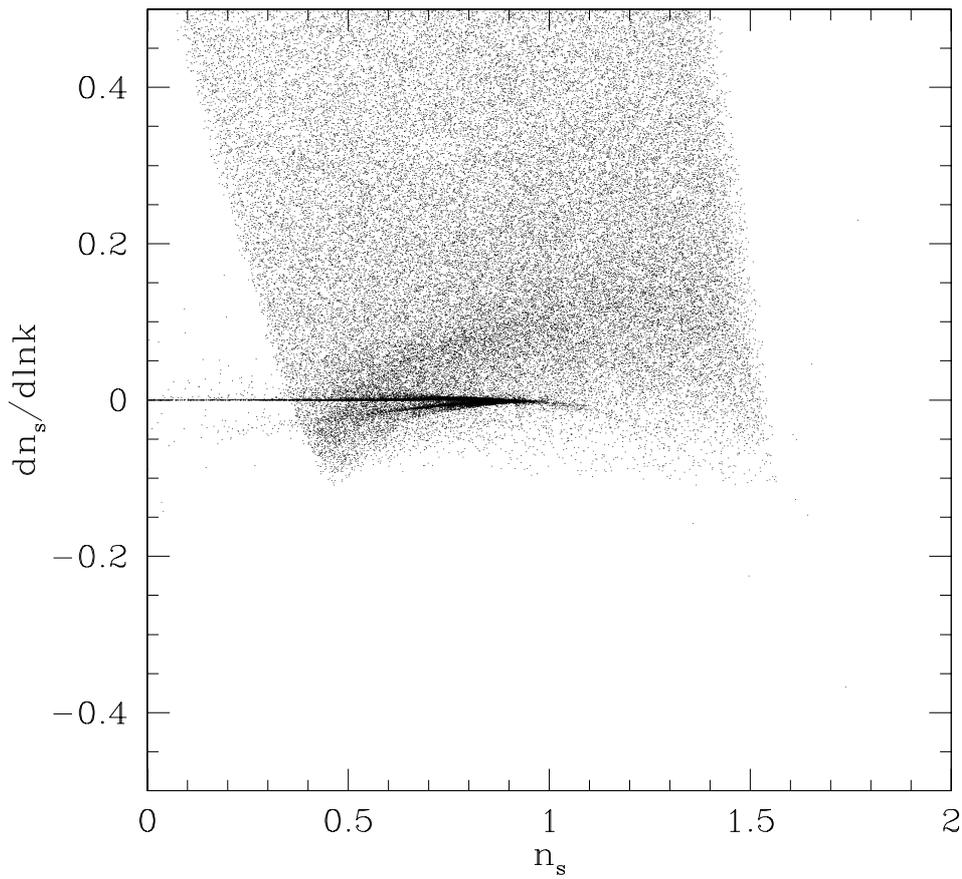
Figure 5.8: The parameter space of observables $(n_s, \mathrm{d}n_s/\mathrm{d}\ln k)$ obtained from the same sample of 250,000 inflation models. Models are evolved to the end of inflation defined by $N = 0$ or $\epsilon_{\mathrm{H}} = 1$ as discussed in the text.

5.9 PBH constraints applied to stochastically generated models of inflation

We use the modified flow algorithm described in Sec. 5.8 to generate the same ensemble (250,000) of inflation models as in Sec 5.8.3. To apply the PBH constraints we use the Stewart-Lyth expression for the power spectrum, Eq. (5.24), to identify inflation models where the amplitude of the perturbations on small scales which exit the horizon close to the end of inflation is large, and may lead to the over-production of PBHs. For these models, we then carry out an accurate numerical evolution of the primordial perturbations, as described in Sec. 5.5.

In Sec. 3.8 we compiled, and where relevant updated, the PBH abundance constraints
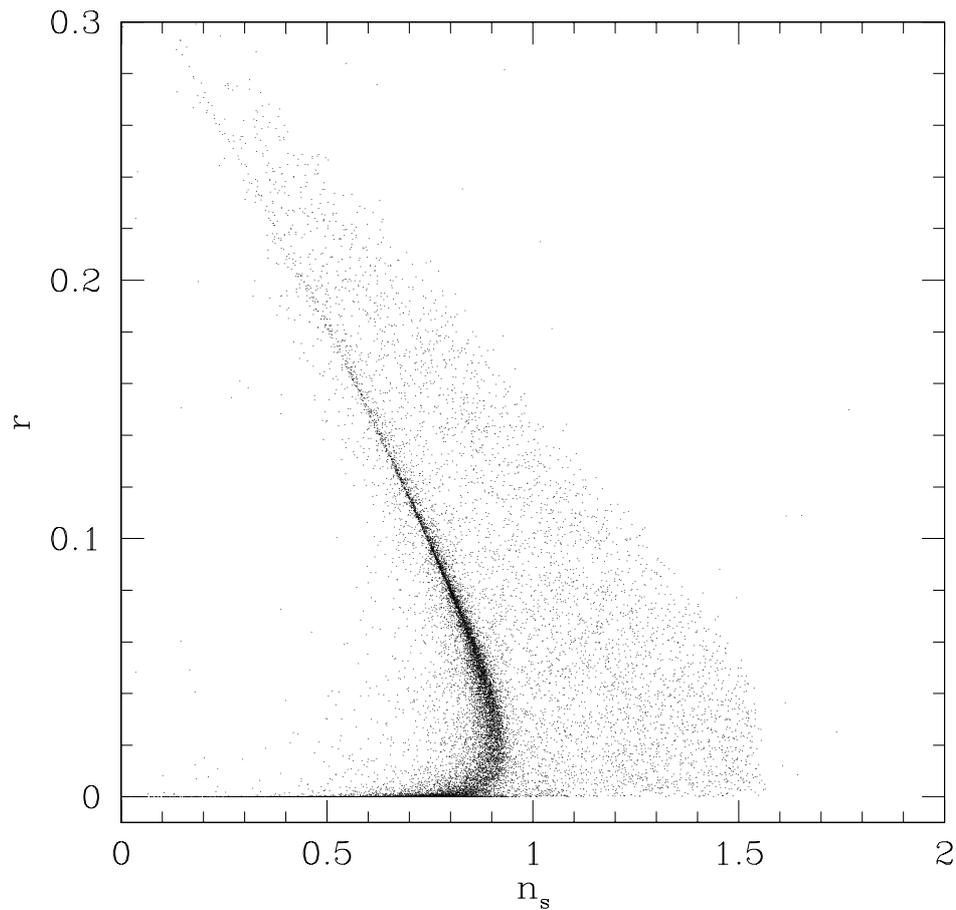
Figure 5.9: The parameter space of observables (n_s, r) obtained from the same sample of 250,000 inflation models. The power spectrum for each inflation model is calculated using the Stewart-Lyth equation and those which violate PBH bounds are excluded.

and translated these into constraints on the power spectrum of curvature perturbations. We found that $\mathcal{P}_\mathcal{R} < 10^{-2} - 10^{-1}$ in order to avoid the over production of PBHs. We use the conservative constraint $\mathcal{P}_\mathcal{R} < 10^{-1}$ to constrain models of inflation numerically. Figs. 5.9 and Figs. 5.10 show the cosmological observables for the models which remain once those which over-produce PBHs are excluded.

The 7% of original models for which inflation ends naturally (diagonal swathe) generally have $n_\mathrm{s} < 1$ on all scales and so are unaffected by the PBH constraints. Of the remaining models, in which inflation continues indefinitely ($\epsilon_\mathrm{H} \rightarrow 0$) in the absence of a secondary mechanism, 92% are excluded by PBH overproduction. Hence, of the models initially generated, only approximately 1% end via a secondary mechanism and do not overproduce PBHs. With an accurate numerical calculation of the perturbations,
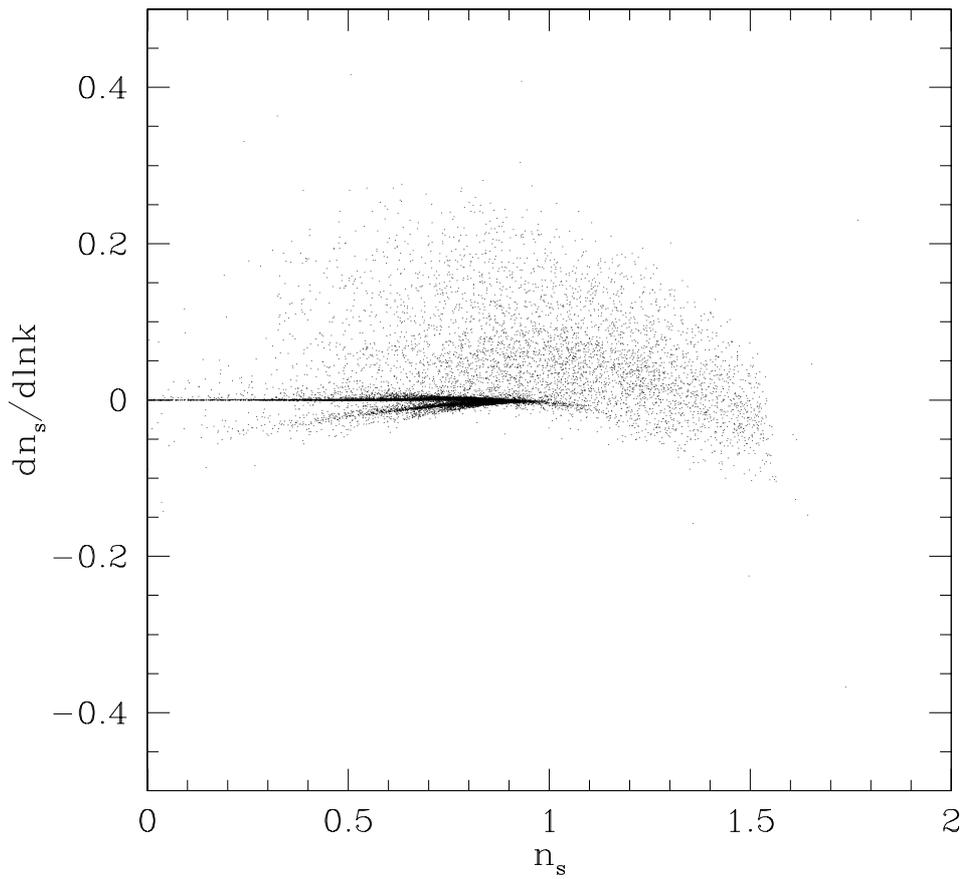
Figure 5.10: The parameter space of observables $(n_s, \mathrm{d}n_s/\mathrm{dln}k)$ obtained from the same sample of 250,000 inflation models. The power spectrum for each inflation model is calculated using the Stewart-Lyth equation and those which violate PBH bounds are excluded.

we find that the number of these models decreases by approximately 10%.

Large positive running is now excluded as expected (see Fig. 5.10). Cosmological constraints on $\mathrm{d}n_\mathrm{s}/\mathrm{dln}k$ eliminate a significant fraction of the models generated using flow algorithms [190]. A full MCMC analysis of cosmological data is beyond the scope of this work. However a simple application of the observational constraints shows that a significant fraction of cosmologically viable models are excluded by PBH constraints. Of the models generated using our modified flow analysis which have cosmological observables within the 3σ ranges found by WMAP7 [9], 19% are excluded by PBH over-production. This illustrates that in the era of precision cosmological measurements PBH still provide a powerful constraint on inflation models.

We conclude that significant PBH formation can occur in models in which inflation can

continue indefinitely and is ended via a secondary mechanism (such as hybrid infla-
tion). The algorithm presented in Sec. 5.8 finds models of inflation compatible with all
cosmological data and where the amplitude of perturbations is large on small scales.
This differs from the original algorithm used by Kinney. We demonstrate that PBH
constraints provide a significant constraint on models of inflation. Furthermore to ex-
ploit their full power an accurate numerical calculation of the amplitude of primordial
perturbations on small scales, which exit the horizon close to the end of inflation, is
required.

Chapter 6

Conclusions

WMAP and large scale structure surveys have taken us into an era of precision cosmology. In Chapter 1 we review the Big Bang and shortfalls that arise within this theory. We discuss how a period of rapidly accelerating expansion called inflation overcomes these shortfalls. A simple way of generating a period of inflation is with a scalar field (known as the inflaton field) evolving in a potential. A suitable form for the potential results in a Universe dominated by negative pressure which drives an accelerated expansion. Scalar fields, although not yet observed, have long been an integral part of particle physics. This connection between particle physics and cosmology has resulted in a much studied area of physics. We review the slow-roll formalism which relates the dynamics of the inflaton field in a potential to the dynamics of an expanding Universe.

Inflation naturally predicts the generation of perturbations in the early Universe from quantum vacuum fluctuations. This, along with the resolution of the problems associated with the Big Bang, has led to inflation becoming a part of the 'standard cosmological model' describing our Universe. In Chapter 2 we review cosmological perturbation theory and the issue of gauge ambiguity. We use metric perturbations in the comoving total matter gauge to derive a new expression relating the primordial curvature perturbations generated during inflation to density perturbations. Here we take into account the full time evolution of perturbations prior to and post horizon entry. We use this new expression to calculate constraints on the power spectrum of perturbations based on observational data from small-scale structure.

WMAP and large scale structure surveys have strongly constrained the spectrum of perturbations on very narrow range of large-scales. However, the spectrum of perturbations on small-scales is poorly constrained. Two particular examples of small-scale structure that we concentrate on are primordial black holes and ultra compact dark matter mini halos. PBHs can form from large density perturbations generated at the end of inflation. Constraints on the abundance of PBHs can be translated to constraints on the spectrum of perturbations on these small-scales. In Chapter 3 we review the criteria for PBH formation. We then compile, and where relevant, update the PBH abundance constraints. We find that to avoid the over production of PBHs, the power spectrum of curvature perturbations is constrained to $\mathcal{P}_\mathcal{R} < 10^{-2} - 10^{-1}$ across the relevant range of scales. Compared to the latest WMAP 7 year data finding $\mathcal{P}_\mathcal{R} = (2.43 \pm 0.11) \times 10^{-9}$, the PBH constraints are relatively weak. They are, however, applicable across a very wide range of scales.

In Chapter 4 we discuss the possible formation of ultra compact dark matter mini halos. These dark matter structures may form from primordial density perturbations generated by inflation in a similar manner as PBHs. We describe their formation and possible detection. If dark matter is in the form of Weakly Interacting Massive Particles (WIMPs) then WIMP annihilation may lead to a detectable gamma-ray signature. We investigate constraints on the power spectrum of perturbation in the event of detection or non-detection of gamma-rays from UCMHs by the Fermi satellite. We find that a positive detection by Fermi would place very strong constraints on the power spectrum on small scales of the order $\mathcal{P}_\mathcal{R} \gtrsim 10^{-6.6} - 10^{-5.9}$.

Finally in Chapter 5 we discuss a stochastic method of generating models of inflation. This is an important development in the area of inflation model building and is complementary to the more usual model by model approach. We apply our constraints on the primordial power spectrum from PBHs to models of inflation generated by a modified flow algorithm. The power spectrum of perturbations is usually calculated using the Stewart-Lyth expression. We demonstrate that the break down of the Stewart-Lyth equation at the end of inflation has important consequences for the application of PBH constraints. We therefore advocate a numerical approach along with our modified algorithm in order to apply PBH constraints on models of inflation.

Particle physics phenomenology has now become one of the largest areas of active research. Experiments such as the newly built Large Hadron Collider (LHC) promise to reach energies which existed during the very early Universe. However, observations from WMAP and large-scale structure provide a unique opportunity to observe the largest physics experiment. With the recent launch of the Planck satellite and continued data gathering from Fermi, the era of precision cosmology will continue to improve our understanding of the early Universe.

Bibliography

[1] A. H. Guth, *The Inflationary Universe: A Possible Solution to the Horizon and Flatness Problems*, Phys. Rev. **D23** (1981) 347–356.

[2] A. H. Guth and S. Y. Pi, *Fluctuations in the New Inflationary Universe*, Phys. Rev. Lett. **49** (1982) 1110–1113.

[3] A. A. Starobinsky, *A new type of isotropic cosmological models without singularity*, Phys. Lett. **B91** (1980) 99–102.

[4] S. W. Hawking, *The Development of Irregularities in a Single Bubble Inflationary Universe*, Phys. Lett. **B115** (1982) 295.

[5] B. J. Carr, K. Kohri, Y. Sendouda and J. Yokoyama, *New cosmological constraints on primordial black holes*, Phys. Rev. **D81** (2010) 104019 [0912.5297].

[6] A. S. Josan, A. M. Green and K. A. Malik, *Generalised constraints on the curvature perturbation from primordial black holes*, Phys. Rev. **D79** (2009) 103520 [arXiv:0903.3184].

[7] A. S. Josan and A. M. Green, *Gamma-rays from ultracompact minihalos: potential constraints on the primordial curvature perturbation*, arXiv:1006.4970.

[8] E. Hubble, *A relation between distance and radial velocity among extra–galactic nebulae*, Proc. Nat. Acad. Sci. **15** (1929) 168–173.

[9] E. Komatsu *et. al.*, *Seven-Year Wilkinson Microwave Anisotropy Probe (WMAP) Observations: Cosmological Interpretation*, arXiv:1001.4538.

[10] A. Einstein, *The foundation of the general theory of relativity*, Annalen Phys. **49** (1916) 769–822.

[11] Supernova Search Team Collaboration, A. G. Riess *et. al.*, *Observational Evidence from Supernovae for an Accelerating Universe and a Cosmological Constant*, Astron. J. **116** (1998) 1009–1038 [astro-ph/9805201].

[12] Supernova Cosmology Project Collaboration, S. Perlmutter *et. al.*, *Measurements of Omega and Lambda from 42 High-Redshift Supernovae*, Astrophys. J. **517** (1999) 565–586 [astro-ph/9812133].

[13] E. J. Copeland, M. Sami and S. Tsujikawa, *Dynamics of dark energy*, *Int. J. Mod. Phys.* **D15** (2006) 1753–1936 [hep-th/0603057].

[14] R. Bean, *TASI Lectures on Cosmic Acceleration*, 1003.4468.

[15] A. A. Penzias and R. W. Wilson, *A Measurement of excess antenna temperature at 4080- Mc/s*, *Astrophys. J.* **142** (1965) 419–421.

[16] G. F. Smoot *et. al.*, *Structure in the COBE differential microwave radiometer first year maps*, *Astrophys. J.* **396** (1992) L1–L5.

[17] R. K. Sachs and A. M. Wolfe, *Perturbations of a cosmological model and angular variations of the microwave background*, *Astrophys. J.* **147** (1967) 73–90.

[18] D. H. Lyth and A. R. Liddle, *The primordial density perturbation: Cosmology, inflation and the origin of structure*. Cambridge, UK: Cambridge Univ. Pr. (2009) 497 p.

[19] N. Jarosik *et. al.*, *Seven-Year Wilkinson Microwave Anisotropy Probe (WMAP) Observations: Sky Maps, Systematic Errors, and Basic Results*, 1001.4744.

[20] T. W. B. Kibble, *Topology of Cosmic Domains and Strings*, *J. Phys.* **A9** (1976) 1387–1398.

[21] C. T. Hill, D. N. Schramm and J. N. Fry, *Cosmological structure formation from soft topological defects*, *Comments Nucl. Part. Phys.* **19** (1989) 25.

[22] R. H. Brandenberger, *Topological defects and structure formation*, *Int. J. Mod. Phys.* **A9** (1994) 2117–2190 [astro-ph/9310041].

[23] R. Durrer, M. Kunz and A. Melchiorri, *Cosmic structure formation with topological defects*, *Phys. Rept.* **364** (2002) 1–81 [astro-ph/0110348].

[24] A. D. Linde, *Scalar Field Fluctuations in Expanding Universe and the New Inflationary Universe Scenario*, *Phys. Lett.* **B116** (1982) 335.

[25] A. A. Starobinsky, *Dynamics of Phase Transition in the New Inflationary Universe Scenario and Generation of Perturbations*, *Phys. Lett.* **B117** (1982) 175–178.

[26] D. S. Salopek and J. R. Bond, *Nonlinear evolution of long wavelength metric fluctuations in inflationary models*, *Phys. Rev.* **D42** (1990) 3936–3962.

[27] A. R. Liddle, P. Parsons and J. D. Barrow, *Formalizing the slow roll approximation in inflation*, *Phys. Rev.* **D50** (1994) 7222–7232 [arXiv:astro-ph/9408015].

[28] A. R. Liddle and D. H. Lyth, *Cosmological Inflation and Large-Scale Structure*. Cambridge University Press, 2000.

[29] J. M. Bardeen, P. J. Steinhardt and M. S. Turner, *Spontaneous Creation of Almost Scale - Free Density Perturbations in an Inflationary Universe*, *Phys. Rev.* **D28** (1983) 679.

[30] D. H. Lyth, *Large Scale Energy Density Perturbations and Inflation*, *Phys. Rev.* **D31** (1985) 1792–1798.

[31] A. R. Liddle and S. M. Leach, *How long before the end of inflation were observable perturbations produced?*, *Phys. Rev.* **D68** (2003) 103503 [astro-ph/0305263].

[32] H. V. Peiris and R. Easther, *Primordial Black Holes, Eternal Inflation, and the Inflationary Parameter Space after WMAP5*, *JCAP* **0807** (2008) 024 [arXiv:0805.2154].

[33] J. Khoury, B. A. Ovrut, P. J. Steinhardt and N. Turok, *The ekpyrotic universe: Colliding branes and the origin of the hot big bang*, *Phys. Rev.* **D64** (2001) 123522 [hep-th/0103239].

[34] J. Khoury, B. A. Ovrut, N. Seiberg, P. J. Steinhardt and N. Turok, *From big crunch to big bang*, *Phys. Rev.* **D65** (2002) 086007 [hep-th/0108187].

[35] J. Khoury, B. A. Ovrut, P. J. Steinhardt and N. Turok, *Density perturbations in the ekpyrotic scenario*, *Phys. Rev.* **D66** (2002) 046005 [hep-th/0109050].

[36] J. M. Bardeen, *Gauge Invariant Cosmological Perturbations*, *Phys. Rev.* **D22** (1980) 1882–1905.

[37] K. A. Malik and D. Wands, *Cosmological perturbations*, arXiv:0809.4944.

[38] K. A. Malik, *Cosmological perturbations in an inflationary universe*, astro-ph/0101563.

[39] H. Kodama and M. Sasaki, *Cosmological Perturbation Theory*, *Prog. Theor. Phys. Suppl.* **78** (1984) 1–166.

[40] V. F. Mukhanov, H. A. Feldman and R. H. Brandenberger, *Theory of cosmological perturbations. Part 1. Classical perturbations. Part 2. Quantum theory of perturbations. Part 3. Extensions*, *Phys. Rept.* **215** (1992) 203–333.

[41] J. C. Hwang, *Curved space quantum scalar field theory with accompanying metric fluctuations*, *Phys. Rev.* **D48** (1993) 3544–3556.

[42] A. Riotto, *Inflation and the theory of cosmological perturbations*, hep-ph/0210162.

[43] J. Martin and D. J. Schwarz, *The influence of cosmological transitions on the evolution of density perturbations*, *Phys. Rev.* **D57** (1998) 3302–3316 [gr-qc/9704049].

[44] D. Wands, K. A. Malik, D. H. Lyth and A. R. Liddle, *A new approach to the evolution of cosmological perturbations on large scales*, *Phys. Rev.* **D62** (2000) 043527 [astro-ph/0003278].

[45] A. M. Green, A. R. Liddle, K. A. Malik and M. Sasaki, *A new calculation of the mass fraction of primordial black holes*, *Phys. Rev.* **D70** (2004) 041502 [arXiv:astro-ph/0403181].

[46] A. M. Green, S. Hofmann and D. J. Schwarz, *The first WIMPy halos*, JCAP **0508** (2005) 003 [arXiv:astro-ph/0503387].

[47] Zel'Dovich, Y. B. and Novikov, I. D., *The Hypothesis of Cores Retarded during Expansion and the Hot Cosmological Model*, *Soviet Astronomy* **10** (1967) 602.

[48] S. Hawking, *Gravitationally collapsed objects of very low mass*, *Mon. Not. Roy. Astron. Soc.* **152** (1971) 75.

[49] B. J. Carr and S. W. Hawking, *Black holes in the early Universe*, *Mon. Not. Roy. Astron. Soc.* **168** (1974) 399–415.

[50] K. Jedamzik, *Primordial black hole formation during the QCD epoch*, *Phys. Rev.* **D55** (1997) 5871–5875 [astro-ph/9605152].

[51] K. Jedamzik and J. C. Niemeyer, *Primordial Black Hole Formation during First-Order Phase Transitions*, *Phys. Rev.* **D59** (1999) 124014 [astro-ph/9901293].

[52] S. W. Hawking, *BLACK HOLES FROM COSMIC STRINGS*, *Phys. Lett.* **B231** (1989) 237.

[53] M. Nagasawa, *Primordial black hole formation by stabilized embedded strings in the early universe*, *Gen. Rel. Grav.* **37** (2005) 1635–1649.

[54] V. A. Berezin, V. A. Kuzmin and I. I. Tkachev, *THIN WALL VACUUM DOMAINS EVOLUTION*, *Phys. Lett.* **B120** (1983) 91.

[55] S. G. Rubin, A. S. Sakharov and M. Y. Khlopov, *The formation of primary galactic nuclei during phase transitions in the early universe*, *J. Exp. Theor. Phys.* **91** (2001) 921–929 [hep-ph/0106187].

[56] M. Crawford and D. N. Schramm, *Spontaneous generation of density perturbations in the early universe*, *Nature* **298** (1982) 538–540.

[57] R. V. Konoplich, S. G. Rubin, A. S. Sakharov and M. Y. Khlopov, *Formation of black holes in first-order phase transitions as a cosmological test of symmetry-breaking mechanisms*, *Phys. Atom. Nucl.* **62** (1999) 1593–1600.

[58] B. J. Carr, *Primordial Black Holes: Do They Exist and Are They Useful?*, arXiv:astro-ph/0511743.

[59] B. J. Carr, *Primordial black holes - recent developments*, astro-ph/0504034.

[60] M. Y. Khlopov, *Primordial Black Holes*, arXiv:0801.0116.

[61] B. J. Carr, *Some cosmological consequences of primordial black-hole evaporations*, *Astrophys. J.* **206** (1976) 8–25.

[62] D. N. Page and S. W. Hawking, *Gamma rays from primordial black holes*, *Astrophys. J.* **206** (1976) 1–7.

[63] D. N. Page, *Particle Emission Rates from a Black Hole: Massless Particles from an Uncharged, Nonrotating Hole*, *Phys. Rev.* **D13** (1976) 198–206.

[64] J. H. MacGibbon and B. J. Carr, *Cosmic rays from primordial black holes*, *Astrophys. J.* **371** (1991) 447–469.

[65] T. N. Ukwatta *et. al.*, *Sensitivity of the FERMI Detectors to Gamma-Ray Bursts from Evaporating Primordial Black Holes (PBHs)*, 1003.4515.

[66] A. Gould, *Femtolensing of gamma-ray bursters*, *Astrophys. J.* **386** (1992) L5–L7.

[67] C. R. Canizares, *Manifestations of a cosmological density of compact objects in quasar light*, *Astrophys. J.* **263** (1982) 508–517.

[68] A. Kassiola, I. Kovner and R. D. Blandford, *Bounds on intergalactic compact objects from observations of compact radio sources*, *Astrophys. J.* **381** (1991) 6–13.

[69] (Macho) C. Alcock Collaboration, R. A. Allsman *et. al.*, *MACHO Project Limits on Black Hole Dark Matter in the 1-30 Solar Mass Range*, astro-ph/0011506.

[70] D. Blais, C. Kiefer and D. Polarski, *Can primordial black holes be a significant part of dark matter?*, *Phys. Lett.* **B535** (2002) 11–16 [astro-ph/0203520].

[71] I. D. Novikov, A. G. Polnarev, A. A. Starobinskii and I. B. Zeldovich, *Primordial black holes*, A&A **80** (Nov., 1979) 104–109.

[72] B. J. Carr, J. H. Gilbert and J. E. Lidsey, *Black hole relics and inflation: Limits on blue perturbation spectra*, *Phys. Rev.* **D50** (1994) 4853–4867 [arXiv:astro-ph/9405027].

[73] A. M. Green and A. R. Liddle, *Constraints on the density perturbation spectrum from primordial black holes*, *Phys. Rev.* **D56** (1997) 6166–6174 [arXiv:astro-ph/9704251].

[74] A. R. Liddle and A. M. Green, *Cosmological constraints from primordial black holes*, *Phys. Rept.* **307** (1998) 125–131 [gr-qc/9804034].

[75] B. Carr, edited by J.L Sanz and L. Goicoechea, eds., *in Observational and theoretical aspects of relativistic astrophysics and cosmology*, (World Scientific Singapore), 1985.

[76] T. Harada and B. J. Carr, *Upper limits on the size of a primordial black hole*, *Phys. Rev.* **D71** (2005) 104009 [astro-ph/0412134].

[77] I. Musco, J. C. Miller and L. Rezzolla, *Computations of primordial black hole formation*, *Class. Quant. Grav.* **22** (2005) 1405–1424 [arXiv:gr-qc/0412063].

[78] M. W. Choptuik, *Universality and scaling in gravitational collapse of a massless scalar field*, *Phys. Rev. Lett.* **70** (1993) 9–12.

[79] C. Gundlach, *Critical phenomena in gravitational collapse*, *Phys. Rept.* **376** (2003) 339–405 [arXiv:gr-qc/0210101].

[80] C. Gundlach and J. M. Martin-Garcia, *Critical phenomena in gravitational collapse*, *Living Rev. Rel.* **10** (2007) 5 [arXiv:0711.4620].

[81] J. C. Niemeyer and K. Jedamzik, *Near-Critical Gravitational Collapse and the Initial Mass Function of Primordial Black Holes*, *Phys. Rev. Lett.* **80** (1998) 5481–5484 [arXiv:astro-ph/9709072].

[82] J. C. Niemeyer and K. Jedamzik, *Dynamics of Primordial Black Hole Formation*, *Phys. Rev.* **D59** (1999) 124013 [arXiv:astro-ph/9901292].

[83] M. Shibata and M. Sasaki, *Black hole formation in the Friedmann universe: Formulation and computation in numerical relativity*, *Phys. Rev.* **D60** (1999) 084002 [arXiv:gr-qc/9905064].

[84] J. M. Bardeen, J. R. Bond, N. Kaiser and A. S. Szalay, *The Statistics of Peaks of Gaussian Random Fields*, *Astrophys. J.* **304** (1986) 15–61.

[85] S. W. Hawking, *Black hole explosions*, *Nature* **248** (1974) 30–31.

[86] S. W. Hawking, *Particle Creation by Black Holes*, *Commun. Math. Phys.* **43** (1975) 199–220.

[87] J. H. MacGibbon and B. R. Webber, *Quark and gluon jet emission from primordial black holes: The instantaneous spectra*, *Phys. Rev.* **D41** (1990) 3052–3079.

[88] J. H. MacGibbon, *Quark and gluon jet emission from primordial black holes. 2. The Lifetime emission*, *Phys. Rev.* **D44** (1991) 376–392.

[89] WMAP Collaboration, J. Dunkley *et. al.*, *Five-Year Wilkinson Microwave Anisotropy Probe (WMAP) Observations: Likelihoods and Parameters from the WMAP data*, *Astrophys. J. Suppl.* **180** (2009) 306–329 [arXiv:0803.0586].

[90] J. H. MacGibbon, B. J. Carr and D. N. Page, *Do Evaporating Black Holes Form Photospheres?*, *Phys. Rev.* **D78** (2008) 064043 [arXiv:0709.2380].

[91] The 2dFGRS Collaboration, S. Cole *et. al.*, *The 2dF Galaxy Redshift Survey: Power-spectrum analysis of the final dataset and cosmological implications*, *Mon. Not. Roy. Astron. Soc.* **362** (2005) 505–534 [arXiv:astro-ph/0501174].

[92] SDSS Collaboration, M. Tegmark *et. al.*, *Cosmological Constraints from the SDSS Luminous Red Galaxies*, *Phys. Rev.* **D74** (2006) 123507 [arXiv:astro-ph/0608632].

[93] H. Peiris and R. Easther, *Slow Roll Reconstruction: Constraints on Inflation from the 3 Year WMAP Dataset*, *JCAP* **0610** (2006) 017 [arXiv:astro-ph/0609003].

[94] B. J. Carr and J. E. Lidsey, *Primordial black holes and generalized constraints on chaotic inflation*, *Phys. Rev.* **D48** (1993) 543–553.

[95] H. I. Kim and C. H. Lee, *Constraints on the spectral index from primordial black holes*, *Phys. Rev.* **D54** (1996) 6001–6007.

[96] T. Bringmann, C. Kiefer and D. Polarski, *Primordial black holes from inflationary models with and without broken scale invariance*, Phys. Rev. **D65** (2002) 024008 [arXiv:astro-ph/0109404].

[97] A. Vallinotto, E. J. Copeland, E. W. Kolb, A. R. Liddle and D. A. Steer, *Inflationary potentials yielding constant scalar perturbation spectral indices*, Phys. Rev. **D69** (2004) 103519 [arXiv:astro-ph/0311005].

[98] D. H. Lyth, K. A. Malik, M. Sasaki and I. Zaballa, *Forming sub-horizon black holes at the end of inflation*, JCAP **0601** (2006) 011 [arXiv:astro-ph/0510647].

[99] I. Zaballa, A. M. Green, K. A. Malik and M. Sasaki, *Constraints on the primordial curvature perturbation from primordial black holes*, JCAP **0703** (2007) 010 [arXiv:astro-ph/0612379].

[100] I. Zaballa and M. Sasaki, *Boosted perturbations at the end of inflation*, arXiv:0911.2069.

[101] J. C. Hidalgo, *The effect of non-Gaussian curvature perturbations on the formation of primordial black holes*, arXiv:0708.3875.

[102] J. C. Hidalgo and A. G. Polnarev, *Probability of primordial black hole formation and its dependence on the radial profile of initial configurations*, Phys. Rev. **D79** (2009) 044006 [arXiv:0806.2752].

[103] E. W. Kolb and M. S. Turner, *The Early universe*, Front. Phys. **69** (1990) 1–547.

[104] B. J. Carr, *The Primordial black hole mass spectrum*, Astrophys. J. **201** (1975) 1–19.

[105] H. I. Kim, C. H. Lee and J. H. MacGibbon, *Diffuse gamma-ray background and primordial black hole constraints on the spectral index of density fluctuations*, Phys. Rev. **D59** (1999) 063004 [arXiv:astro-ph/9901030].

[106] A. M. Green and A. R. Liddle, *Critical collapse and the primordial black hole initial mass function*, Phys. Rev. **D60** (1999) 063509 [arXiv:astro-ph/9901268].

[107] J. Yokoyama, *Cosmological constraints on primordial black holes produced in the near-critical gravitational collapse*, Phys. Rev. **D58** (1998) 107502 [gr-qc/9804041].

[108] A. M. Green, *Viability of evaporating primordial black holes as short period gamma-ray bursts*, Phys. Rev. **D65** (2002) 027301 [astro-ph/0105253].

[109] G. D. Kribs, A. K. Leibovich and I. Z. Rothstein, *Bounds from Primordial Black Holes with a Near Critical Collapse Initial Mass Function*, Phys. Rev. **D60** (1999) 103510 [arXiv:astro-ph/9904021].

[110] E. V. Bugaev and K. V. Konishchev, *Constraints on diffuse neutrino background from primordial black holes*, Phys. Rev. **D65** (2002) 123005 [arXiv:astro-ph/0005295].

[111] E. V. Bugaev and K. V. Konishchev, *Cosmological constraints from evaporations of primordial black holes*, Phys. Rev. **D66** (2002) 084004 [arXiv:astro-ph/0206082].

[112] A. Barrau, D. Blais, G. Boudoul and D. Polarski, *Galactic Cosmic Rays from PBHs and Primordial Spectra with a Scale*, Phys. Lett. **B551** (2003) 218–225 [arXiv:astro-ph/0210149].

[113] E. Bugaev and P. Klimai, *Constraints on amplitudes of curvature perturbations from PBHs*, arXiv:0812.4247.

[114] W. H. Press and J. E. Gunn, *Method for Detecting a Cosmological Density of Condensed Objects*, Astrophys. J. **185** (1973) 397–412.

[115] J. J. Dalcanton, C. R. Canizares, A. Granados, C. C. Steidel and J. T. Stocke, *Observational limits on omega in stars, brown dwarfs, and stellar remnants from gravitational microlensing*, Astrophys. J. **424** (1994) 550–568.

[116] G. F. Marani, R. J. Nemiroff, J. P. Norris, K. Hurley and J. T. Bonnell, *Gravitationally Lensed Gamma-Ray Bursts as Probes of Dark Compact Objects*, Astrophys. J. Lett. **512** (1999) L13–L16 [arXiv:astro-ph/9810391].

[117] P. N. Wilkinson *et. al.*, *Limits on the cosmological abundance of supermassive compact objects from a search for multiple imaging in compact radio sources*, Phys. Rev. Lett. **86** (2001) 584–587 [arXiv:astro-ph/0101328].

[118] B. Paczynski, *Gravitational microlensing by the galactic halo*, Astrophys. J. **304** (1986) 1–5.

[119] K. Griest, *galactic microlensing as a method of detecting massive compact halo objects*, Astrophys. J. **366** (1991) 412–421.

[120] MACHO Collaboration, C. Alcock *et. al.*, *The macho project: Microlensing results from 5.7 years of lmc observations*, Astrophys. J. **542** (2000) 281–307 [arXiv:astro-ph/0001272].

[121] EROS-2 Collaboration, P. Tisserand *et. al.*, *Limits on the macho content of the galactic halo from the eros-2 survey of the magellanic clouds*, Astron. Astrophys. **469** (2007) 387–404 [arXiv:astro-ph/0607207].

[122] C. Alcock *et. al.*, *EROS and MACHO Combined Limits on Planetary-Mass Dark Matter in the Galactic Halo*, Astrophys. J. Lett. **499** (1998) L9–L12 [arXiv:astro-ph/9803082].

[123] H. A. Abt, *Normal and abnormal binary frequencies*, Ann. Rev. Astron. Astrophys. **21** (1983) 343–372.

[124] D. A. Fischer and G. W. Marcy, *Multiplicity among M dwarfs*, Astrophys. J. **396** (1992) 178–194.

[125] J. N. Bahcall, P. Hut and S. Tremaine, *Maximum mass of objects that constitute unseen disk material*, Astrophys. J. **290** (1985) 15–20.

[126] M. D. Weinberg, S. L. Shapiro and I. Wasserman, *The dynamical fate of wide binaries in the solar neighborhood*, Astrophys. J. **312** (1987) 367–389.

[127] J. Chaname and A. Gould, *Disk and Halo Wide Binaries from the Revised Luyten Catalog: Probes of Star Formation and MACHO Dark Matter*, Astrophys. J. **601** (2004) 289–310 [astro-ph/0307434].

[128] J. Yoo, J. Chaname and A. Gould, *The End of the MACHO Era: Limits on Halo Dark Matter from Stellar Halo Wide Binaries*, Astrophys. J. **601** (2004) 311–318 [arXiv:astro-ph/0307437].

[129] D. P. Quinn *et. al.*, *On the Reported Death of the MACHO Era*, arXiv:0903.1644.

[130] C. G. Lacey and J. P. Ostriker, *Massive black holes in galactic halos?*, ApJ **299** (Dec., 1985) 633–652.

[131] B. J. Carr and M. Sakellariadou, *Dynamical constraints on dark compact objects*, Astrophys. J. **516** (1999) 195–220.

[132] B. Carr, *Some cosmological consequences of primordial black-hole evaporations*, Astrophys. J. **206** (1976) 8–25.

[133] F. Halzen, E. Zas, J. H. MacGibbon and T. C. Weekes, *Gamma-rays and energetic particles from primordial black holes*, Nature **353** (1991) 807–815.

[134] K. Yoshimura, *Cosmic-ray antiprotons and antinuclei*, Advances in Space Research **27** (2001) 693–703.

[135] A. Barrau *et. al.*, *Antideuterons as a probe of primordial black holes*, Astron. Astrophys. **398** (2003) 403–410 [arXiv:astro-ph/0207395].

[136] B. V. Vainer and P. D. Naselskii, *Observational consequences of the evaporation of low-mass primordial black holes*, Pis ma Astronomicheskii Zhurnal **3** (1977) 147–151.

[137] S. Miyama and K. Sato, *the upper bound of the number density of primordial black holes from the big bang nucleosynthesis*, Prog. Theor. Phys. **59** (1978) 1012.

[138] I. B. Zeldovich, A. A. Starobinskii, M. I. Khlopov and V. M. Chechetkin, *Primordial black holes and the deuterium problem*, Soviet Astronomy Letters **3** (1977) 110–112.

[139] B. V. Vainer, O. V. Dryzhakova and P. D. Naselskii, *Primordial black holes and cosmological nucleosynthesis*, Soviet Astronomy Letters **4** (1978) 185–187.

[140] K. Kohri and J. Yokoyama, *Primordial black holes and primordial nucleosynthesis. I: Effects of hadron injection from low mass holes*, Phys. Rev. **D61** (2000) 023501 [arXiv:astro-ph/9908160].

[141] D. Lindley, *Primordial black holes and the deuterium abundance*, Mon. Not. Roy. Astron. Soc. **193** (1980) 593–601.

[142] D. Clancy, R. Guedens and A. R. Liddle, *Primordial black holes in braneworld cosmologies: Astrophysical constraints*, Phys. Rev. **D68** (2003) 023507 [arXiv:astro-ph/0301568].

[143] P. D. Naselskii, *Hydrogen recombination kinetics in the presence of low-mass primordial black holes*, Soviet Astronomy Letters **4** (1978) 209–211.

[144] J. C. Mather *et. al.*, *Measurement of the Cosmic Microwave Background spectrum by the COBE FIRAS instrument*, Astrophys. J. **420** (1994) 439–444.

[145] H. Tashiro and N. Sugiyama, *Constraints on Primordial Black Holes by Distortions of Cosmic Microwave Background*, Phys. Rev. **D78** (2008) 023004 [arXiv:0801.3172].

[146] A. M. Green, *Supersymmetry and primordial black hole abundance constraints*, Phys. Rev. **D60** (1999) 063516 [arXiv:astro-ph/9903484].

[147] M. Lemoine, *Moduli constraints on primordial black holes*, Phys. Lett. **B481** (2000) 333–338 [arXiv:hep-ph/0001238].

[148] M. Y. Khlopov, A. Barrau and J. Grain, *Gravitino production by primordial black hole evaporation and constraints on the inhomogeneity of the early universe*, Class. Quant. Grav. **23** (2006) 1875–1882 [arXiv:astro-ph/0406621].

[149] J. H. MacGibbon, *Can Planck-mass relics of evaporating black holes close the universe?*, Nature **329** (1987) 308–309.

[150] M. J. Bowick, S. B. Giddings, J. A. Harvey, G. T. Horowitz and A. Strominger, *Axionic Black Holes and a Bohm-Aharonov Effect for Strings*, Phys. Rev. Lett. **61** (1988) 2823.

[151] S. R. Coleman, J. Preskill and F. Wilczek, *Dynamical effect of quantum hair*, Mod. Phys. Lett. **A6** (1991) 1631–1642.

[152] Y. I. Izotov, T. X. Thuan and G. Stasinska, *The primordial abundance of 4He: a self-consistent empirical analysis of systematic effects in a large sample of low-metallicity HII regions*, Astrophys. J. **662** (2007) 15–38 [astro-ph/0702072].

[153] M. Fukugita and M. Kawasaki, *Primordial Helium Abundance: A Reanalysis of the Izotov- Thuan Spectroscopic Sample*, Astrophys. J. **646** (2006) 691–695 [astro-ph/0603334].

[154] M. Pettini, B. J. Zych, M. T. Murphy, A. Lewis and C. C. Steidel, *Deuterium Abundance in the Most Metal-Poor Damped Lyman alpha System: Converging on Omegabaryons*, 0805.0594.

[155] J. Geiss and G. Gloeckler, *Abundances of Deuterium and Helium-3 in the Protosolar Cloud*, Space Sci. Rev. **84** (Apr., 1998) 239–250.

[156] M. Asplund, D. L. Lambert, P. E. Nissen, F. Primas and V. V. Smith, *Lithium isotopic abundances in metal-poor halo stars*, Astrophys. J. **644** (2006) 229–259 [astro-ph/0510636].

[157] J. Hisano, M. Kawasaki, K. Kohri, T. Moroi and K. Nakayama, *Cosmic Rays from Dark Matter Annihilation and Big-Bang Nucleosynthesis*, Phys. Rev. **D79** (2009) 083522 [0901.3582].

[158] D. E. Gruber, J. L. Matteson, L. E. Peterson and G. V. Jung, *The Spectrum of Diffuse Cosmic Hard X-Rays Measured with HEAO-1*, astro-ph/9903492.

[159] A. W. Strong, I. V. Moskalenko and O. Reimer, *A new determination of the extragalactic diffuse gamma-ray background from EGRET data*, Astrophys. J. **613** (2004) 956–961 [astro-ph/0405441].

[160] The Fermi-LAT Collaboration, A. A. Abdo *et. al.*, *The Spectrum of the Isotropic Diffuse Gamma-Ray Emission Derived From First-Year Fermi Large Area Telescope Data*, Phys. Rev. Lett. **104** (2010) 101101 [1002.3603].

[161] Fermi LAT Collaboration, A. A. Abdo *et. al.*, *Fermi LAT Observation of Diffuse Gamma-Rays Produced Through Interactions between Local Interstellar Matter and High Energy Cosmic Rays*, Astrophys. J. **703** (2009) 1249–1256 [0908.1171].

[162] W. H. Press and P. Schechter, *Formation of galaxies and clusters of galaxies by selfsimilar gravitational condensation*, Astrophys. J. **187** (1974) 425–438.

[163] G. Efstathiou, C. S. Frenk, S. D. M. White and M. Davis, *Gravitational clustering from scale free initial conditions*, Mon. Not. Roy. Astron. Soc. **235** (1988) 715–748.

[164] C. G. Lacey and S. Cole, *Merger rates in hierarchical models of galaxy formation. 2. Comparison with N body simulations*, Mon. Not. Roy. Astron. Soc. **271** (1994) 676 [astro-ph/9402069].

[165] S. M. Leach, I. J. Grivell and A. R. Liddle, *Black hole constraints on the running mass inflation model*, Phys. Rev. **D62** (2000) 043516 [arXiv:astro-ph/0004296].

[166] K. Kohri, D. H. Lyth and A. Melchiorri, *Black hole formation and slow-roll inflation*, JCAP **0804** (2008) 038 [0711.5006].

[167] F. Zwicky, *Spectral displacement of extra galactic nebulae*, Helv. Phys. Acta **6** (1933) 110–127.

[168] G. Jungman, M. Kamionkowski and K. Griest, *Supersymmetric dark matter*, Phys. Rept. **267** (1996) 195–373 [hep-ph/9506380].

[169] L. Bergstrom, *Non-baryonic dark matter: Observational evidence and detection methods*, Rept. Prog. Phys. **63** (2000) 793 [arXiv:hep-ph/0002126].

[170] G. Bertone, D. Hooper and J. Silk, *Particle dark matter: Evidence, candidates and constraints*, Phys. Rept. **405** (2005) 279–390 [arXiv:hep-ph/0404175].

[171] J. R. Ellis, J. S. Hagelin, D. V. Nanopoulos, K. A. Olive and M. Srednicki, *Supersymmetric relics from the big bang*, Nucl. Phys. **B238** (1984) 453–476.

[172] M. Ricotti and A. Gould, *A New Probe of Dark Matter and High-Energy Universe Using Microlensing*, Astrophys. J. **707** (2009) 979–987 [arXiv:0908.0735].

[173] P. Scott and S. Sivertsson, *Gamma-Rays from Ultracompact Primordial Dark Matter Minihalos*, Phys. Rev. Lett. **103** (2009) 211301 [arXiv:0908.4082].

[174] A. S. Josan and A. M. Green, *Constraints from primordial black hole formation at the end of inflation*, Phys. Rev. **D82** (2010) 047303 [1004.5347].

[175] V. Berezinsky, V. Dokuchaev, Y. Eroshenko, M. Kachelriess and M. A. Solberg, *Superdense cosmological dark matter clumps*, arXiv:1002.3444.

[176] K. J. Mack, J. P. Ostriker and M. Ricotti, *Growth of structure seeded by primordial black holes*, Astrophys. J. **665** (2007) 1277–1287 [arXiv:astro-ph/0608642].

[177] M. Ricotti, J. P. Ostriker and K. J. Mack, *Effect of Primordial Black Holes on the Cosmic Microwave Background and Cosmological Parameter Estimates*, arXiv:0709.0524.

[178] B. C. Lacki and J. F. Beacom, *Primordial Black Holes as Dark Matter: Almost All or Almost Nothing*, 1003.3466.

[179] G. R. Blumenthal, S. M. Faber, R. Flores and J. R. Primack, *Contraction of Dark Matter Galactic Halos Due to Baryonic Infall*, Astrophys. J. **301** (1986) 27.

[180] PAMELA Collaboration, O. Adriani *et. al.*, *An anomalous positron abundance in cosmic rays with energies 1.5-100 GeV*, Nature **458** (2009) 607–609 [0810.4995].

[181] The Fermi LAT Collaboration, A. A. Abdo *et. al.*, *Measurement of the Cosmic Ray e+ plus e- spectrum from 20 GeV to 1 TeV with the Fermi Large Area Telescope*, Phys. Rev. Lett. **102** (2009) 181101 [0905.0025].

[182] P. Ullio, L. Bergstrom, J. Edsjo and C. G. Lacey, *Cosmological dark matter annihilations into gamma-rays: A closer look*, Phys. Rev. **D66** (2002) 123502 [arXiv:astro-ph/0207125].

[183] P. Gondolo *et. al.*, *DarkSUSY: Computing supersymmetric dark matter properties numerically*, JCAP **0407** (2004) 008 [arXiv:astro-ph/0406204].

[184] `http://fermi.gsfc.nasa.gov/science/instruments/table1-1.html`.

[185] J. F. Navarro, C. S. Frenk and S. D. M. White, *A Universal Density Profile from Hierarchical Clustering*, Astrophys. J. **490** (1997) 493–508 [arXiv:astro-ph/9611107].

[186] A. Klypin, H. Zhao and R. S. Somerville, *LCDM-based models for the Milky Way and M31 I: Dynamical Models*, Astrophys. J. **573** (2002) 597–613 [astro-ph/0110390].

[187] E. D. Stewart, *Flattening the inflaton's potential with quantum corrections*, *Phys. Lett.* **B391** (1997) 34–38 [arXiv:hep-ph/9606241].

[188] E. D. Stewart, *Flattening the inflaton's potential with quantum corrections. II*, *Phys. Rev.* **D56** (1997) 2019–2023 [arXiv:hep-ph/9703232].

[189] M. B. Hoffman and M. S. Turner, *Kinematic constraints to the key inflationary observables*, *Phys. Rev.* **D64** (2001) 023506 [arXiv:astro-ph/0006321].

[190] W. H. Kinney, *Inflation: Flow, fixed points and observables to arbitrary order in slow roll*, *Phys. Rev.* **D66** (2002) 083508 [arXiv:astro-ph/0206032].

[191] D. H. Lyth and A. Riotto, *Particle physics models of inflation and the cosmological density perturbation*, *Phys. Rept.* **314** (1999) 1–146 [hep-ph/9807278].

[192] L. Covi, D. H. Lyth and L. Roszkowski, *Observational constraints on an inflation model with a running mass*, *Phys. Rev.* **D60** (1999) 023509 [hep-ph/9809310].

[193] L. Covi and D. H. Lyth, *Running-mass models of inflation, and their observational constraints*, *Phys. Rev.* **D59** (1999) 063515 [hep-ph/9809562].

[194] D. H. Lyth and L. Covi, *Observational constraints on the spectral index of the cosmological curvature perturbation*, *Phys. Rev.* **D62** (2000) 103504 [astro-ph/0002397].

[195] L. Covi, D. H. Lyth, A. Melchiorri and C. J. Odman, *The running-mass inflation model and WMAP*, *Phys. Rev.* **D70** (2004) 123521 [astro-ph/0408129].

[196] L. Alabidi and K. Kohri, *Generating Primordial Black Holes Via Hilltop-Type Inflation Models*, *Phys. Rev.* **D80** (2009) 063511 [0906.1398].

[197] E. Bugaev and P. Klimai, *Large curvature perturbations near horizon crossing in single-field inflation models*, *Phys. Rev.* **D78** (2008) 063515 [0806.4541].

[198] A. R. Liddle, *On the inflationary flow equations*, *Phys. Rev.* **D68** (2003) 103504 [astro-ph/0307286].

[199] E. Ramirez and A. R. Liddle, *Stochastic approaches to inflation model building*, *Phys. Rev.* **D71** (2005) 123510 [arXiv:astro-ph/0502361].

[200] S. Chongchitnan and G. Efstathiou, *Accuracy of slow-roll formulae for inflationary perturbations: Implications for primordial black hole formation*, *JCAP* **0701** (2007) 011 [arXiv:astro-ph/0611818].

[201] B. A. Powell and W. H. Kinney, *Limits on primordial power spectrum resolution: An inflationary flow analysis*, *JCAP* **0708** (2007) 006 [0706.1982].

[202] P. Adshead and R. Easther, *Constraining Inflation*, *JCAP* **0810** (2008) 047 [0802.3898].

[203] W. H. Kinney, E. W. Kolb, A. Melchiorri and A. Riotto, *WMAPping inflationary physics*, *Phys. Rev.* **D69** (2004) 103516 [hep-ph/0305130].

[204] S. Chongchitnan and G. Efstathiou, *Dynamics of the inflationary flow equations*, *Phys. Rev.* **D72** (2005) 083520 [astro-ph/0508355].

[205] R. Easther and W. H. Kinney, *Monte Carlo reconstruction of the inflationary potential*, *Phys. Rev.* **D67** (2003) 043511 [astro-ph/0210345].

[206] R. Easther and J. T. Giblin, *The Hubble slow roll expansion for multi field inflation*, *Phys. Rev.* **D72** (2005) 103505 [astro-ph/0505033].

[207] E. D. Stewart and D. H. Lyth, *A more accurate analytic calculation of the spectrum of cosmological perturbations produced during inflation*, *Phys. Lett.* **B302** (1993) 171–175 [arXiv:gr-qc/9302019].

[208] J. E. Lidsey *et. al.*, *Reconstructing the inflaton potential: An overview*, *Rev. Mod. Phys.* **69** (1997) 373–410 [arXiv:astro-ph/9508078].

[209] V. F. Mukhanov, *Quantum Theory of Gauge Invariant Cosmological Perturbations*, *Sov. Phys. JETP* **67** (1988) 1297–1302.

[210] M. Sasaki, *Large Scale Quantum Fluctuations in the Inflationary Universe*, *Prog. Theor. Phys.* **76** (1986) 1036.

[211] F. Lucchin and S. Matarrese, *Power Law Inflation*, *Phys. Rev.* **D32** (1985) 1316.

[212] S. M. Leach and A. R. Liddle, *Inflationary perturbations near horizon crossing*, *Phys. Rev.* **D63** (2001) 043508 [astro-ph/0010082].

[213] I. J. Grivell and A. R. Liddle, *Accurate determination of inflationary perturbations*, *Phys. Rev.* **D54** (1996) 7191–7198 [astro-ph/9607096].

[214] J. Lesgourgues, A. A. Starobinsky and W. Valkenburg, *What do WMAP and SDSS really tell about inflation?*, *JCAP* **0801** (2008) 010 [arXiv:0710.1630].

[215] J. Hamann, J. Lesgourgues and W. Valkenburg, *How to constrain inflationary parameter space with minimal priors*, *JCAP* **0804** (2008) 016 [0802.0505].

[216] A. D. Linde, *Hybrid inflation*, *Phys. Rev.* **D49** (1994) 748–754 [astro-ph/9307002].